Winter 1989

Development of a glucose sensor based on competitive binding and laser-excited fluorescence

Richard William Bauer
University of New Hampshire, Durham

Order Number 9022634

Development of a glucose sensor based on competitive binding and laser excited fluorescence

Bauer, Richard William, Ph.D.

University of New Hampshire, 1989

U·M·I

300 N. Zeeb Rd.
Ann Arbor, MI 48106

DEVELOPMENT OF A GLUCOSE SENSOR BASED ON COMPETITIVE BINDING AND LASER EXCITED FLUORESCENCE

BY

RICHARD W. BAUER
B.S., Bates College, 1983

DISSERTATION

Submitted to the University of New Hampshire
in Partial Fulfillment of
the Requirements for the Degree of

Doctor of Philosophy

in

Chemistry

December, 1989

This dissertation has been examined and approved.

Dissertation Director, W. Rudolf Seitz,
Professor of Chemistry

Kenneth K. Andersen,
Professor of Chemistry

L. C. Balling,
Professor of Physics

Christopher F. Bauer,
Associate Professor of Chemistry

Sterling A. Tomellini,
Associate Professor of Chemistry

October 6, 1989
Date October 6, 1989

I am dedicating this dissertation to my parents in appreciation for their continued support and encouragement.

Thanks

William and Charlotte Bauer.

ACKNOWLEDGMENTS

I would like to thank my research adviser Dr. Rudi Seitz for his guidance and support during my graduate studies.

I would also like to thank my friends who made my time at the University of New Hampshire enjoyable as well as educational. In addition, I want to thank Scott, without his computer expertise, I would still be trying to print my dissertation.

Once again I wish to thank my parents and sisters.

Finally I want to extend a special thanks to Lyn for her love and encouragement.

TABLE OF CONTENTS

LIST OF TABLES

LIST OF FIGURES

ABSTRACT

DEVELOPMENT OF A GLUCOSE SENSOR BASED ON COMPETITIVE BINDING AND LASER EXCITED FLUORESCENCE

By

Richard W. Bauer

University of New Hampshire, December 1989

An optical glucose sensor has been developed using competitive binding in conjunction with energy transfer. Sensor response is based on competition between glucose and dextran for a limited number of binding sites on the protein concanavalin A (conA). The system is optically monitored using fluorescent donor-acceptor dye pairs labeled to concanavalin A and dextran. When the dyes are sufficiently close, on the order of 50 Å, energy is transferred from the donor emission band to the overlapping excitation band of the acceptor. This nonradiative, singlet-singlet transfer of energy enhances the acceptor emission at the expense of donor emission.

In absence of glucose, the conA and dextran are bound together and energy transfer takes place. Upon addition of glucose, the dextran is displaced, and energy transfer is disrupted. The ratio of the two emission intensities can be related to glucose concentration. Donor-acceptor sytems investigated included energy transfer from fluorescein (FITC) to three different types of rhodamine, TRITC, XRITC, and Texas Red, and both coumarin and fluorescamine donating energy to FITC. The system that gave the largest change in intensity involved FITC labeled conA as the donor and TRITC labeled dextran as the donor.

Fluorescence was measured with both conventional fluorescence instrumentation and a computer controlled, laser excited spectrometer. The laser instrument was developed specifically for the optical glucose sensor, but was designed to support a wide range of fiber optic sensors. Instrument components include a nitrogen pumped dye laser, fiber optic beam splitters, photomultiplier tubes fitted with interference filters for wavelength selection, and boxcar averagers.

Instrument development included calibration of the dye laser, evaluation of different fiber optic beam splitter arrangements, reduction of stray light, and evaluation of the boxcar averagers. The spectrometer was interfaced to an Apple IIc computer which was programmed to collect the data, perform baseline corrections, ratio the two channels, and trigger the laser to initiate the next data point.

The instrument's detection level, using Rhodamine 6G standards, is 1.0×10^{-9} molar and is limited by stray light. Precision of the instrument is approximately 3 % and is limited by drift of the boxcar averagers.

CHAPTER I

INTRODUCTION

For decades electrochemical sensors have been employed for chemical measurements. Electrochemical sensors are based on the conversion of chemical information to a current or a voltage, which is then transmitted via a wire to a readout device. Recently a new class of optical sensors has been developed in which optical chemical information is carried from the sample by fiber optic cables.

Both electrochemical and optical sensors must have certain characteristics to make them useful as analytical measurement devices. An ideal sensor will not perturb the system being investigated, will be selective, easily calibrated, readily inserted into the analyte solution, and be capable of long term continuous measurment, with a single calibration. The degree to which sensors fulfill these ideal requirements determines their practicality. Electrochemical sensors meet many of the above requirements as indicated by their extensive use over the last fifty years.

However, for certain measurements, optical sensors offer advantages over electrodes. First, with optical sensors information is carried by light waves, and thus is free from the electromagnetic interferences that can affect systems where information is transmitted electronically. Secondly, because of the absence of electrical hazard, optical sensors are preferred for in vivo measurements. In addition, optical sensors can be used to study analytes previously inaccessible to electrochemical devices.

Other advantages of optical sensors are that unlike electrodes, they do not require a reference sensor and that multiwavelength measurements are possible with optical sensors. Also, when analyte concentration can be related to a ratio of

intensities at two wavelengths, optical sensors, are likely to be stable with respect to calibration.

Optical sensor development is considered in review articles by Seitz [1,2], Peterson and Vurek [3], Wolfbeis [4,5] and Angel [6]. Fiber optic sensors can be classified into three types: photometric, physical, and chemical. Photometric sensors are bare ended fibers which directly observe the absorption or luminescence of an analyte in situ. Physical sensors operate when the shape or size of a micro-transducer is physically altered. For example, pressure sensors have been developed based on effects of pressure on the position of a reflecting surface [7]. Other physical sensors measure the distortion of the fibers themselves [8].

More recently fiber optic chemical sensors have attracted increasing attention. These sensors are based on a chemical reaction between a reagent immobilized at the end of an optical fiber and the analyte of interest. Both reversible and non-reversible systems are available. Reversible chemical sensors are more practical since they can be used for continuous measurements.

Reversible chemical fiber optic probes may be further classified as direct and indirect. Direct sensors monitor an optical change involving a reaction with the analyte. Indirect sensors involve a reaction where the analyte perturbs the system in a way which creates an optical change through an intermediate reaction.

The concept of merging chemical sensing with fiber optic waveguides was first demonstrated by Hardy et al. [9]. By immobilizing sodium picrate on the core of a fiber, he developed an optical sensor for cyanide. Other early work included an oxygen sensor based on fluorescence quenching [10] and a chemiluminescence probe for hydrogen peroxide, based on the luminol reaction [11].

Considerable work has been performed on the development of optic pH sensors. Of particular interest are sensors for in vivo pH measurements to monitor the respiratory status of patients in critical care. The primary advantages of the op-

tical approach are that it combines small size with calibration stability.

Peterson et al. [12] designed the first pH sensor in the late 1970's taking advantage of the different acid/base absorption peaks of phenol red. Gehrich et al. used optical fluorescence to sense pH in an intravascular blood gas monitoring system [13]. Seitz and coworkers have developed sensors based on immobilized fluoresceinamine [14] and HPTS (1-hydroxy-pyrene-3,6,8-trisulfonate) [15].

Wolfbeis has been active in pH sensor development. He also found HPTS to be an ideal indicator since its pKa of about 7.4 is suitable for pH measurements in the physiological range [16]. In an alkaline solution, HPTS has a strong excitation peak at 460 nm which is not observed when the solution becomes acidic. HPTS in an acidic medium is excited at 403 nm. By alternately exciting fluorescence bands at 403 and 460 nm an intensity ratio can be measured using a regular incandescent source and inexpensive glass fibers.

Efforts have also been made to develop optical sensors for in vivo pO_2 and pCO_2 measurements. Most pO_2 sensors are based on fluorescence quenching. The theory of oxygen quenching was first described in 1939 [17] and utilized by Bergman [18] in the 60's. Both Wolfbeis [19] and Peterson [20] used this approach as the basis for pO_2 sensors.

Oxygen complexation with hemoglobin provided Zhujun and Seitz [21] with a pO_2 probe using reflectance. Deoxyhemoglobin is immobilized on a cation exchange resin and is isolated from the sample by an oxygen permeable membrane. A spectral shift is observed upon oxygenation of the hemoglobin. This fiber optic chemical sensor (FOCS) ratios the deoxyhemoglobin and oxyhemoglobin reflectance at 405 and 435 nm, respectively.

Sensors which detect CO_2 are prepared from optical pH probes. Both Vurek et al. [22], and Zhujun and Seitz [23] have made carbon dioxide devices suitable for in vivo measurements. Cardiovascular Devices of Irvine, CA [13] currently pro-

duces a commercial instrument which will monitor all three blood gases during surgery.

Wolfbeis recently developed a single fiber probe to simultaneously detect O_2 and CO_2 using fluorescence [24]. Both the oxygen and CO_2 sensitive materials are entrapped in a gas permeable polymer matrix that is attached to the distal (bare) end of the fiber. Both indicators have similar excitation spectra but have different fluorescence wavelengths.

In addition to biomedical applications, there are possible environmental applications for fiber optic sensors, including the measurement of ground water pollutants [25-27] and potentially hazardous gases [28,29]. Chemical sensors are also readily adapted for detection of ions and ionic strength [30-33].

Competitive Binding Theory

The applicability of "direct" fiber optic sensing is limited by the availability of reactions which have the appropriate equilibrium constant, selectivity, and also give a detectable optical change. Competitive binding represents a way of extending optical sensing to other analytes.

Competitive binding is a system where an analyte competes with a second component, called a ligand, for a specific binding site on an immobilized reagent. This system is practical if the analyte and ligand are structurally similar and if the ligand can be labeled with a tracer. A significant advantage afforded by the system is that the analyte concentration can be monitored indirectly via the ligand.

The theory for competitive binding fiber optic sensor was first presented by Schultz and Sims [34]. The reactions may be represented:

$$A + R \leftrightarrow AR$$

$$L + R \leftrightarrow LR$$

The corresponding equilibrium constants are:

$$K_A = [AR]/\{[R][A]\}$$
$$K_L = [LR]/\{[R][L]\}$$

The ligand and reagent are in solution and contained by a size permeable membrane through which the small analyte can freely pass.

Total concentrations of L and R are derived from the mass balance equations:

$$C_L = [L] + [LR]$$
$$C_R = [LR] + [AR] + [R]$$

Assuming K_A and K_L are large, [R] can be dropped from consideration and through further substitution:

$$A = \left[\frac{(C_R - [LR])[L]}{[LR]} \right] X \frac{K_L}{K_A}$$

From this equation it is seen that the analyte concentration is proportional to the ratio of the equilibrium constants. This means that the effect of temperature, pH, and ionic strength on response will be minimized since variations in these parameters is likely to affect both of the reactions similarly.

Besides proposing the theory for competitive binding sensors, Schultz also developed the first fiber optic sensor of this type [35]. Schultz's glucose sensor employs the protein concanavalin A (conA) as the reagent to which both the

analyte, glucose, and the ligand, dextran, specifically and reversibly bind. The system is monitored optically by labeling dextran with fluorescein-isothiocyanate (dex-FITC). The reversible reaction is:

$$\text{conA} + \text{glucose} \leftrightarrow \text{conA-glucose}$$
$$\text{conA} + \text{Dex-FITC} \leftrightarrow \text{conA-Dex-FITC}$$

Increasing the glucose concentration drives the first reaction to the right, forming more conA-glucose, and pushes the second reaction to the left, freeing the fluorescent labeled dextran.

Schultz's original design [36] immobilized conA along the inner walls of a capped length of hollow dialysis tubing, Figure 1.1. Dextran, bound to the conA, is held out of the optical path of the excitation light coming from the fiber. As the low molecular weight glucose diffuses from the analyte solution through the membrane, dextran is displaced from the conA and is free to migrate into the illumination zone. Once in the illumination zone, the FITC label is excited, creating an increase in observed fluorescence intensity.

This optical glucose sensor offers several attractive features for detection of blood sugar. This chemical sensor is reversible and can be used continuously as long as concanavalin A is stable. The flexibility and small size of the optical cable used in this sensor make it ideal for in vivo measurements.

Development of an optical glucose sensor is important for the treatment of diabetes. It could be used in a self-contained system that detects blood sugar levels and dispenses insulin automatically.

However, while Schultz's glucose sensor is important as being the first competitive binding sensor, the actual system has several limitations. The design requires that there be an excess of fluorescein labeled dextran to insure that the conA

Figure 1.1: Competitive Binding Glucose Sensor

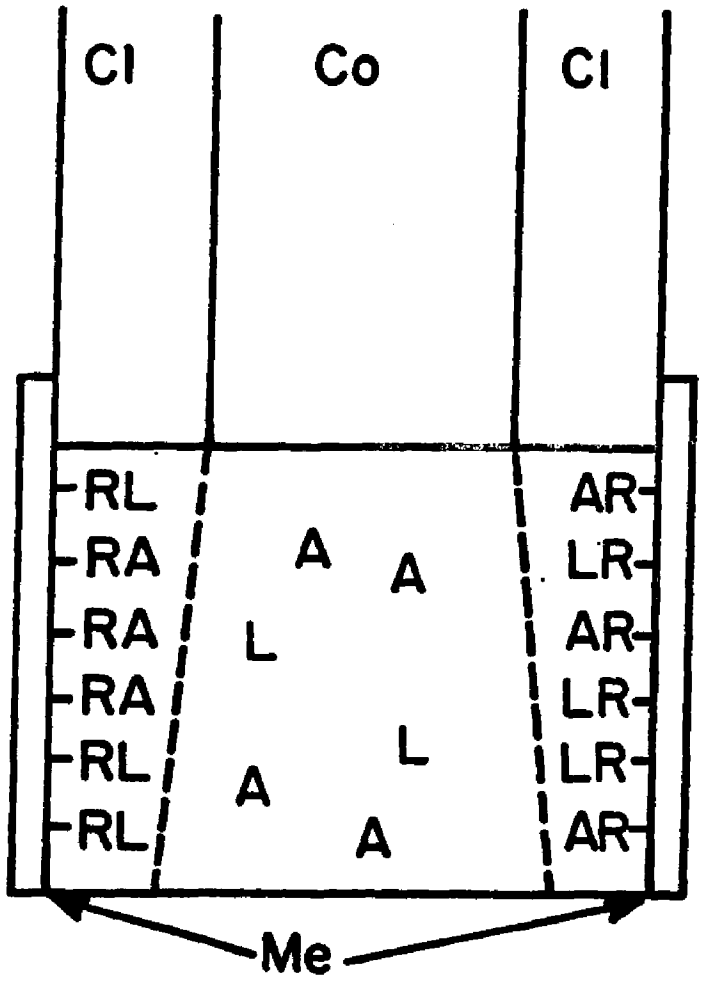

Schultz's fluorescence sensor for glucose based on competitive binding.

R is the reagent (ConA)
L is the ligand (Dex-Fluor.)
A is the analyte (Glucose).
Co = Fiber Core.
Cl = Fiber Cladding.

binding sites are saturated. This means that any fluorescence change, upon addition or removal of glucose, has to be measured above a significant background. Since the sensor is based on a single wavelength measurement, the fluorescence intensity, even in the absence of glucose, is subject to variations due to environmental changes such as temperature and pH. Also, photodecomposition of the fluorescent dye can not be distinguished from changes in glucose concentration.

Since Schultz's work, there have been other efforts to develop fiber optic chemical sensors based on competitive binding. Most of these probes utilize antibody/antigen interactions [37-40].

Introduction to Energy Transfer

One of the goals of this dissertation is to improve upon Schultz's glucose sensor by combining competitive binding with fluorescence energy transfer so that sensing can be based on an intensity ratio measurement.

Energy transfer is long range, nonradiative, singlet-singlet transfer of fluorescence energy from donor dye to an acceptor fluorophore, Figure 1.2 [41]. Spectral overlap between the donor emission band and acceptor absorption spectrum is necessary for energy transfer. In addition, for energy to be transferred, the donor and acceptor molecules have to be close spatially, on the order of 50 angstroms apart or less.

Förster developed the theory of energy transfer in the mid 1950's [41]. Since then it has been useful in several contexts including immunoassay. Ullman and coworkers [42] first studied competitive binding reactions by monitoring energy transfer between donor-labeled antigens and acceptor-labeled antibodies. When donor-labeled antigen is bound to acceptor-labeled antibody, the distance between the donor and acceptor is small enough to allow for significant energy transfer. Dis-

Figure 1.2: Ideal Exitation and Emission Spectra for a Fluorescence Energy Transfer Pair

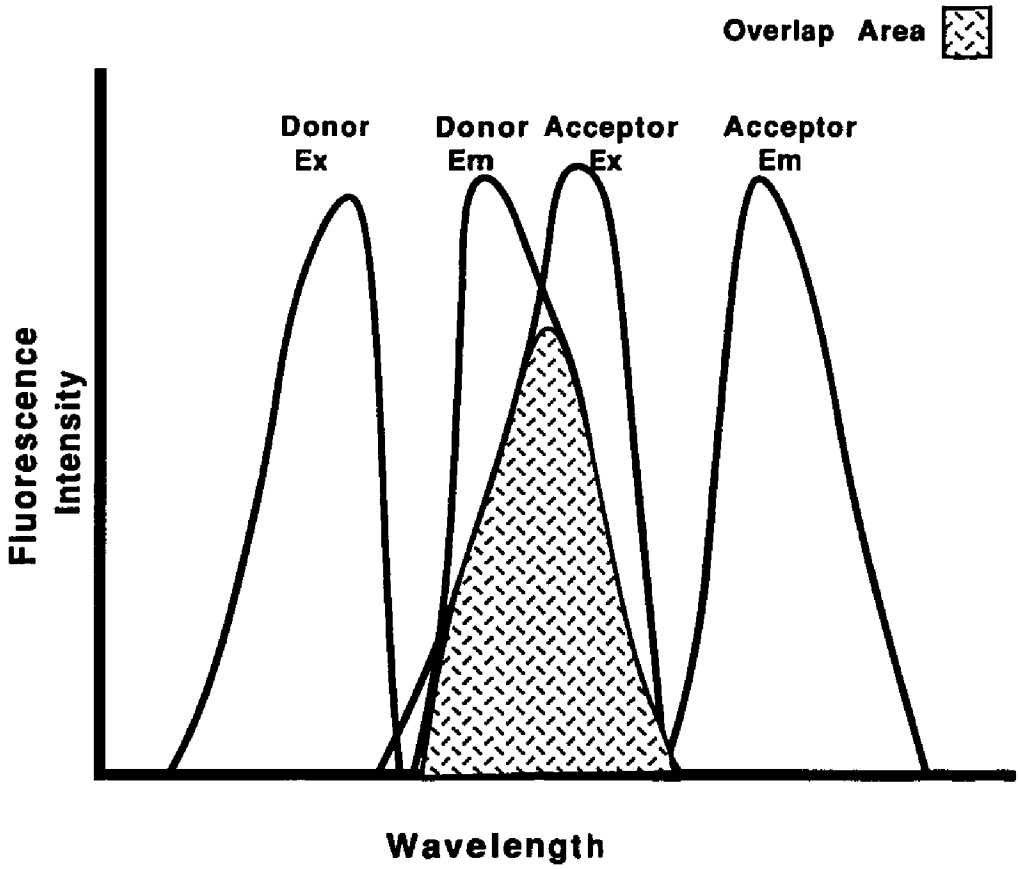

Ex = Excitation
Em = Emission

placement of donor-labeled antigen by unlabeled antigen, disrupts energy transfer and leads to an increase in observed donor fluorescent intensity.

More recently energy transfer has been utilized in the development of a physiological fiber optic pH sensor [43] where eosin is the donor and phenol red is the acceptor. The radius necessary for energy transfer is maintained by immobilizing both dyes on the end of an optical fiber.

An important feature of sensing based on energy transfer is the possibility of monitoring both the donor and acceptor emission peaks. The ratio measurement is insensitive to instrument drift and variations in the optical properties of the reagent phase.

Chemical Components of the Glucose Sensor

The glucose sensor presented in this dissertation combines both competitive binding and energy transfer. Energy transfer enhances the relative change in fluorescence intensity and provides the advantages of the ratio measurement. The competitive binding process is the same as in Schultz's sensor since the same substrates are used. Concanavalin A is the reagent, the ligand is dextran, and glucose is the analyte.

Concanavalin A is a lectin obtained in a crystalline form from the jack bean (Canavalia ensiformis). It reversibly binds saccharides and polysaccharides [44]. The protein was first crystallized in 1919, but it was not until 1936 that it was shown to react with carbohydrates [45]. The specific binding of conA, with dextran, provides a simple method for purification by affinity chromatography. ConA is adsorbed on cross-linked dextran gels (Sephadex) [46,47] and eluted with D-glucose. The proposed sensor works with the same principle.

Crystalline concanavalin A can be separated into several subunits, each con-

sisting of 238 amino acids. The sequence has been tentatively established by Edelman et al. [48,49]. Each subunit or "monomer" is made up of two polypeptide chains, one NH-terminal (MW 12,500) and the other is COOH-terminal (MW 13,000) [44]. X-Ray crystallographic studies show that each conA unit is globular in shape with overall dimensions of 42 x 40 x 39 Å [50,51].

The number of subunits which aggregate to form the conA molecule in solution is pH dependent. In a solution below pH 5.6 a dimer is formed while at pH's above 5.6 the conA molecule is made up of four subunits with a total molecular weight of 112,000 amu [52] and four saccharide binding sites, Figure 1.3 [48]. The psuedotetrahedral shaped tetramer is formed from a pair of dimers which in turn is formed from a pair of monomers. The association is reversible.

Crystallographic studies have also shown that the saccharide binding site is contained with in a deep but narrow pocket of approximately 6 x 7.5 x 18 Å [48]. Before the saccharide can bind to the conA a calcium ion must first fill a separate binding site on the surface of the conA. However, the calcium ion binding must be preceded by the binding of a transition metal to yet another site on each subunit [53].

Through a series of masking studies it has been shown that the carboxyl groups [54], not the amino or phenolic groups [55], of the concanavalin A, are responsible for the interaction with the saccharides. The carboxyl groups bind to the saccharides through polar interactions such as hydrogen bonding and charge-dipole interactions.

Further studies indicate the formation of these complexes involve the non-reducing ends of α-D-glucopyranosyl, α-D-mannopyranose, and sterically related sugars. It is thought that the oxygen atoms of the C-1, C-2, and C-3 hydroxyl groups, Figure 1.4, form the strongest interactions with the conA and that the saccharide binds to the protein in a C-1 chair conformation [56], Figure 1.5.

Figure 1.3: Schematic Representation of the Tetrameric Structure of ConA

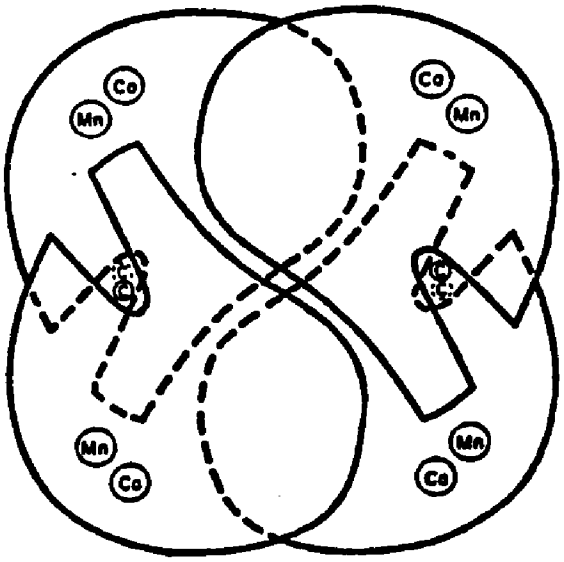

Viewed down the z axis.
Proposed binding sites for transition metals, calcium and saccharides are indicated by Mn, Ca, and C, respectively. [Edelman, G. M. etal *Proc. Nat. Acad. Sci. USA* vol 69, p. 2580, 1972.]

Figure 1.4: Fisher Projection of D-Glucose

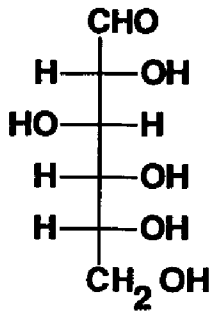

Figure 1.5: D-Glucopyranose Subunit of Dextran (1-6 Linkage)

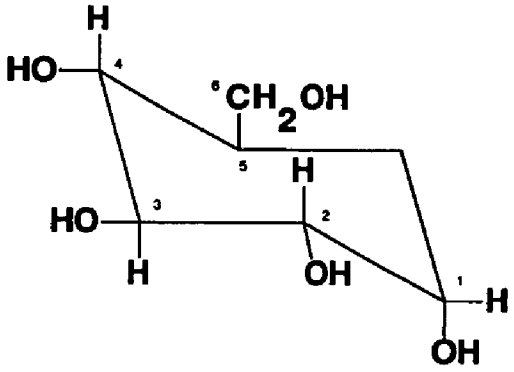

The proposed glucose sensor is feasible for the treatment of diabetics because α-D-glucose is the only low molecular weight carbohydrate present is blood plasma with both the right structure and in sufficient concentration to interact with concanavalin A, Table 1.1 [36].

The binding of glucose to concanavalin A is uncomplicated since it is a monosaccharide. However, dextran, which is a long chain of glucose units is multivalent. Dextran has predominantly α-D-(1-6)-glucosidic linkages, Figure 1.5, with many non-reducing branched chain ends. This enables a single dextran to bind to a number of conA binding sites. Because multivalent binding can occur, the binding constant for conA-dextran is almost two orders of magnitude stronger than for the conA-glucose interaction, 1.5×10^4 and 4.0×10^2, respectively [35].

Glucose and dextran are soluble in water, their structures are well known and their chemistry has been extensively characterized, facilitating their use in the proposed glucose sensor. Concanavalin A, on the other hand, is difficult to work with and characterize. The protein is sensitive to pH, temperature, and solvent, all of which cause the conA to denature, thus limiting its lifetime as a sensor reagent.

Another problem with conA is that it has limited solubility in aqueous solutions which restricts the sensor's dynamic range and sensitivity. To increase the sensitivity and working range, the ratio of fluorophore to conA can be increased and/or the source intensity can be enhanced. The ratio of dye to conA is limited by the number of binding sites on conA and by other constraints.

Optical Sensor Instrumentation

All fluorescence-based fiber optic sensors require a radiation source to generate measurable fluorescence. The more excitation wavelengths the source emits, the more versatile the instrument. The more intense the light, the better the

Table 1.1: Low Molecular Weight Sugars in Blood that can Bind to ConA

Carbohydrate	Conc. (mg/liter)
Glucose	800-1000
Pentones	4
L-Xylulose	1
Galactose	16
Mesoinositol	6
Glucose-6-phosphate	25
Fructose-6-phosphate	5
Fructose-1,6-phosphate	5

sensor's detection level. Presented in this dissertation is an instrument utilizing a tunable dye laser which emits intense, monochromatic, excitation throughout the entire visible spectrum.

Vurek and Bowman [57] were the first to use a laser source with an optical waveguide. Since then lasers have been used as sources for a number of optical sensors. In published work, the laser of choice has been the argon ion laser which has two intense emission lines at 488.0 and 514.5 nm. Schultz used the argon laser as the source, in his optical glucose sensor [35]. Argon laser emission has also been utilized in an energy transfer based pH sensor [43], in a competitive binding fluoroimmunoassy sensor [38], in an in vivo CO_2 probe [58], and for a host of other applications [59-64]. Hirschfeld used the argon ion laser for monitoring ground water via optical fibers [65].

Argon ion lasers are attractive since they emit continuous, high intensity, visible light. However, they have a high initial cost, a high maintenance cost, and since they only emit strongly at two wavelengths, their versatility is limited. In addition, the high intensity of the beam often requires attenuation, to avoid excess photodegradation of the sensor dyes.

A goal of this dissertation is to develop a low cost, versatile instrument which can be mated to a number of fluorescence based chemical sensors. Cost considerations preclude the use of the expensive argon ion laser, therefore a nitrogen-pumped dye laser is employed as the radiation source.

Nitrogen laser radiation (337 nm) excites a laser dye which emits broad band fluorescence. This emission band defines the tuning range of the dye. By utilizing a number of different dyes, the output of the dye laser can be tuned from 360 to 1000 nm [66]. In addition, the 337 nm line of the nitrogen laser can also be used.

To date, a nitrogen-pumped dye laser has been used in only one paper dealing with optical sensors. Both a frequency doubled, nitrogen-pumped dye laser, and

a Nd:YAG laser have been used to induce fluorescence in ground water contaminants [26]. It should be noted that this is not a chemical sensor, since it does not involve an indicator.

The advantages of low initial and maintenance costs, wide tunability, and sufficient intensity, for remote sensing, are offset by the pulse to pulse variability of the spark discharge nitrogen laser. This variability requires a two wavelength intensity ratio measurement that compensates for fluctuations in pulse intensity.

Light from the nitrogen laser is conducted to and from the indicator by optical fibers. Optical fiber consists of an inner solid cylinder of light conducting material, called the core, surrounded by a shell of glass or plastic, designated as the cladding, Figure 1.6. As long as the cladding material has a lower index of refraction (n) than the core, light that strikes the core/cladding interface at an angle greater than the critical angle will be totally internally reflected. The critical angle (ϕ_c) depends on the refractive indices of core (n_1) and cladding (n_2).

$$\phi_c = \arcsin (n_2/n_1)$$

The numerical aperture (NA) defines the angle of the acceptance cone of the fiber and determines how much light will be accepted by the fiber, Figure 1.7. The numerical aperture depends on the refractive index of both the core and the cladding.

$$NA = (n_1^2 - n_2^2)^{1/2}.$$

Choosing fiber with a large numerical aperture is important because it is desirable to maximize both the intensity of the light exciting the sample, as well as the collection of the sample fluorescence.

Figure 1.6: Optical Fiber

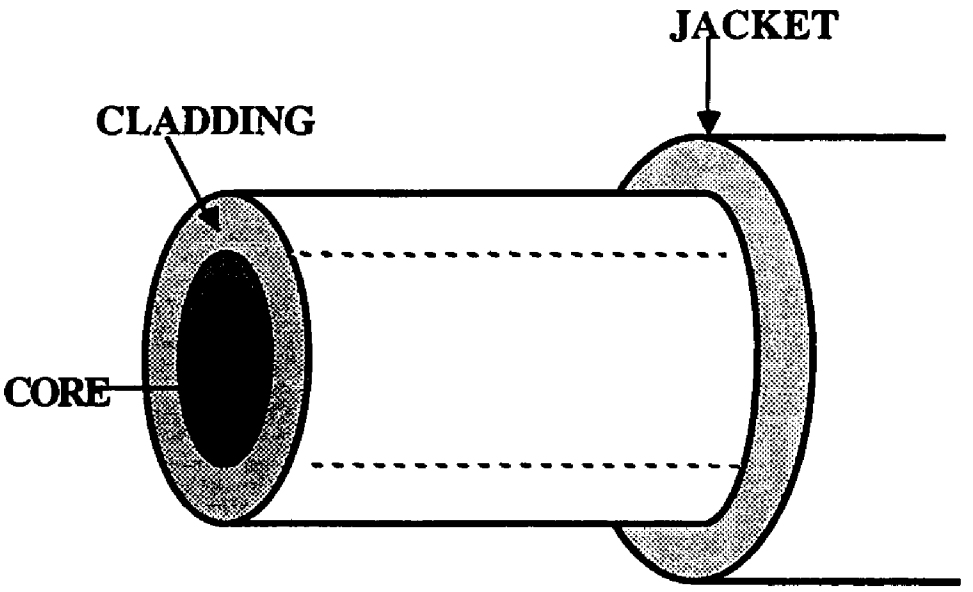

CORE MATERIALS	CLADDING MATERIALS
Fused Silica	Glass
Glass	Plastic
Plastic	

Figure 1.7: Acceptance Cone and Total Internal Reflectance in an Optical Fiber

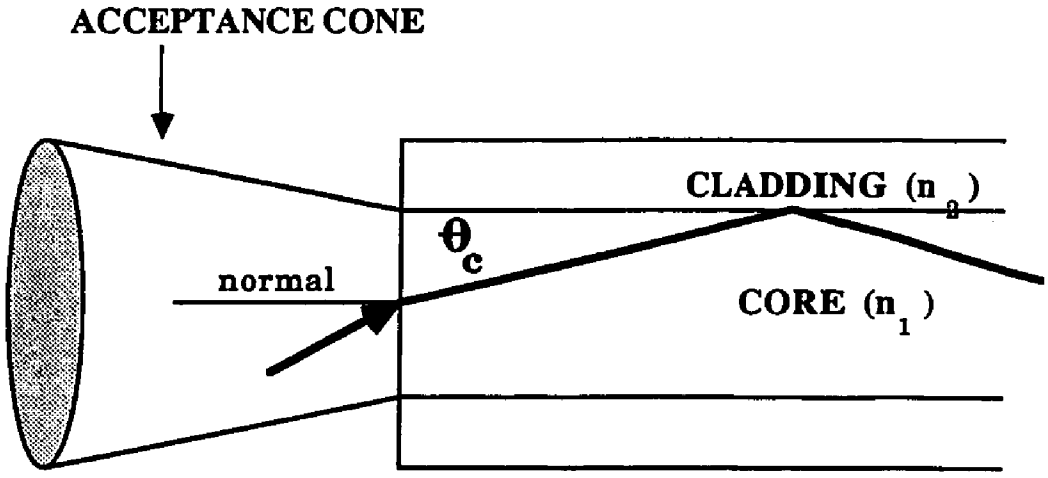

$$NA = \sqrt{n_1^2 - n_2^2} = n_1 \sin \theta_c$$

Presently there are three main types of optical fiber cores: fused silica, glass, and plastic, each of which can be doped with impurities to obtain specific performance characteristics. Fused silica cores (n=1.405 at 850 nm), usually with a plastic cladding, are fabricated from high purity natural quartz, allowing low loss, long distance transmission of light down to 200 nm. Less expensive glass fibers (n=1.458 at 850 nm), with glass or plastic cladding, are also common, but transmission is restricted to the visible and infrared regions.

Many early instruments utilized bifurcated fiber optic bundles [67-70]. As many as one hundred single fibers are bundled together, half are used to carry the light to the sensing region and the other half collect the signal from the sample, Figure 1.8. Bundle diameters are on the order of 5 mm which facilitates coupling of large amounts of light to and from the sample.

Other sensors use separate, single, excitation and collection fibers [71,72]. One fiber carries the excitation light to the sample and fluorescence is collected by up to six surrounding fibers, Figure 1.9 [73]. Since different fibers are employed, this requires only conventional optics to focus the excitation light into the fiber and to detect the emitted sample signal. The only difference between this arrangement and the bifurcated bundle are the number of fibers employed.

A significant advantage of using separate fibers, to carry the excitation and emission light, is that reflected excitation light is not a problem. Due to different refractive indexes, of the fiber optic core material and the sensing environment, there is a certain amount of reflected excitation light, called backscatter.

Fresnel reflections constitute the major portion of backscatter. These reflections occur at the fiber ends and are exacerbated by large differences in the refractive indices of the fiber core and the surrounding medium. For a glass-air interface the reflected power, P_{ref}, for light (of power P_o) incident perpendicular to the interface is:

Figure 1.8: Bifurcated Fiber

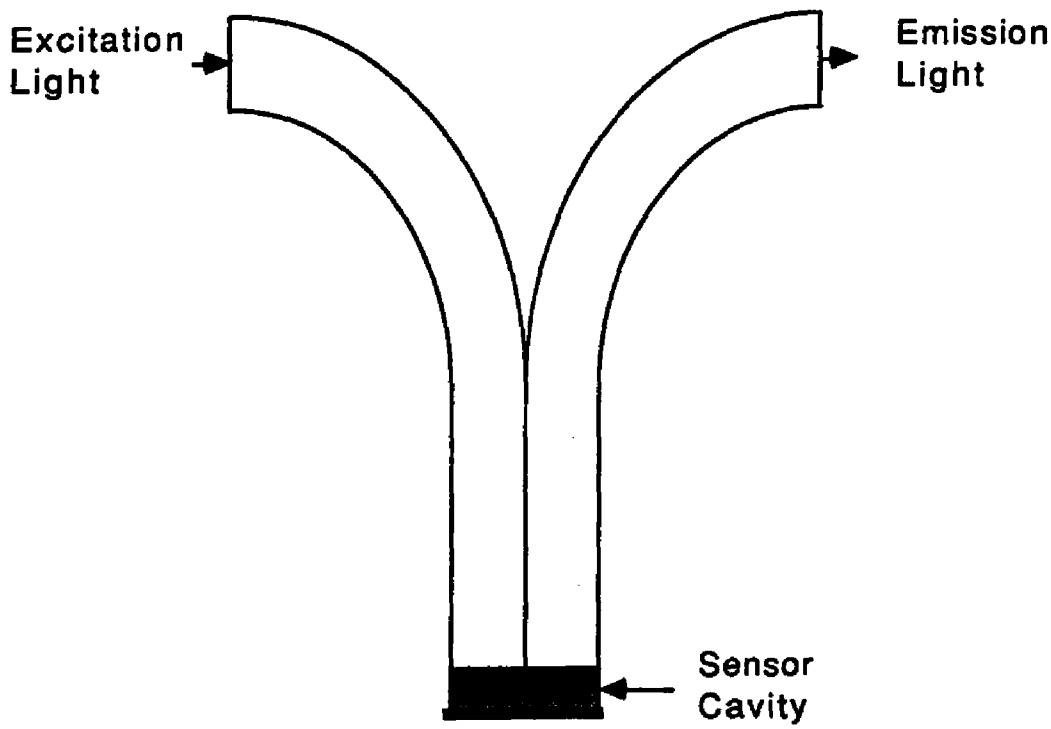

Figure 1.9: Multiple Fiber Design

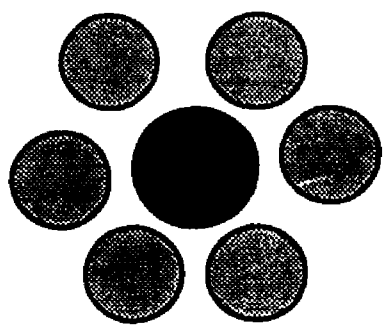

Center excitation fiber surronded by emission fibers.

$$P_{ref} = P_o\{(n_{fiber} - n_{air})/(n_{fiber} + n_{air})\}^2$$

where n_{fiber} and n_{air} are the refractive indices of the fiber core and air [74]. An air/glass interface reflects about 4 % of an incident beam normal to the interface.

Because Fresnel reflections depend on the difference in refractive index between the fiber and surrounding medium, use of index of refraction matching gel at the fiber ends can greatly reduce backscatter. Refractive index gel is a viscous, optically clear, fluid which has a refractive index close to that of the fiber core. If the index of the gel matches the core material exactly, all the backscatter would be a result of Rayleigh scatter, and would be infinitesimal. However, a perfect match is not possible. Therefore, when using a single fiber, the red shifted fluorescence needs to be resolved spectrally from reflected excitation light.

Because backscatter is not a factor when using separate fibers, only conventional optics are necessary. Light is coupled from the source into the fiber with a lens, and sample emission from the second fiber is directed to the detector, Figure 1.8. However, to achieve maximum stability of measurement, it is advantageous to use a single fiber for sample illumination and collection of the sample emission. A single fiber maximizes the overlap between the illumination and collection zones, as well as eliminating problems of fiber alignment, thus increasing sensitivity [65]. Single fiber sensors are also smaller and less costly.

The disadvantage of using the same fiber, to carry both the excitation and emission light, is that the emission needs to be directed towards a detector and away from the source. This requires a more complex optical arrangement than used for bifurcated systems. Redirection of the emission signal is most easily performed using a conventional beam splitter, but, the method is hampered by significant light loss.

A dichroic mirror, which is basically a wavelength dependent beam splitter, has been used in some applications [35,43,61,64]. Shorter wavelength excitation light passes through a splitter which reflects the red shifted sample fluorescence, Figure 1.10. The greatest advantage of this configuration is that backscatter of reflected excitation light is not split off to the detector. However, cost and the need to employ fluorophors with a large Stokes shifts diminish the applicability of the dichroic splitter.

A third method to extract the sample emission is to use a perforated mirror [38,76]. Excitation light passes through a small hole in the middle of a concave mirror and into the fiber. Sample emission exits the fiber in a cone, determined by the numerical aperture, and is reflected by the mirror to the detector, Figure 1.11. This method is only practical with laser sources.

All of the above optical arrangements require precise alignment and thus are not well suited for portable instruments. The instrument presented in this dissertation uses a fiber optic beam splitter which minimize the optical alignment and stability problems encountered with conventional splitter/lens systems.

Fiber optic beam splitters (FOBS) provide a way to transfer light directly between two fibers, Figure 1.12. Most fiber optic beam splitters are fabricated by the fused-pull-and-taper method [76]. The plastic buffer is stripped off the fibers. Then, while heating to melt the two fibers together, the fibers are drawn or stretched. The degree of fusion between the two fiber cores determines the splitting ratio of the FOBS [77,78].

Figure 1.12 represents a 2 x 2 fused biconical taper coupler. Light entering port 1 is evanescently coupled to the second fiber. In other words, light travels out of the first core into a second core, with a similar refractive index. A portion of the light travels down one arm and the remainder travels down the other. Anderson and Miller utilized a fiber optic beam splitter in their immunosensor [79].

Figure 1.10: Single Fiber Measurements With a Dichroic Mirror

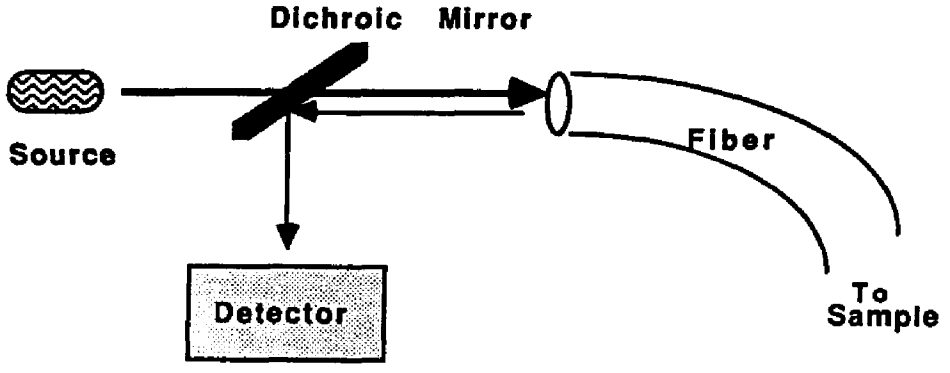

Figure 1.11: Single Fiber Measurements With a Perforated Mirror

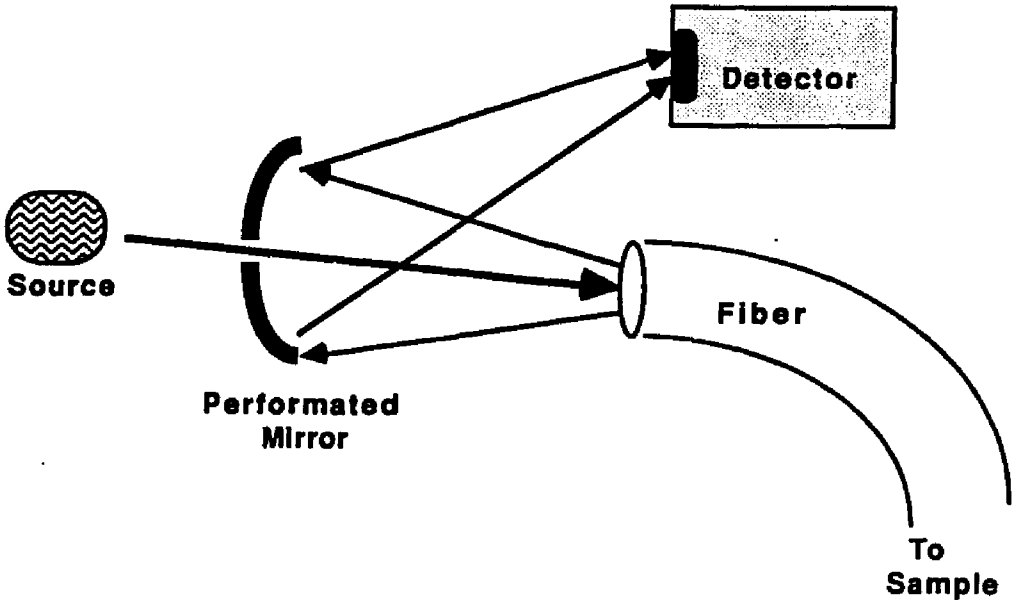

Figure 1.12: 2 X 2 Fiber Optic Beam Splitter

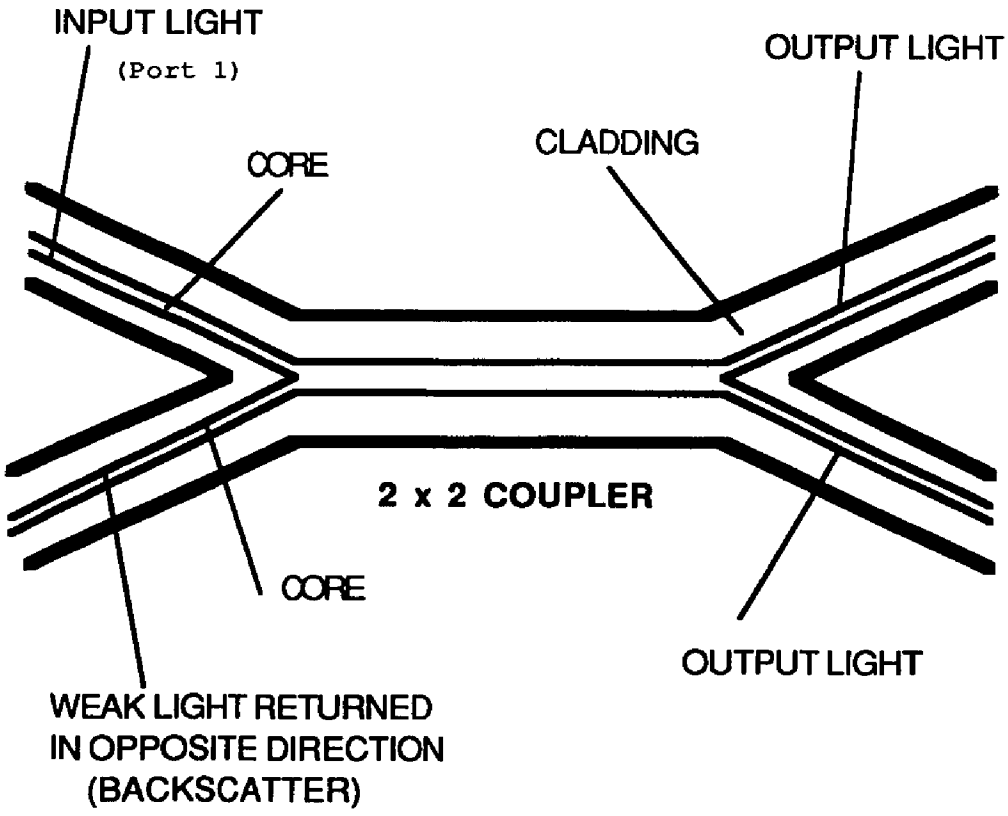

Summary

This dissertation had two objectives, the design and characterization of an instrument for single fiber chemical sensors based on laser excited fluorescence, and the development of an optical glucose sensor, based on competitive binding and fluorescence energy transfer.

Different instrument designs were considered, evaluated, and characterized. Of special interest are versatility provided by the nitrogen-pumped dye laser and the multiple configurations of fiber optic beam splitter(s). A discussion of the computer interface and data acquisition is also presented.

In developing the fluorescence based chemical glucose sensor, a number of donor acceptor fluorescence pairs were evaluated as labels for the concanavalin A and dextran. Of particular interest was the compatibility of the dyes with the dextran and conA, and the energy transfer donor-acceptor spectral characteristics.

CHAPTER II

INSTRUMENT DEVELOPMENT AND EVALUATION

Introduction

This chapter describes the development, and evaluation of a laser-excited fiber optic, fluorescence instrument. The instrument is configured expressly for the optical glucose sensor but can support a wide array of fiber optic chemical sensors.

Each of the components is evaluated individually. Various optical beam splitters and boxcar integrators configurations are investigated. Finally, the performance of the whole instrument is studied with emphasis on detection limits, precision and working range.

Components

Source

The source is a Phase-R Micro Dye Laser pumped by a Phase-R Nitrogen Laser, Figure 2.1. (Phase-R Corporation, Box G-2, New Durham, NH). The air cooled nitrogen laser emits light at 337.1 nm with a spectral band width of 0.1 nm. It has a repetition rate up to 20 pulses per second (pps). Each pulse has a 1.0 ns lifetime. Energy per pulse is reported to be 150 uJ with $\mp$ 5% pulse-to-pulse reproducibility. Peak power is 150 kW and average power at 20 Hz is 3mW. (All specifications from Phase-R manual.) Laser stability and power are controlled by adjusting the high voltage, repetition rate, nitrogen flow, and air pressure.

During normal operation, the nitrogen laser is fired remotely using a computer controlled relay. In some of the characterization work, and for certain ap-

Figure 2.1: Diagram of the Nitrogen Laser

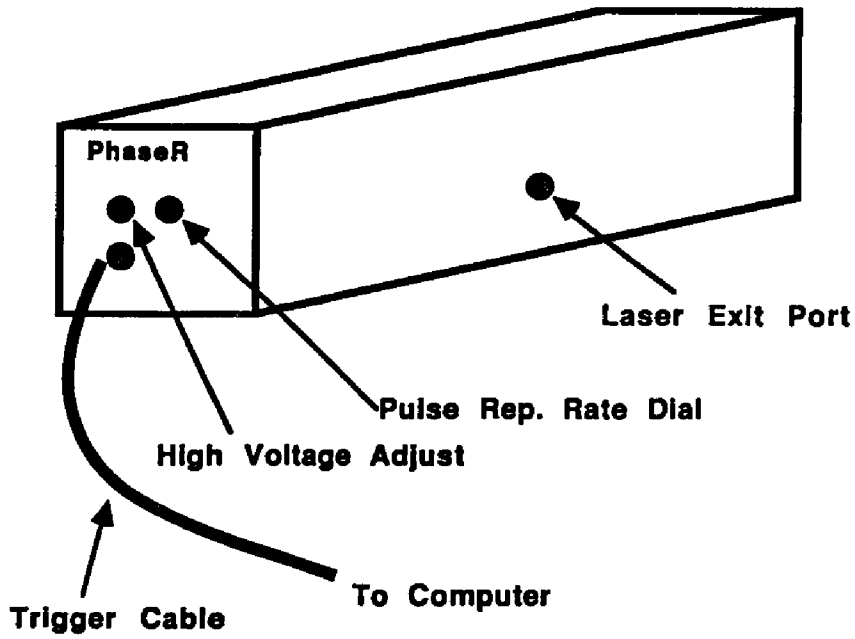

Nitrogen and Air inputs are on the back panel.

plications, the auto fire mode was also used.

While the nitrogen laser can directly induce fluorescence from UV absorbing fluorophores, its primary function is to pump the Phase-R Tunable Dye Laser. The MICRO-DYE laser produces tunable laser light radiation with a line width of 0.001 nm. Wavelengths from 360 to 1000 nm are possible using a series of laser dyes with tuning curves of approximately∓ 50 nm. Laser quality dyes (Exciton Inc. P.O. Box 31126, Overlook Station, Dayton, OH) were used for best results.

Highly concentrated dye solutions are added to a 3.0 x 3.0 x 40.0 mm fused silica dye cell, which is tilted 10 to 15 degrees forward to prevent reflections onto the grating. The dye cell has two unobstructed cell faces which are oriented so that lasing occurs along the clear face, Figure 2.2. Given the high dye concentration, up to 1.0×10^{-3} M, there is total self absorption within the first 1 to 1.5 mm of dye solution.

Lasing is achieved by amplifying the dye fluorescence within the optical cavity, Figure 2.3 [80]. A cylindrical lens focuses the nitrogen laser light into a thin line across the dye cell. Dye emission is reflected by a stationary maximum reflector on to an 1800 line/mm holographic grating which diffracts the light onto a movable mirror controlled by a micrometer. The wavelength of the dye laser is selected by adjusting the tuning mirror with the micrometer to a position which reflects the desired wavelength back to the grating. The zero order band of the grating is the output of the lasing cavity.

Efficient dyes produce secondary fluorescence spots which are easily distinguished from the crisp, speckled laser output. Pump light conversion can reach 25% [81]. Beam diameter at the output port is stated to be 6 mm. The beam is directed at a microscope objective lens (Ealing X10 power, 0.25 numerical aperture) which focuses the laser light onto the end of the input fiber of the fiber optic beam splitter. Both the objective lens and an adjustable 3 axis fiber holder are mounted

Figure 2.2: Dye Laser Cell
Top View

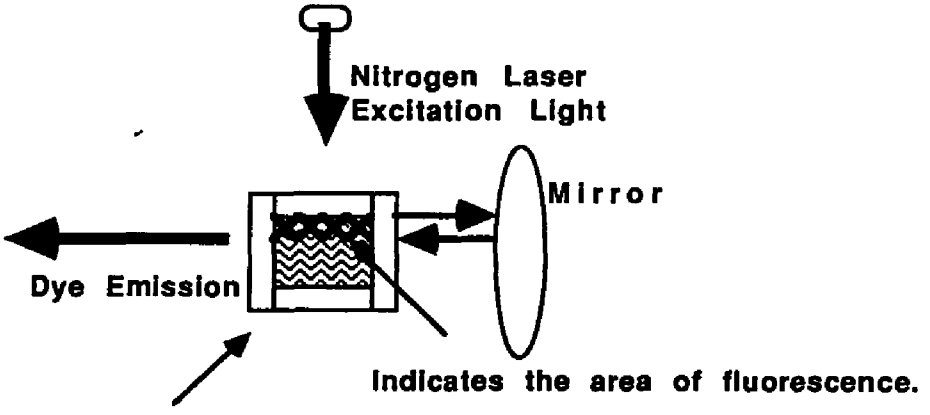

Dye Cell oriented so that dye emission passes through two clear faces.

Figure 2.3: Dye Laser Optical Cavity

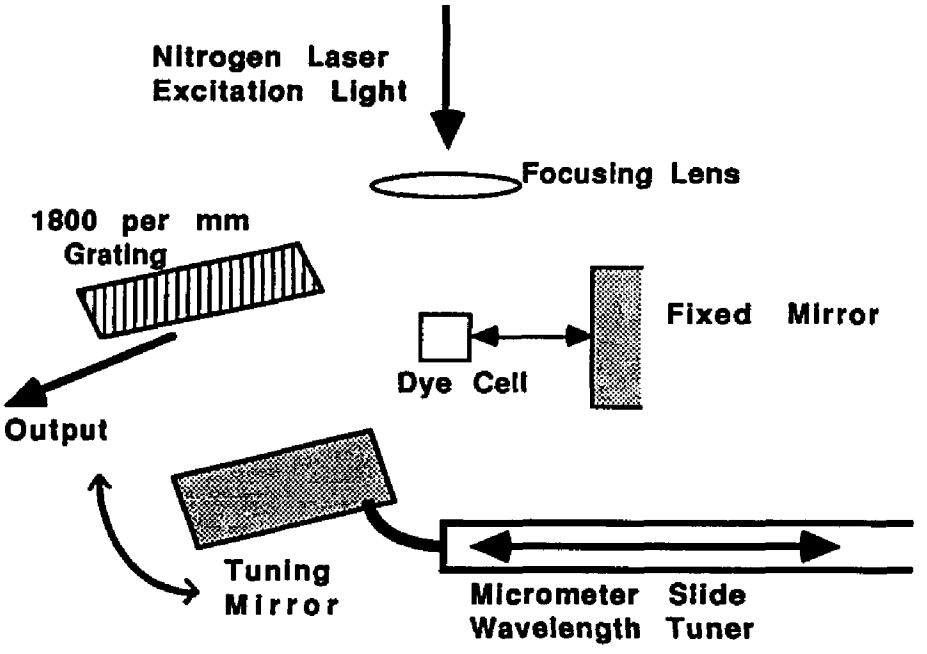

on an Ealing Minibench (Ealing Electro-Optics, South Natick, MA).

Optical Beam Splitters

A fiber optic beam splitter (FOBS) is a device that divides, or combines light, from the input port to the output ports in a predetermined splitting ratio, Figure 2.4.

Two types of FOBS were utilized in this instrument. Initial studies were performed with both a 3 and 4 Port ADC FOBS (Westborough, MA) fabricated from glass/glass fiber with a 200 micron diameter core and 240 micron cladding. Measurements in the ultraviolet region require a fused silica splitter which was obtained from Aster (113 Cedar St., Milford, MA). This FOBS utilizes a 200/230 (core/cladding) high numerical aperture (NA) fused silica core with a plastic cladding (Ensign Bickford Optics Co. Avon, CT 06001). Both beam splitters were suppose to have a 50/50 splitting ratio. The ratio is determined by measuring the intensity of light from Port 4 (X) over the light emitted from both Ports (X + Y).

Connections between fibers are made with SMA type connectors. Splice bushings act as in-line connectors to mate two assembled SMA terminated fibers, while bulkhead adaptors mate SMA terminated fibers with the detectors and fiber bundles. SMA connectors are available from a number of suppliers and the fiber can either be secured with epoxy (OFTI, Nutting Lake, MA and General Fiber Optics, Cedar Grove, NJ) or by crimping (Ensign Bickford Optics Co.). Backscatter from the air/fiber interface and at fiber to fiber connections was minimized with index of refraction matching gel.

Detectors

Sample light is measured with a RCA 1P21 photomultiplier tube (PMT). The reference intensity and the boxcar trigger signals were detected with RCA 1P28 PMTs. All three PMTs were held in Hamamatsu sockets, Figure 2.5. The trigger

Figure 2.4: Four Port ADC Fiber Optic Beam Splitter

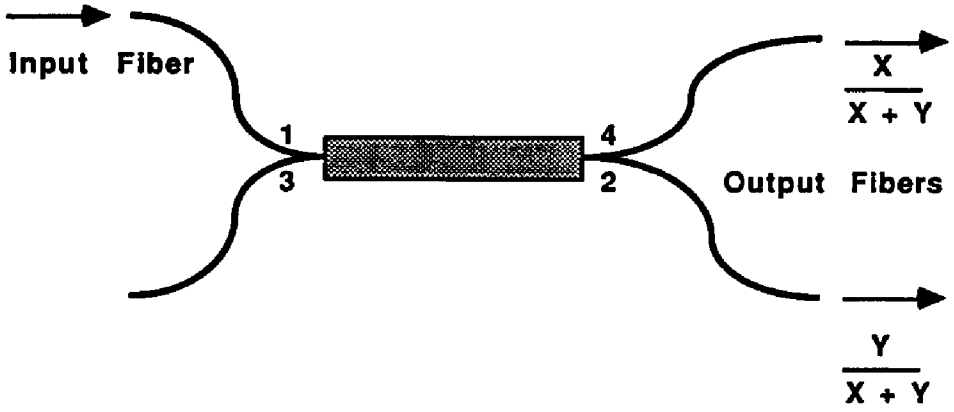

Figure 2.5: Sample Photomultiplier Tube

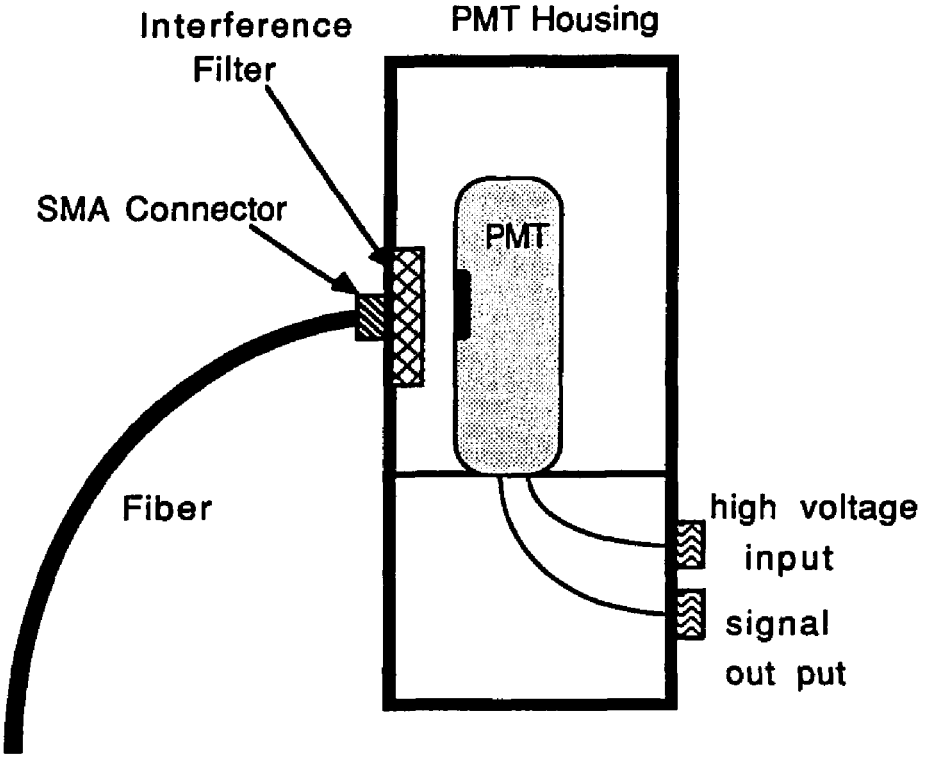

In the Reference and Trigger PMTs the Interference Filter is replaced with Neutral Density Filters.

PMT was powered by a PAR model 280/281 High Voltage Power Supply, a Kepco 2500 volt unit is used to power the reference PMT and the sample PMT was powered by a Fluke Model 412B.

The emission wavelength was selected by interference filters incorporated into the sample PMT housing. Filter selection is covered in the evaluation section of this chapter.

Boxcar Averagers

Signal integration was performed with boxcar averagers (EG & G Princeton Applied Research, P.O. Box 2565, Princeton, NJ). The sample, reference, and trigger signals from the photomultiplier tubes were carried to the boxcars by 50 ohm impedance coaxial cables (RG 58C/U), terminated with BNC connectors.

Boxcar averaging is a process of controlled sampling and averaging. The process involves repeatedly measuring the amplitude of a specific point on a repetitive waveform while computing the average value of the measurements taken. Since the average value of noise over an infinite number of repetitions is zero, an improvement in signal-to-noise ratio occurs. Signal averaging is applicable when three conditions are satisfied: signals must be repetitive, each sample signal pulse must be preceded by a clean trigger signal, and both signal and trigger must be synchronized to each other [82].

The principles of boxcar operation are illustrated in Figure 2.6.A, where a repetitive signal and a synchronous trigger are applied to the boxcar [83]. At a precisely selected moment, after receipt of a the trigger, the electronic sampling switch closes for a relatively short time interval known as the Aperture Duration (AD). The exact moment that the AD switch opens is determined by the aperture delay range (ADR) and the percent delay knob. When the switch opens, the accumulated signal is held "indefinitely" and the balance of the waveform is ignored until the next

Figure 2.6.A: Simplified Boxcar Operation

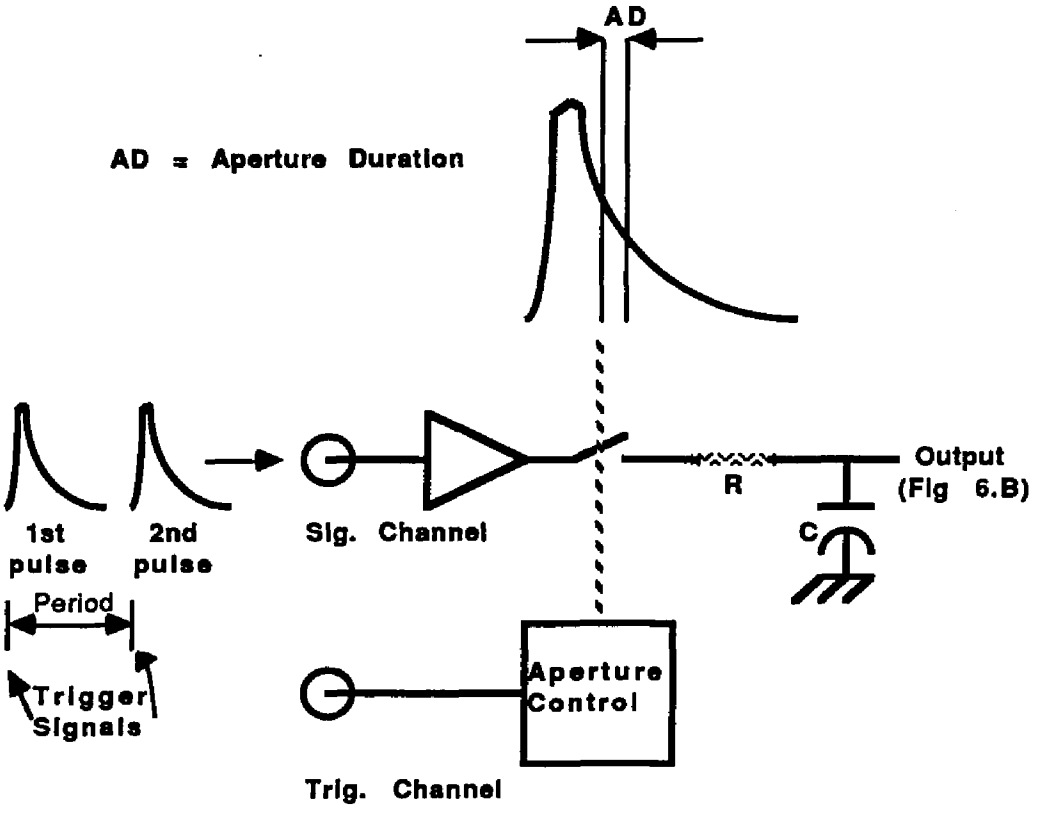

Figure 2.6.B: Boxcar Output

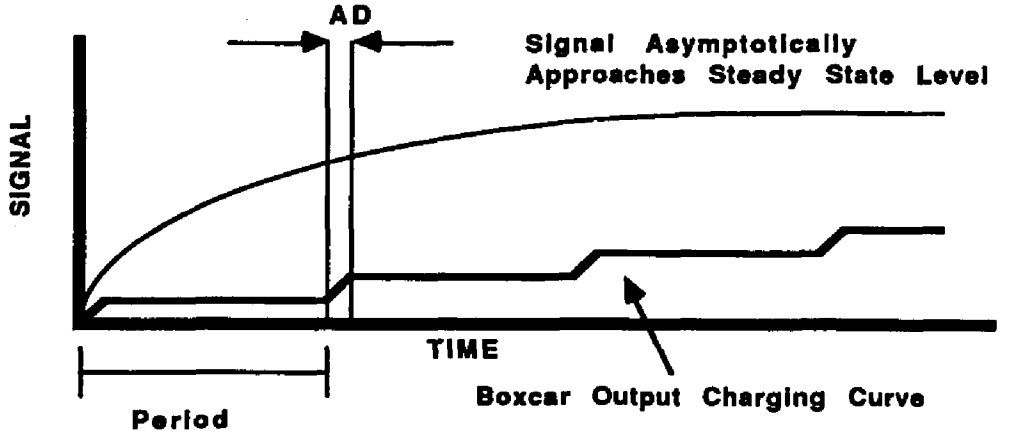

trigger. Complete definitions of boxcar terminology are presented in Appendix 1.

Assuming that the same waveform segment is repetitively sampled the boxcar voltage output asymptotically approaches the average value of the input signal, Figure 2.6.B. After an elapsed time of five Observed Time Constants (OTC), $5(TC)T_P/AD$, (TC is the low-pass time constant and T_P is the period between successive triggers), the output is within 0.7% of the steady state average. Noise is similarly sampled, but its presence at the boxcar output will be reduced. The maximum signal to noise improvement ratio (SNIR) for a white noise background is $(2TC/AD)^{1/2}$.

The boxcars consist of a Model 162 Mainframe with two ports for gated integrators. The Model 162 mainframe contains most of the timing and control functions including the aperture positioning and aperture duration. Also included on the 162 mainframe are the trigger input and control. The mainframe accommodates two plug in modules to perform the actual gated integration. Models 164 and 166 Gated Integrators were evaluated. Both perform the same function but the 166 allows for faster signal recovery. The 162 mainframe and the gated integrators, as well as their controls are discussed in more detail in the instrument evaluation section of this dissertation.

Computer and the Computer Interfacing Card

The boxcars are interfaced to an Apple IIe computer through an ADALAB Interface Card (Interactive Microware Inc., P.O. Box 139, State College, PA) in the computer. The ADALAB interface allows both analog input to collect voltage information from an instrument, and digital output to send information from the Apple IIe. The Analog to Digital (A/D) converter subsystem reads voltages with a precision of 0.025% and has an overall accuracy of better than 0.1%. The dual slope integrating A/D converter smooths out noisy signals and can accept up to 20

voltage readings per second.

An ADA-MUX (Interactive Microware) Multiplexer enables the ADALAB card to read both channels of the boxcars by sequentially sampling the boxcar channels and sending the voltage signals to the interface card. Channel-to-Channel sampling rate varies between 3 and 16 channels per second, depending on signal level. In addition to its function as an input multiplexer, the ADA-MUX was also configured to act as double-pole, single-throw switch for operating the relay which triggers the Nitrogen laser. System programing for laser triggering, data acquisition, and data manipulation was done using QUICK I/O software (Interactive Microware) in BASIC, Appendices 2 and 3.

Laser triggering is initiated by a 1.0 V signal from the ADALAB to an AMF Potter & Brumfield Model KRP 11DG relay powered by a Burr-Brown Model 551 15 volt power supply, Figure 2.7.

Component testing and instrument diagnostics were performed with a 100 MHz Model SS-5711 Iwatsu Oscilloscope.

Figure 2.7: Laser Trigger Relay Wiring Diagram

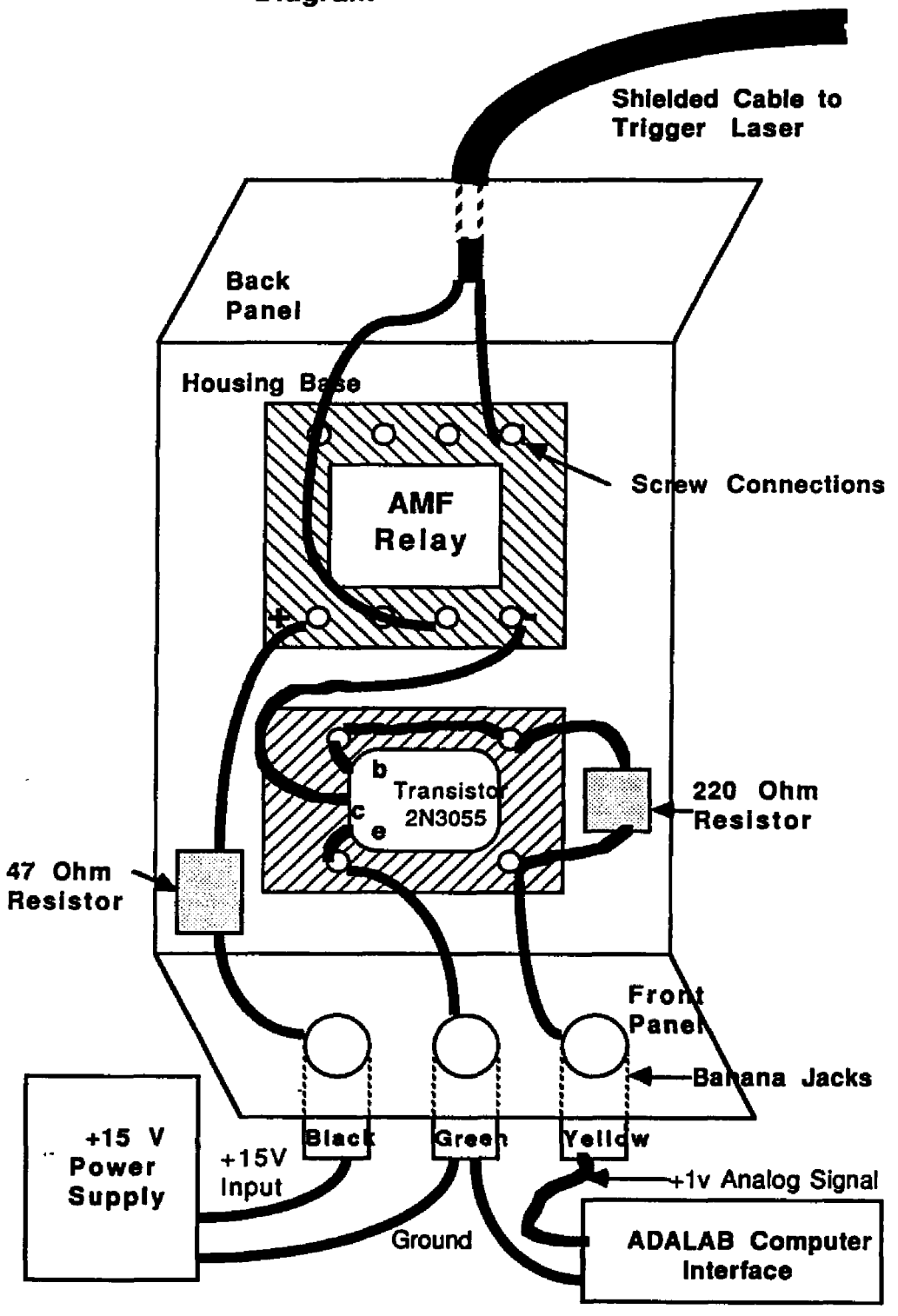

Instrument Component Evaluation

Nitrogen Laser

Pulse-to-pulse reproducibility of nitrogen laser intensity is of primary importance to instrument performance since sample fluorescence is directly proportional to source intensity. In the manufactere's literature the replication is reported to be ∓5%. Long term drift, the increase or decrease in laser intensity over hundreds of laser shots, also needs to be considered.

The nitrogen laser is remotely fired by the computer at 1 pulse per second (pps) and the 337.1 nm light intensity is monitored indirectly by measuring the intensity of the dye emission. Dye laser emission was collected with an 1P28 photomultiplier tube and the output was monitored on a 1MHz oscilloscope. Precision studies were performed at off peak hours to reduce line voltage and air pressure variability. The laser high voltage was set above the minimum level necessary for efficient laser firing. Air pressure must be maintained above 10 psi to ensure that waste gases are removed and the spark gap remains within the working temperature range. During these studies air pressure from in-house lines was maintained at 14 psi by continually adjusting the pressure valve. The nitrogen flow is critical and should be kept near 4 psi with a very slow flow rate. As the nitrogen level in the cylinder decreases the pressure also diminishes. This problem can be reduced by utilizing a double stage regulator for accurate delivery at low pressures. Although not easily characterized, humidity seems to affect short term reproducibility with better precision on slightly humid days.

As long as the above conditions are maintained long term drift is minimized.

However, pulse-to-pulse variability was greater than the reported ∓5%. Even when carefully monitoring and correcting the laser high voltage, air pressure, and N_2 flow, pulse-to-pulse reproducibility of ∓ 10% is difficult to attain. If these parameters are not maintained at constant levels pulse-to-pulse variability is only slightly affected, but long term stability can deteriorate drastically, even reaching the point where the nitrogen laser will fail to fire.

Dye Laser and Dyes

There are two main factors to consider when discussing the dye laser: wavelength calibration and long term drift. Long term drift is primarily due to the photodegradation of the laser dyes leading to an intensity loss, but also includes dye solvent evaporation and alterations in the dye cell position.

Dye laser calibration was performed using a series of laser dyes combined with a sequence of interference filters. There are dozens of dyes suitable for use with the nitrogen pump source allowing for nearly continuous wavelength tuning from 357 to 890 nm. However, other instrument components can place practical limitations on the useful dye laser tuning range. The use of glass fiber optic beam splitters sets the lower wavelength at approximately 400 nm while the upper limit is set by the wavelength range detected by the photomultiplier tube. For the 1P21 PMT the cut off is at 650 nm. Five dyes emitting from 400 to 650 nm were chosen for the calibration study.

The laser dye emission maxima and bands for the five laser dyes were measured on the SLM fluorimeter. The spectra were obtained with the excitation wavelength set to 340 nm and were normalized with the sensitivity controls to produce spectra of approximately the same intensity, Figure 2.8. Laser dye micrometer

Figure 2.8: Emission Spectra of Selected Laser Dyes

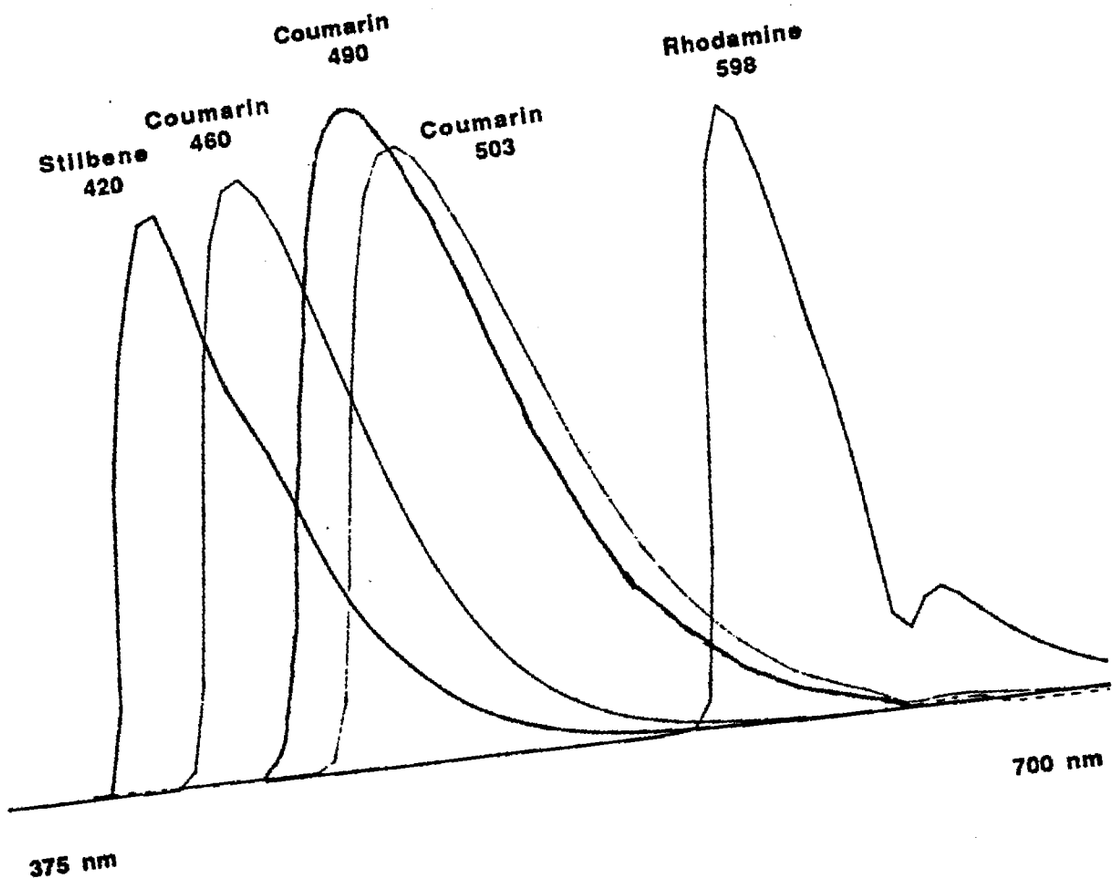

readings for the lasing ranges were then recorded for each dye. The outer limits were established when the lasing signal, monitored on an oscilloscope, is 5% above the broad band laser dye background.

The micrometer readings were then correlated with a series of interference filters, 10 nm band width at half height, to establish a dye laser micrometer calibration. Micrometer settings corresponding to the maxima and half height signal levels were then recorded, Table 2.1. Analysis of the data indicates that over the 400 to 650 nm range of interest the calibration is linear and the best correlation between wavelength and the micrometer is 1 nm per 0.0035 ∓ 0.0003 micrometer units. A more exact calibration could have been obtained using 1.0 nm wide interference filters.

Setting the dye laser micrometer for a chosen wavelength can be performed by extrapolating the reading from Figure 2.9 or by using the above correction factor. When using the correction factor 500 nm, corresponding to 1.433 micrometer units, acts as a convenient reference point. The micrometer setting for 525 nm light can be calculated using Equation 2.1.

Equation 2.1

(Desired λ - Ref. λ)(Cal. Factor) + Ref. Setting= Micrometer Setting

Reference Wavelength	**500 nm**
Reference Micrometer Setting	**1.433 units**
Calibration Factor	**0.0035 units/nm**

Sample Calculation:

(525 nm - 500 nm)(0.0035 units/nm)
+ 1.433 units = a micrometer setting of 1.520 units

It is interesting, though not surprising, that the experimental tuning curves for the individual laser dyes were not as broad as presented in the manufacture's literature [84]. Calculations based on Equation 1 indicate that the tuning curve for

Table 2.1. DYE LASER MICROMETER SETTINGS CORRESPONDING TO SPECIFIC INTERFERENCE FILTERS.

LASER DYE FILTER	LITERATURE VAUES MAX	RANGE	MICROMETER UNITS MAX	RANGE
Stilbene 420 Dye	425	408-453		
420 Filter			1.133	1.125-1.147
Coumarin 460 Dye	464	434-500		
450 Filter			1.250	1.241-1.262
460 Filter			1.279	1.264-1.289
480 Filter			1.333	1.305-1.342
Coumarin 490 Dye	490	465-530		
480 Filter			1.365	1.350-1.382
500 Filter			1.430	1.418-1.467
Coumarin 503 Dye	500	472-555		
500 Filter			1.435	1.420-1.456
Rhodamine 590 Dye	585	571-616		
598 Filter			~1.715	

Interference Filters - 10 nm at half height

Figure 2.9. CORRELATION OF DYE LASER WAVELENGHT EMISSION TO MICROMETER READING

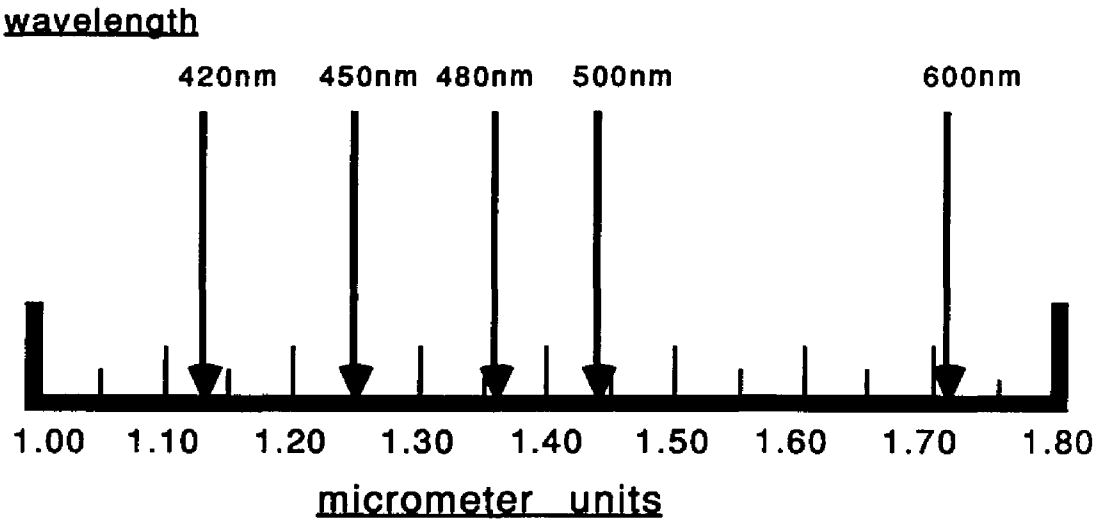

stilbene 420 is 411 to 428 nm, much smaller than the cited range of 408 to 453 nm. Similarly, the experimental coumarin 490 range from 482 to 538 nm is smaller than the literature range of 477 to 555 nm.

It is critical to note that the micrometer/wavelength calibration is dependent on the alignment of the mirrors and grating in the dye laser cavity. Therefore, once the alignment necessary for lasing is reached, it is important not to readjust any of the set screws.

The second dye laser characteristic which needs to be evaluated is the variability in emitted laser intensity. Of primary importance is long term intensity drift which is mainly due to photobleaching of the laser dye. Of secondary importance are alterations in the dye cell position and concentration changes due to dye solvent evaporation.

Increases in dye concentration due to evaporation of the solvent, usually ethanol or methanol, can affect the intensity, wavelength maximum and range of the laser light. With the best fitting dye cell cap currently used, ethanol evaporation is limited to 0.4 ml per 10 hours at room temperature (68°C). This is 10% of the total cell volume. Variations in temperature, cap positioning, and dye solvent can lead to greater or lesser concentration changes.

Long term drift of the dye laser intensity can result from slight alterations in the position of the dye cell due to vibrations. The cell seat is poorly designed in that the cavity is shallow, the supporting material is pliable and not aligned well. Maintenance of cell position is critical when performing a series of related experiments since variations can affect the signal-to-background ratio.

The change in signal-to-background is due to the constant broad band fluorescence of the laser dye. This background fluorescence is detected along with the monochromatic laser light. When the cell is adjusted for maximum lasing efficiency the laser light signal is much larger than the broad band background. Once maxi-

mum efficiency is obtained, any movement of the cell results in a decrease in the signal to background ratio. When the cell was intentionally moved, while being careful to maintain lasing, a 14% difference in the signal to reference ratio was noted. This makes it impractical to replace a photobleached dye during an experiment.

The need to replace the dye solution depends on the individual dye and is determined by the number of dye source pulses. After 100,000 laser pulses coumarin 490 lost approximately 40% of its light conversion efficiency. This was determined by firing the nitrogen laser, measuring the dye laser intensity with the PMT, and monitoring the signal on the oscilloscope. Nitrogen laser drift, during this experiment, is minimized by closely regulating the N_2 at 4 psi, with a low flow rate, and maintaining air pressure at 14 psi. A constant nitrogen laser high voltage is maintained and the work was performed at night, when other instruments where not in use, to minimize line current fluctuations.

Data in Table 2.2 show that after 6 hours of continuous firing at 5 pulses per second, or just over 100,000 shots, a 40% reduction in the dye laser intensity results. The inability to change the dye solution during an experiment would be particularly restrictive if working at a 20 pps repetition rate, since at this rate the 40% reduction would be reached in less than an hour and a half. However, data acquisition constraints of the computer interface card limit the repetition rate to about 1 pps, meaning that 6 hours of use, 21600 shots, would result in a dye laser intensity loss between 5 and 10%.

Fiber Optic Beam Splitters

In place of conventional optics, i.e. mirrors, beam splitters, and lenses, the excitation and emission light is transported through fiber optic cables and divided using fiber optic beam splitters (FOBS). Optical waveguide theory has previously

Table 2.2: PHOTOBLEACHING OF COUMARIN 490 LASER DYE.

TIME	VOLTAGE*	NUMBER OF SHOTS	% INTENSITY LOSS
0	2.0 v	-	-
10 min	2.0	3000	0%
30	1.9	9000	5%
60	1.9	18000	5%
90	1.8	27000	10%
120	1.6	36000	20%
180	1.5	54000	25%
240	1.4	72000	30%
300	1.3	90000	35%
360	1.2	108000	40%

Dye Laser Micrometer Setting = 1.450 (500 nm)
Coumarin 490 dye concentration = 5 micromolar
*Voltage readings are background corrected (0.2 v).

been discussed including the characteristics of different fiber materials. This section will therefore be limited to the evaluation of three different fiber optic beam splitters, as well as of fused silica fiber, with regard to light throughput, splitting ratios, and backscatter.

The function of the FOBS is to efficiently transfer excitation light to the sample chamber and then deliver the emission light to the detector. Because light is split twice during this process it is desirable to know the splitting ratio of each port of the FOBS. The splitting ratio of three fiber optic beam splitters was determined over a broad region of the visible spectrum and their relative throughput compared.

Pulse-to-pulse laser intensity variations were too large for the accurate single channel measurements necessary to determine the FOBS splitting ratio. Therefore, the xenon arc lamp of the SLM spectrofluorimeter was used as a stable reproducible light source. Fiber ends of the FOBS were terminated with SMA connectors and successively polished with 32, 15, 3, and 0.3 micron grit polishing paper.

Splitting ratios were calculated by connecting the input port of the FOBS, port 1, to a specially adapted fitting at the excitation monochromator exit slit. The exit ports, 2 and 4, (2 and 3 with the 3 Port ADC FOBS) were alternately connected to an RCA 1P21 PMT, and the signal intensity was measured on an oscilloscope, Figure 2.10. The unmonitored end was covered with black cloth. The incident wavelength was set using the SLM monochromator. Splitting ratios were taken at 50 nm intervals from 400 to 700 nm.

The fiber optic beam splitters evaluated include: a 4 port Aster, a 4 port ADC, and a 3 port ADC. In each experiment the maximum signal is generated and measured by rotating the SMA connector in the PMT bulkhead mount.

The splitting ratios for the two ADC fiber optic beam splitters were calculated and listed in Table 2.3. The splitting ratio for the Aster FOBS was 55/45, at 500 nm. However, because the total throughput was over two orders of magnitude

Figure 2.10: FOBS Splitting Ratio Configuration

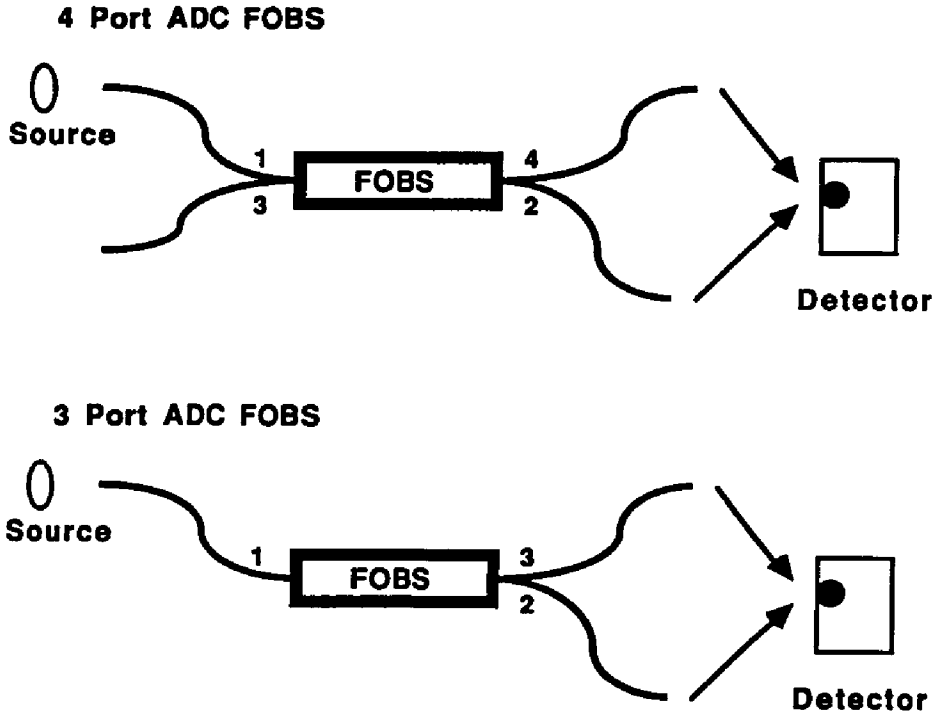

Table 2.3: SPLITTING RATIOS FOR TWO ADC FIBER OPTIC BEAM SPLITTERS.

WAVELENGTH (nm)	3 PORT ADC FOBS Port 3/Port 2 (%/ %)	4 PORT ADC FOBS Port 4/Port 2 (%/%)
400	67/33	61/39
450	64/36	64/36
500	59/41	63/37
550	62/38	61/39
600	59/41	60/40
650	62/38	61/39
700	64/36	60/40

Input Port is Port #1. Refer to Figure 2.4.

less than for the ADC FOBSs, the Aster FOBS was not evaluated further.

None of the couplers displayed the 50/50 ratio specified in manufactures literature. But, the uneven splitting can be used to advantage when configuring the FOBS. The port with the larger percentage of light is used to excite the sample while the less efficient port supplies the signal for triggering the boxcars or provides a reference intensity.

Choosing the port with the higher throughput increases excitation intensity but also leads to more stray light due to backscatter. To minimize stray light it is important to reduce the differences in the refractive index of the fiber core and the medium to which the fiber end is exposed. Because glass, the core material of the ADC FOBS, has an index of refraction (n) of about 1.5, the unused fiber end should be placed in an index of refraction matching gel with n close to 1.5.

Stray light was measured using both the SLM's xenon lamp and the nitrogen dye laser as excitation sources connected to Port 1 of the 4 port ADC coupler. The ends of ports 2 and 4 are where most light is reflected. Port 3 was used to monitor the stray light. The port 3 fiber is terminated with an SMA connector and mated to a housing containing an RCA 1P21 PMT. An oscilloscope was used to measure the relative stray light signals for Port 2 and 4 fibers immersed in air, water, and index of refraction matching gel.

Using 520 nm light, immersion of both the 2 and 4 Port fiber ends in distilled H_2O reduced backscatter by 50% compared to a measurement with both fibers in air. The index of refraction matching gel caused stray light to be reduced by more than an order of magnitude. The data are presented in Table 2.4.

Because the laser source is more intense than the xenon lamp, higher stray light intensities would be expected. However, the laser is also more monochromatic, so that when combined with an interference filter, the overall intensity of stray light was similar to that observed for the xenon source. The effects

Table 2.4: STRAY LIGHT REDUCTION USING INDEX OF REFRACTION MATCHING GEL.

PORT 2	PORT 4	VOLTAGE	% REDUCTION
Air	Air	7.5 v	N.A
Air	Gel*	1.0 v	87%
Gel	Gel	0.4 v	94%

*Index of refraction matching gel.
Rhodamine 590 sample, excited by 525 nm light (Xenon Lamp), and emission wavelength selection with a 580 nm bandpass filter.

Table 2.5: STRAY LIGHT FROM DIFFERENT FIBER ENVIRONMENTS.

PORT 2	PORT 4	VOLTAGE	% REDUCTION
Air	Air	1.51 v	N.A.
Gel	MeOH	0.80	47 %
Gel	Water	0.75	50 %
Gel	Gel	0.55	64 %

Same conditions as in Table 2.4 except a Laser source (525 nm) is used and neutral density filters were used to prevent saturation of PMT

of different index of refraction media on stray light with a laser source, are shown in Table 2.5. The importance of using the index of refraction matching gel at any fiber end is clear. For similar reasons the gel should be used at fiber-to-fiber connections.

Because single fibers, as well as other fiber optic beam splitters, were routinely connected to each other, the throughput loss due to these connections was evaluated. While SMA splice bushings hold two SMA terminated fiber ends very close together, transfer of light between fibers is not perfect. Dispersion of light, reflection, surface roughness, imperfect SMA connectors, and other mechanical problems can reduce fiber to fiber transfer of light by 85% or more.

Throughput experiments were performed with and without gel for both the 3 and 4 Port ADC couplers, fused silica fibers, and different combinations of these fibers. Steady state light at 525 nm was provided by the SLM's xenon lamp, stray light was collected by a RCA 1P28 PMT, and throughput was measured on the oscilloscope. The fiber in the SMA bulkhead mount on the PMT housing was rotated to get maximum intensity. This was necessary because fiber ends may not be flush with the SMA connector surface and emitted light may not directly impinge on the PMT collection window.

All fiber-to-fiber connections were made with the same SMA splice bushing with both SMA terminated fiber ends fully tightened in the bushing. It was noted that, unlike fiber orientation relative to the PMT, which could cause signal variations of 50%, fiber-to-fiber orientation differences produced no more than a 3 % fluctuations in signal in the absence of index of refraction matching gel.

Table 2.6 summarizes the light throughput characteristics of the couplers alone and with different fiber-to-fiber connections. All the voltages in Table 2.6 were measured without the use of index of refraction matching gel. Voltage measurements 1 to 4 were made by connecting port 1 of each FOBS to the SLM and measuring the light exiting the coupler from both output ports with a PMT.

Table 2.6: LIGHT THROUGHPUT MEASUREMENTS OF FIBER OPTIC BEAM SPLITTERS

#	Throughput Measurements with no Connections	Output measured at Port X	RELATIVE VOLTAGE
1	4 Port ADC FOBS	Port 2	11.0 v
2		Port 4	14.0
3	3 Port ADC FOBS	Port 2	16.0
4		Port 3	22.0
5	Fused Silica Fiber		2.0

{Refer to Figure 2.10 for Optical Configuration}

	Fiber to Fiber Connections			
	3 Port FOBS or Fiber	attached to	Arm X of 4 Port ADC FOBS	RELATIVE VOLTAGE
6	Port 2 of 3 Port ADC		Arm 2 of 4 Port ADC	3.0
7	Port 3 of 3 Port ADC		Arm 2 of 4 Port ADC	3.7
8	Port 2 of 3 Port ADC		Arm 4 of 4 Port ADC	1.8
9	Port 3 of 3 Port ADC		Arm 4 of 4 Port ADC	2.0
10	Single Fiber		Arm 2 of 4 Port ADC	0.50
11	Single Fiber		Arm 4 of 4 Port ADC	0.25

{Refer to Figure 2.11 for Optical Configuration}

Measurement number 5 is the direct throughput of the fused silica fiber terminated at both ends with SMA connectors. Even though the fused silica fiber has a larger numerical aperture than the glass fibers of the ADC FOBS, the throughput of the fused silica fiber is more than an order of magnitude less than the total light throughput of the FOBS measurements.

Signals 6 to 11 measure the light throughput when either an additional length of fused silica fiber or the 3 Port ADC fiber optic beam splitter was connected to the 4 Port ADC FOBS. Voltage measurements numbers 6 and 7 were made by connecting port 1 of the 3 Port ADC FOBS to exit port 2 of the 4 Port ADC FOBS, and then sequentially monitoring the outputs of ports 2 and 3, Figure 2.11. Voltages 8 and 9 were measured after switching port 1 of the 3 Port FOBS to exit port 4 of the 4 Port FOBS. The final two voltages are throughput measurements when a single fused silica fiber was connected to the exit ports of the 4 Port FOBS.

It is apparent from the data in Table 2.6, that a significant amount of light loss occurs at fiber to fiber connections. In addition, analysis of the light throughput data presents some interesting observations. Even though port 4 of the 4 Port ADC FOBS emitted more light than arm 2, 56% versus 44%, respectively, the relative intensity ratio was reversed when additional fiber was connected to the two 4 Port ADC exit ports. Measuring the light from a single fiber, sequentially connected to the two exit ports, shows that the throughput was greatest when connected to port 2. The splitting ratio is now 65:35 for ports 2:4. Approximately the same ratios were measured with the addition of the 3 Port ADC FOBS.

The relative splitting ratio is inverted because higher order modes of light are more efficiently coupled from one fiber to the other in the FOBS. High order modes enter the input fiber at a greater angle from the normal, travel down the fiber with a shorter period, and exit the fiber at a sharper angle, Figure 2.12. At fiber-to-fiber connections, the lower order modes are transferred more efficiently to

Figure 2.11: FOBS Configuration for Light Throughput Measurements

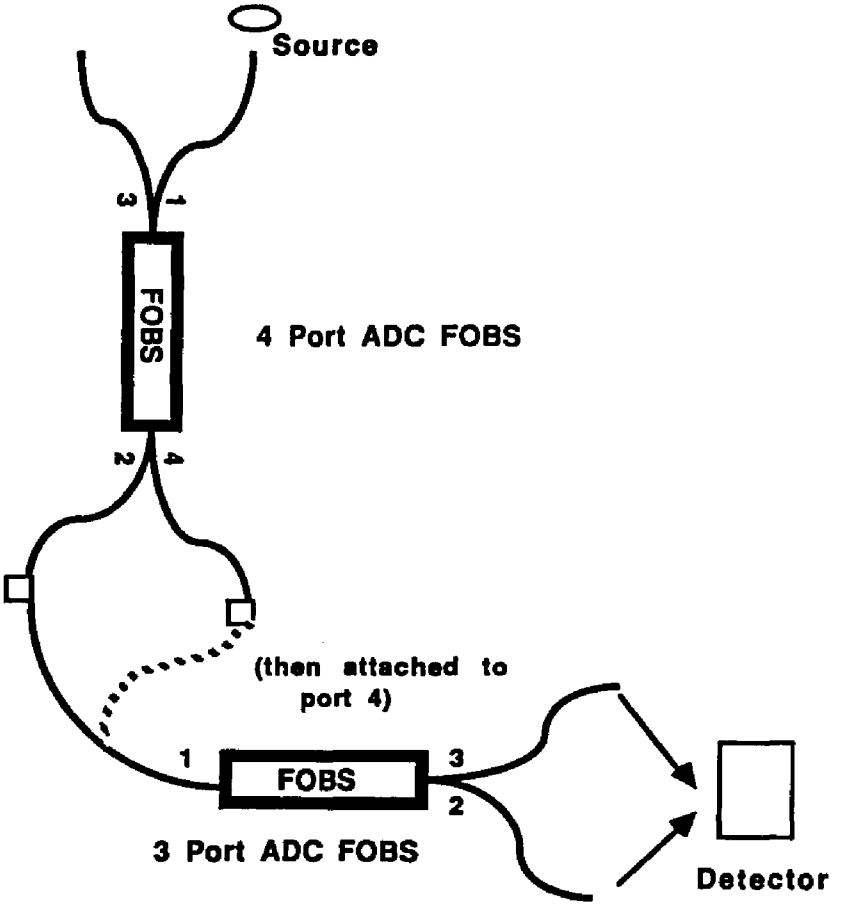

Table 2.6: LIGHT THROUGHPUT MEASUREMENTS OF FIBER OPTIC BEAM SPLITTERS

#	Throughput Measurements with no Connections		RELATIVE VOLTAGE
		Output measured at Port X	
1	4 Port ADC FOBS	Port 2	11.0 v
2		Port 4	14.0
3	3 Port ADC FOBS	Port 2	16.0
4		Port 3	22.0
5	Fused Silica Fiber		2.0

{Refer to Figure 2.10 for Optical Configuration}

	Fiber to Fiber Connections			
	3 Port FOBS or Fiber	attached to	Arm X of 4 Port ADC FOBS	RELATIVE VOLTAGE
6	Port 2 of 3 Port ADC		Arm 2 of 4 Port ADC	3.0
7	Port 3 of 3 Port ADC		Arm 2 of 4 Port ADC	3.7
8	Port 2 of 3 Port ADC		Arm 4 of 4 Port ADC	1.8
9	Port 3 of 3 Port ADC		Arm 4 of 4 Port ADC	2.0
10	Single Fiber		Arm 2 of 4 Port ADC	0.50
11	Single Fiber		Arm 4 of 4 Port ADC	0.25

{Refer to Figure 2.11 for Optical Configuration}

Figure 2.12: High and Low Order Modes In the same Optical Fiber

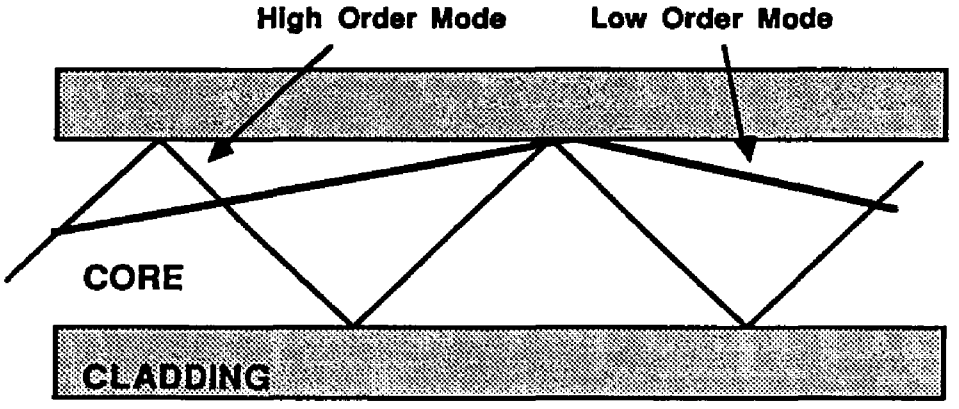

Figure 2.13: Fiber Coupling

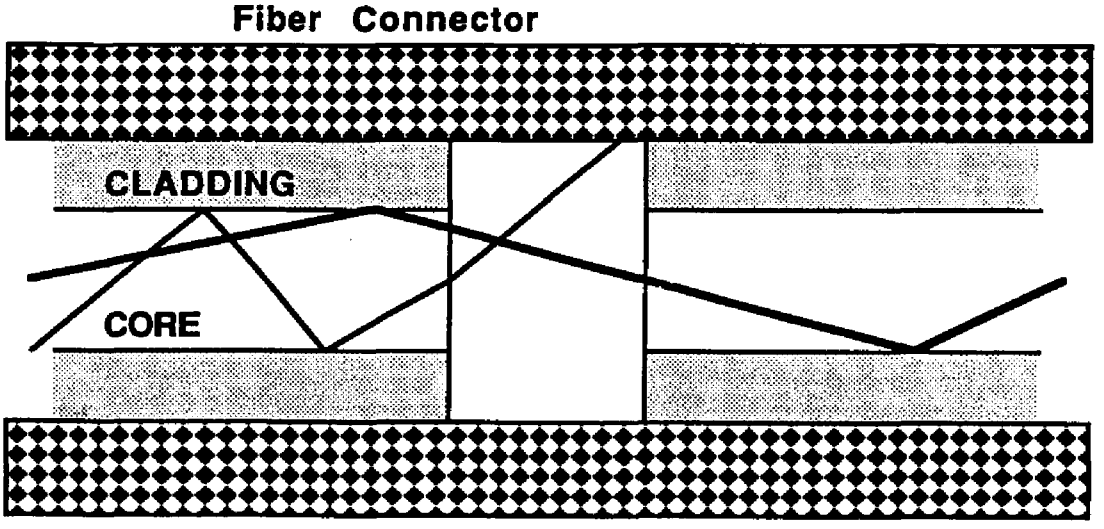

the second fiber since they exit the first fiber at a smaller angle. High order modes exit the first fiber at a greater angle which reduces the collection efficiency of the second fiber, Figure 2.13.

Table 2.7 presents data comparing optical throughput at connections with and without refractive index matching gel. The voltage measurements were made in the same fashion as for the data for Table 2.6. Light throughput was measured at the exit ports, 2 and 3, of the 3 Port FOBS. Refer to Figure 2.11.

The data confirm the importance of the gel. In addition to enhancing light throughput the gel restores the splitting ratio closer to the 4 Port ADC coupler's splitting ratio when no additional fibers are connected. The gel acts as a light pipe between the two fibers so that the high order modes are now coupled into the second fiber instead of being dispersed. In addition the gel minimizes the effect of physical imperfections in the fiber ends in the SMA connectors. Problems such as fiber ends not flush with the SMA connector end, fibers not seated well in the SMA holder and misdirected, slightly off center connections, or imperfect fiber surfaces are reduced by the use of gel, thus improving total optical throughput. This is particularly evident when the 3 Port FOBS is connected to arm 4 of the 4 Port coupler, Table 2.7.

In view of the advantages of placing gel at fiber interfaces, the possibility of placing index of refraction matching gel at the end of the sample fiber was investigated. It was hoped that gel at the fiber tip would reduce the amount of reflected excitation radiation without affecting the fluorescence intensity.

The experiment was performed using 530 nm laser light entering port 1 of the 4 Port ADC FOBS to excite 1.0×10^{-7} M Rhodamine 6G, in a pH 7.2 phosphate buffer, through port 4. The signal was detected at port 3 with a PMT fitted with a 580 nm interference filter (10 nm at 1/2 height).

First, a small dab of gel was placed on the end of the sample fiber which was

Table 2.7: THOUGHPUT MEASURMENTS OF FIBER TO FIBER CONNECTIONS WITH AND WITH OUT INDEX MATCHING GEL

	VOLTAGE		
	NO GEL	GEL	INCREASE
Arm 2 of 3 Port ADC connected to Arm 2 of 4 Port ADC	2.7	3.0	11%
Arm 3 of 3 Port ADC connected to Arm 2 of 4 Port ADC	3.2	3.7	16%
Arm 2 of 3 Port ADC connected to Arm 4 of 4 Port ADC	1.0	3.0	200%
Arm 3 of 3 Port ADC connected to Arm 4 of 4 Port ADC	1.0	3.5	250%

Refer to Figure 2.11 for optical configuration.

then inserted in a solution with no rhodamine. The results indicated that the refractive index matching gel on the sample fiber end reduced stray light.

However, the effect of the gel on the excitation and collection of rhodamine fluorescence intensity was less easy to quantify. Immersing the gel clad fiber into a rhodamine solution created a signal-to-background ratio which varied from zero to 22%. In addition, the gel slowly dissolved in the water/buffer solution creating problems with long term stability and drift. Therefore, placement of gel at the end of the sample fiber was not deemed practical.

The splitting ratio data, as well as the light throughput information, were used to help configure the fiber optic beam splitters to couple excitation light most efficiently from the source to the sample and from the sample to the detector. Specific configurations are discussed below. In all cases the use of index of refraction matching gel in all fiber connections is vital to reduce backscatter and increase throughput.

Three optical designs were investigated utilizing both the 3 and 4 Port ADC couplers. The first configuration in Figure 2.14, requires only the 4 port FOBS and is thus less expensive and involves fewer light divisions. Since the light is split less often a higher degree of overall light throughput is attained. Also, this design requires the reference PMT to play the dual role of referencing the light source and acting as the boxcar trigger. This has the advantage of requiring less space, power, and is less expensive since only one PMT is used. However, the intense laser light is channeled directly to the reference PMT and saturates the dynode chain. PMT overload was evidenced by two observations. The first was that the reference channel showed only a 1% pulse to pulse variation compared to a 12% variation for the sample channel, for the same laser pulses. Also, when scanning the laser decay curve by adjusting the % delay knob, the decay time for the reference PMT was longer than the decay from the sample PMT. The simplest method to reduce the

Figure 2.14: OPTICAL ARRANGEMENTS OF FIBER OPTIC BEAM SPLITTERS

Configuration #1

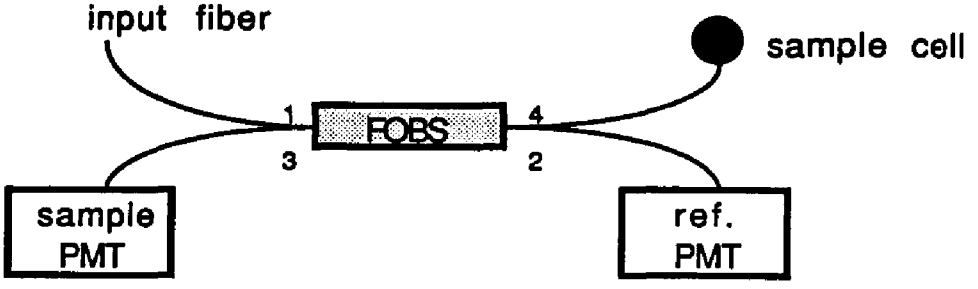

Configuration #2

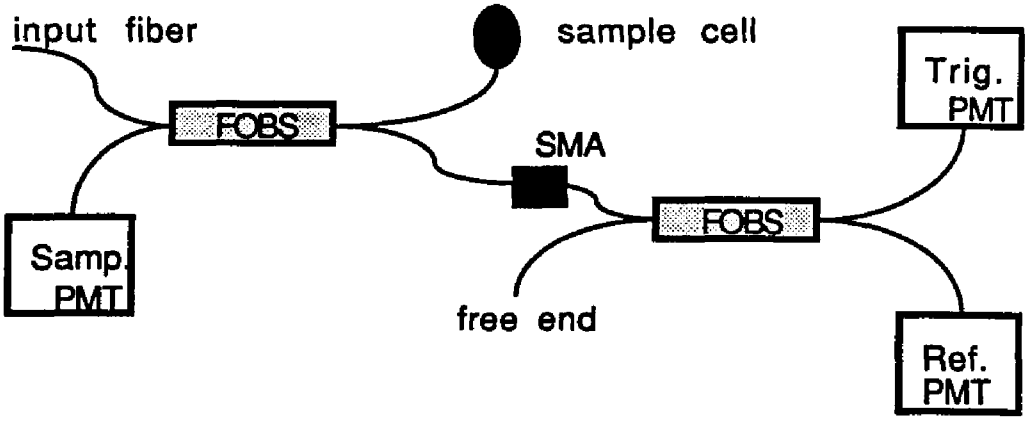

Configuration #3

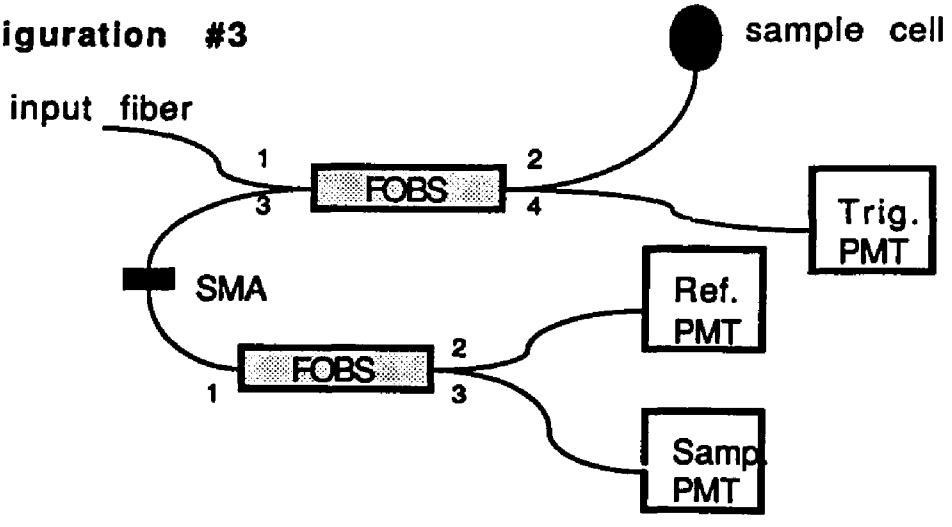

signal at the reference PMT was to use a neutral density filter. Unfortunately this was not practical since lowering the light level also restricted efficient triggering of the boxcars.

To overcome the saturation effect two fiber optic beam splitters were configured to allow independent control of intensities, at the reference and trigger photomultiplier tubes, Figure 2.14, Configuration 2. This design also has the advantage of high transmission since emission is only split once on its way from the sample cell to the detector. One further advantage is that by replacing the 4 Port ADC coupler with the Aster FOBS, which is fabricated from fused silica fiber, UV light can be used to excite the fluorescent sample. A neutral density filter was used to reduce the light to the reference PMT without influencing the light impinging on the trigger PMT. The limitation of this design is that only one sample emission wavelength can be monitored.

The final optical design again utilized both the 3 and the 4 Port ADC fiber optic beam splitters. However, the 3 Port coupler was connected to port 3 of the 4 Port FOBS, on the opposite side from the sample arm, Figure 2.14, Configuration 3. With this configuration not only are the trigger and reference PMTs independently controlled, but also the reference channel can be replaced with a second sample detector. The second sample photomultiplier housing would also be fitted with a suitable interference filter, to enable a second fluorophor, in the analyte solution, to be monitored. This design is useful in optical sensors based on donor-acceptor fluorescence energy transfer.

Replacing the 4 Port ADC with the Aster FOBS permits UV excitation. The emitted light needs to be in the visible region so that it can be transferred via the glass fibers of the 3 Port ADC FOBS. The main drawback of this design is that the sample emission is split twice, reducing the intensity of light reaching the sample PMT. However, the experiments indicated that sufficient sample emission was

transferred to the PMT so FOBS configuration 3 was used in subsequent work.

Filter Selection

The limit of detection for low sample emission intensity is established by stray light from scattered and reflected dye laser excitation radiation. Stray light levels are significantly reduced by the application of index of refraction matching gel to fiber interfaces. However, since the fiber end in the sample solution is not terminated with gel, and an exact match between the fiber core and the index gel is not possible, there will always be stray light superimposed on emission from the sample. Therefore, any further increase in the signal-to-background ratio can only be attained by isolating the stray laser excitation light from the longer wavelength sample emission. This can be accomplished either with a monochromator or with filters. Since, one of the goals of the instrument presented was to maximize utility at minimum cost, it was decided that filters would best fulfill the need.

The affect of fluorophor concentration on the signal-to-backscatter ratio and wavelength characteristics were determined with a series of Rhodamine 6G (Rh 6G) standard solutions (Exciton Corp., Rhodamine 590). First, excitation and emission wavelength maxima for Rh 6G in an aqueous pH 7.2 phosphate buffer were found to be 518 and 550 nm, respectively, on the SLM fluorimeter. These wavelengths were then used to establish the dye laser excitation wavelength and filter selection. When excited with the dye laser, rhodamine emission was detected with an RCA 1P21 PMT coupled to an oscilloscope as the readout device. A 580 nm interference filter was inserted between the fiber output end and the PMT to screen out stray dye laser excitation light.

Maximum rhodamine emission intensity was observed with the dye laser micrometer set to 1.495 units, corresponding to approximately 520 nm. Figure 2.15

Figure 2.15: Rhodamine Fluorescence Correlated To Dye Laser Wavelength

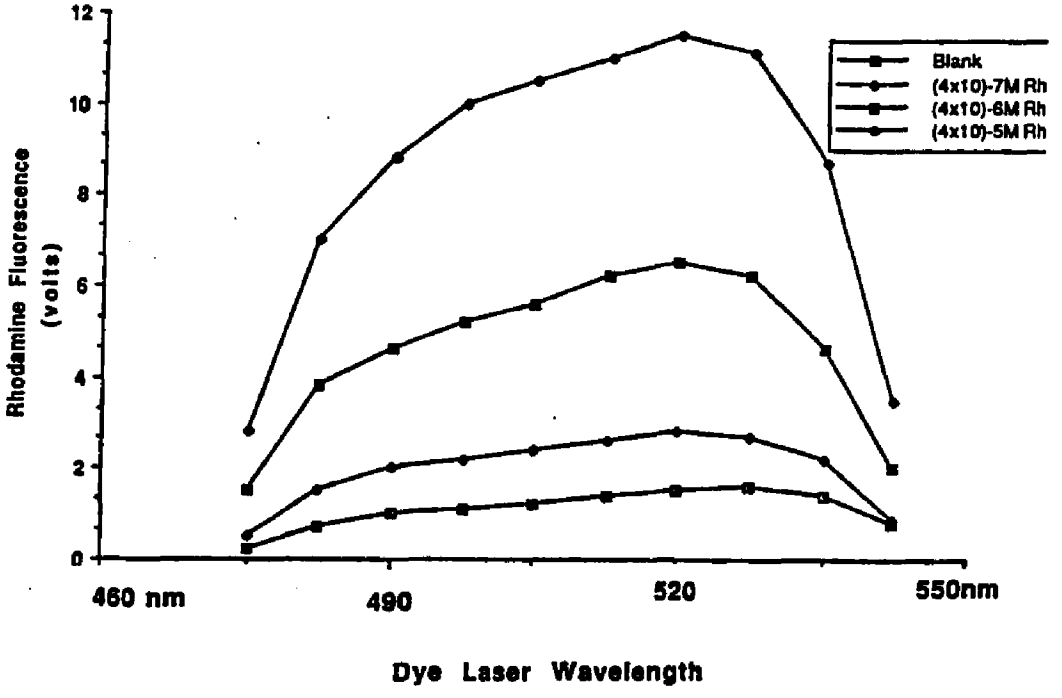

shows emission intensity as a function of wavelength for a blank and three different rhodamine concentrations. The large signal from the blank solution shows that the 580 nm interference filter does not eliminate all stray light. PMT dark current, under the conditions of Figure 2.15, was 3 to 5 mv and does not contribute significantly to the background. To improve the signal-to-background ratio a number of interference and longpass filters were evaluated. However, the stray light due to broad band laser dye fluorescence which matches the filter(s) band width can not be eliminated.

A series of experiments were performed using FOBS Configuration 1, Figure 2.14. 516 nm (1.490 units) dye laser radiation was used to excite the rhodamine 6G sample. The sample PMT was powered with 800 volts and the oscilloscope was employed to monitor the rhodamine signal. The free fiber end was terminated with index of refraction matching gel. Voltage readings were sequentially recorded for rhodamine-free blank solutions and for a 1.0×10^{-7} M Rhodamine 6G standard. Filters and data are summarized in Table 2.8.

Analysis of the data offers no surprises. Light throughputs for the longpass filters are greater than for the interference filters. When longpass and interference filters are combined, stray light throughput decreases further, improving the signal to background. The best signal to background enhancement was achieved by combining the 554 nm long pass and the 560 nm interference filters.

Load Resistance

In principle, stray light can be resolved from longer lived fluorescence. However, because the fluorescence lifetimes are on the nanosecond time scale, this requires low load resistors in the PMT circuit so that the observed response is not dominated by the time constant of the detection system. To simplify the measure-

Table 2.8: STRAY LIGHT REJECTION WITH DIFFERENT LONGPASS AND INTERFERENCE FILTERS

Long Pass Filters (LP)

Wavelength	Blank	1×10^{-7} M Rh	Signal/Background
554 nm	1.7 v	2.7 v	1.6
550 nm	2.0 v	2.8 v	1.4
583 nm	1.4 v	2.0 v	1.4

Interference Filters (IF)

(10 nm at 1/2 peak height)

Wavelength	Blank	1×10^{-7} M Rh	Signal/Background
560 nm	0.58 v	1.21 v	2.1
580 nm	0.42 v	0.94 v	2.2
598 nm	0.15 v	0.40 v	2.7

Combination of Longpass and Interference Filters

Wavelength IF + LP	Blank	1×10^{-7} M Rh	Signal/Background
550 + 554	0.40 v	1.10 v	2.8
560 + 554	0.40 v	1.10 v	2.8
580 + 554	0.38 v	1.00 v	2.6
598 + 554	0.19 v	0.50 v	2.6

ment, larger load resistors can be used to extend the signal lifetime. Both pulse decay time and signal intensity are established by the time constant of the system. Table 2.9 presents different decay times and signal intensities for a series of load resistors. Knowledge of the decay times and signal trade off is helpful when selecting the experimental boxcar timing functions.

Table 2.9: Decay Times and Signal Strengths Associated with Different Load Resistors

RESISTOR	DECAY TIME	VOLTAGE OF 1 nAMP CURRENT
1 MΩ	1 msec	1×10^{-3} v
100 KΩ	100 usec	1×10^{-4} v
50 KΩ	50 usec	5×10^{-5} v
10 KΩ	10 usec	1×10^{-5} v
50 Ω	.05 usec	5×10^{-8} v

(Different load resistors are fabricated by soldering the resistor across a 3 way BNC coaxial cable splitter and capping it with a copper shield.)

Boxcar Averagers

Integrator Modules and Timing Functions. The PAR Boxcar averagers integrate low intensity signals which otherwise would be indistinguishable from background noise.

Original boxcar equipment included two PAR 162 mainframe units each with two ports able to hold any two of the available plug in integrators and included two 164, one 165, and one 166 integration modules. An initial survey established that both mainframes functioned properly as did the two 164 and the 166 modules. However, the 165 integrator failed to zero and could not be calibrated and was not used further.

The boxcar components were evaluated utilizing a number of different input devices including square wave generators, a variable voltage source, and a

photomultiplier tube measuring both steady state and pulsed laser dye light sources.

While the function and principle of the 164 and 166 integration module are the same, the 166 is designed for acquisition of faster signals. The internal load resistor, at the input jack of the 166, is 10 kΩ, versus 1 MΩ for the 164 plug in, which produces a 100 fold decrease in the signal decay time, Table 2.9. To monitor the shorter decay times, the 166 has Aperture Durations (AD) down to 2 nsec and a Time Constant (TC) as short as 0.5 usec. In this application, the most significant advantage of the 166 module is that it has its own signal output, separate from the 162 output port. This allows dual outputs to the computer for a two channel measurement. Also, the gain of the 166 module can be adjusted to amplify low intensity signals. The gain was experimentally determined using a reference voltage (Heathkit model EUW-16) with a TC of 1.0 usec and an AD of 50 nsec. The output for a 10 millivolt input signal was measured on the oscilloscope, Table 2.10. The 164 integrators have a single X40 gain .

The 162 mainframe timing functions include the Aperture Duration (AD), Aperture Delay Range (ADR), and % Delay. The aperture window is opened after a time period, set by the ADR and % Delay. That time period is initiated by a trigger pulse greater than ∓ 0.5 volts in amplitude with a duration of no less than 10 ns. The external trigger of the computer can not be used to trigger both the nitrogen laser and the boxcar simultaneously since there is considerable variability in the time between the trigger pulse to the laser and the actual laser pulse. Therefore, the boxcar is triggered by the laser emission signal. The laser pulse is collected by a PMT situated at an exit port of a fiber optic beam splitter, Figure 2.14. A 50 KΩ load resistor at the trigger input on the 162 mainframe insures that the trigger pulse is of sufficient duration.

Although the signal processing unit is supposedly shielded from the trigger signal, a pulse of approximately 20 mv was measured at the signal output with the

Table 2.10: 166 Integrator Gain Associated with Different Sensitivity Settings

SENSITIVITY SETTING	GAIN
50 mv	200x
100 mv	100x
250 mv	40x
500 mv	20x
1.0 v	10x

TC = 1.0 usec, AD = 50 nsec.

oscilloscope, whenever the boxcar was triggered. This 20 mv signal was present even in the absence of an input signal and remained constant with different trigger signal amplitudes. Integration of this signal caused a drift in baseline voltage.

In principle the drift can be controlled with the zero adjust knobs on the integration modules but in practice zeroing the drift was difficult. While triggering, the zero knob was adjusted to zero the output. Drift typically ranged from 3 to 30% of the 10 volt full scale boxcar reading, after 1,800 trigger pulses.

Since drift was due to integration of the trigger signal the boxcar has to be rezeroed every time the Time Constant, Aperture Duration or Aperture Duration Range are changed.

Fortunately, the drift was not complicated by radio frequency noise from the pulsed nitrogen laser. This was verified by triggering the boxcar averagers with a square wave generator and observing the output while the laser was firing.

Careful selection of the timing functions is vital to measure the sample and reference signals accurately and efficiently. Signals were measured using exponential averaging because in this mode the final steady state output voltage is equal to the input signal strength times the boxcar gain. The time to reach the steady state plateau is five times the Observed Time Constant (OTC) where OTC = TC/(AD*rr). Since the experimental design requires a laser pulse Repetition Rate (rr) of 1 pulse per second OTC = TC/AD. According to the boxcar manual, once the steady state level is reached there should only be a $\mp$ 0.7% change in signal intensity. Trigger drift creates a greater variance.

Also, exponential averaging provides control manipulation of the Signal to Noise Improvement Ratio (SNIR), which is equal to $(2TC/AD)^{1/2}$. The SNIR can be increased by choosing a longer TC or a shorter AD at the expense of an increase in the number of data points necessary for a single run. However, since the computer interface card is limited to a few samples per second, achieving a very high

SNIR can be very time consuming. Also, if the number of data points is too large the gain in SNIR is offset by large trigger drift.

Using a 10 mv steady state input signal with three different combinations of TC and AD settings such that the Five OTC level was reached after 10 triggers, Table 2.11, produced an average precision of 1.5 percent (6 data points). By increasing the Five OTC value to 100 pulses (TC = 100 usec, AD = 5 usec, with a rep. rate of 1 pps) the relative precision was reduced to 0.5% (10 data points), matching the theoretical SNIR.

One hundred pulses was taken as a realistic compromise between SNIR and signal acquisition time.

The AD window was positioned relative to the sample emission decay curve with the Aperture Delay Range (ADR) switch and the % Delay dial. When using the 1 MΩ load resistor of the 164 integrator the laser pulse decay time is 1 msec. Using the 1 msec ADR and a 50 % delay positioned the opening of the AD at 0.50 msec after the start of the decay curve. A 10 % delay places the AD opening at 0.10 msec, where the fluorescence signal intensity is much greater, Figure 2.16. Reproducible timing is attained only when the % Delay dial is set to 5 % or greater. Therefore, to measure very early portions of the decay curve, the ADR needs to be shortened.

Precision. In this section different Aperture Durations and Time Constants will be tested to study their influence on boxcar precision. AD and TC studies were performed employing a steady state voltage source of 10 millivolts and the boxcar output was monitored with the oscilloscope. Boxcar triggering was initiated by the Digital to Analog converter of the ADALAB interface card.

Using different AD's, while holding the input voltage at 10 millivolts and setting the TC to 10 msec (ADR = 1.0 msec with a 10% delay, 166 sensitivity = 100

Table 2.11: Time Constant and Aperture Duration Settings to Consitute Five Observed Time Constants

Time Constant	Apeture Duration
100 usec	50 usec
10 usec	5 usec
1 usec	500 n sec

5 x TC/AD = 10 when pulse repetition rate is 1 pulse per second.

Figure 2.16 A and B: RELATIVE INTENSITY FOR 10 AND 50 PERCENT DELAYS WITH 1.0 AND 0.50 mSEC ADR'S

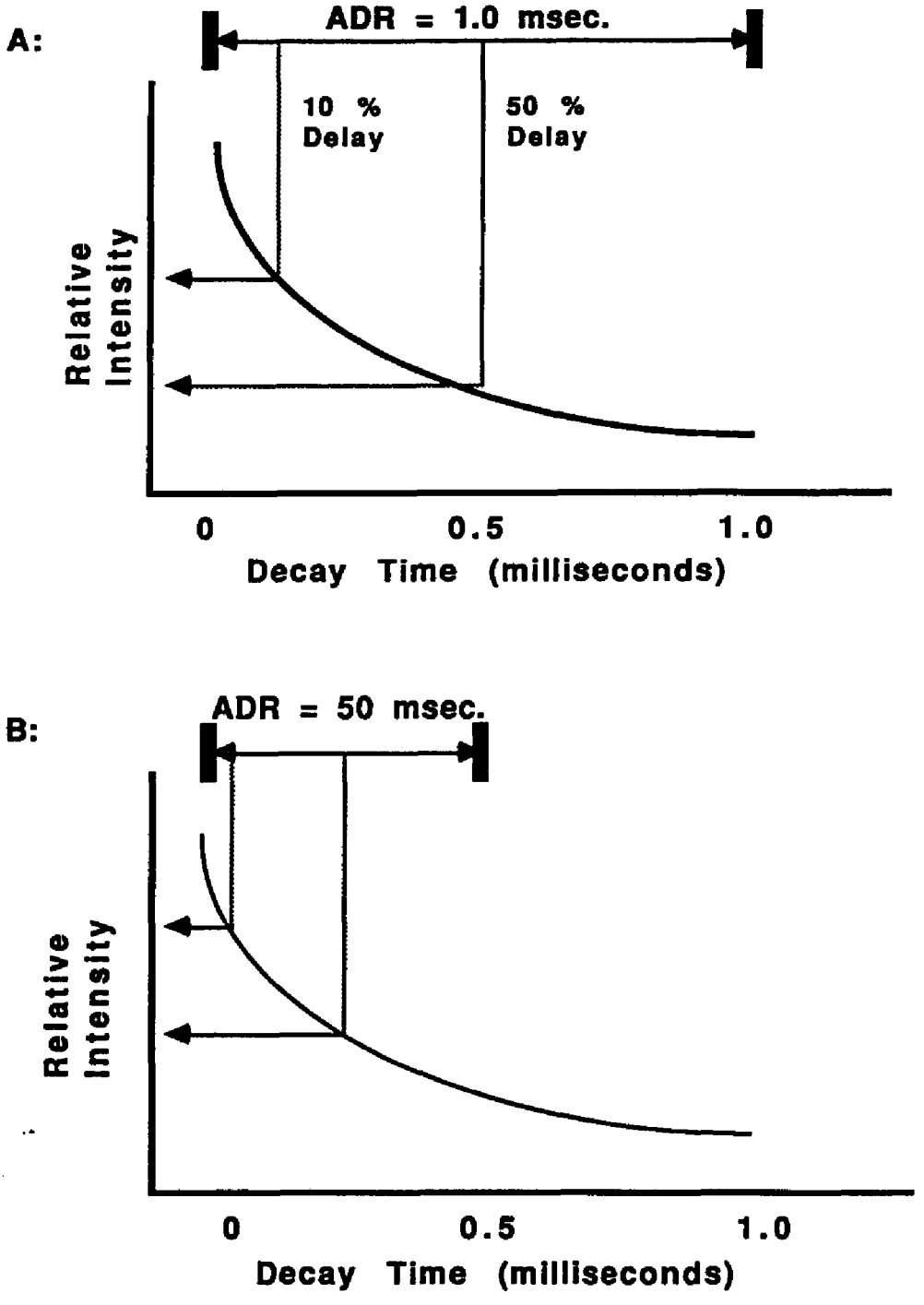

mv), produced signal output values of 0.40∓ 0.01 (six points) and 1.1∓ 0.02 (nine points) volts for the 164 and 166 modules, respectively. Similar values were obtained when holding the AD constant at 50 nsec and changing the Time Constant. Outputs of 0.40 and 1.10 volts were measured for the 164 and 166 units, respectively, each with a precision of about three percent. Rezeroing the trigger drift, after switching AD and TC settings, was required.

Also of importance is how the boxcars handled the input of low intensity signals. The 166 module was used to integrate two different input voltages, with the TC set at 10 usec and a 5 usec AD. The 100 millivolt sensitivity setting on the 166 unit, corresponding to a gain of 100, accurately amplified a relatively strong input of 12 millivolts to 1.2 volts with a 1.2 % precision. In comparison, a signal almost an order of magnitude smaller, 2.2 millivolts, was less accuratly amplified to 0.24 volts with a precision of approximately 10 percent. Three trials were performed for each input level.

Configuration. Initially, 164 and 166 integrators were placed in a single 162 mainframe. However, this proved unsatisfactory because the 166 integrator was subject to severe trigger drift. The second arrangement was to place two 164 integrators in the same mainframe. However, because the 164's do not have independent outputs, this requires that the A/B ratio be obtained directly from the mainframe. This output was found to fluctuate erratically and was attributed to unsynchronized channels. Correction of this function requires an expensive and lengthy factory adjustment.

Since two 162 mainframe units were available, a third boxcar configuration was evaluated with each 164 integrator module in its own 162 mainframe, Figure 2.17. When using separate mainframes, the trigger signal has to be split to simultaneously trigger both units. Also, the initial point for the two 162 mainframes are not

Figure 2.17: BOXCAR INTEGRATOR CONFIGURATION

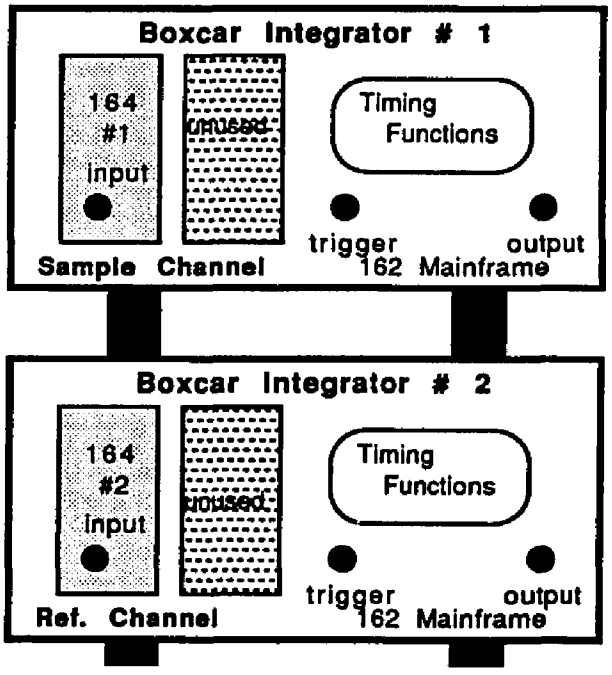

equal. Starting voltages of + 0.5 and - 0.4 volts were established for 162 #1 and 162 #2, respectively, employing the same 164 plug in integrator. These values are reproducible and can be computer corrected.

Adalab-Computer Interface

An ADALAB Interface card and an ADA-MUX Multiplexer interfaced the boxcar integrators to an Apple IIe computer. The multiplexer samples both the reference and sample boxcar channels simultaneously and then sequentially routes the analog voltage signals to the interface card. The interface card, which can only read one signal at a time, is reported to perform the analog to digital (A/D) conversion with a precision of 0.025 % and an overall accuracy of better than 1 percent. Working ranges of $\mp 4.0, \mp 2.0, \mp 1.0$, and ∓ 0.5 volts are selected by moving a jumper switch on the interface card. The ∓ 4.0 voltage option was picked to extend the instrument's working range.

Both precision and accuracy of the interface/computer system were evaluated with a DC voltage source (Micronta Model 22-121) adjustable from 0.0 to +4.0 volts. The analog voltage signal was split between the two ADALAB channels and the digital output was monitored on the Apple IIe. The A/D converter was able to convert voltages up to 3 volts (1600 ADALAB units). Accuracy was 1.0% for low voltage inputs, 0.20 to 0.50 volts, 0.3 percent for a 1.0 volt input, and about 0.1 percent for a 2.0 volt input signal. Theoretically, the ADALAB interface card can convert signals up to 4.0 volts (2047 ADALAB units), but in practice it failed to accurately process signals above 3.0 volts, Figure 2.18. This was observed with two different data collection programs, SENSOR and SENSOR2, Appendices 2 and 3, that have different sampling times which indicates that insufficient time to digitize higher input voltages does not seem to be the problem.

Figure 2.18 ADALAB A/D CONVERSION CHARACTERITICS

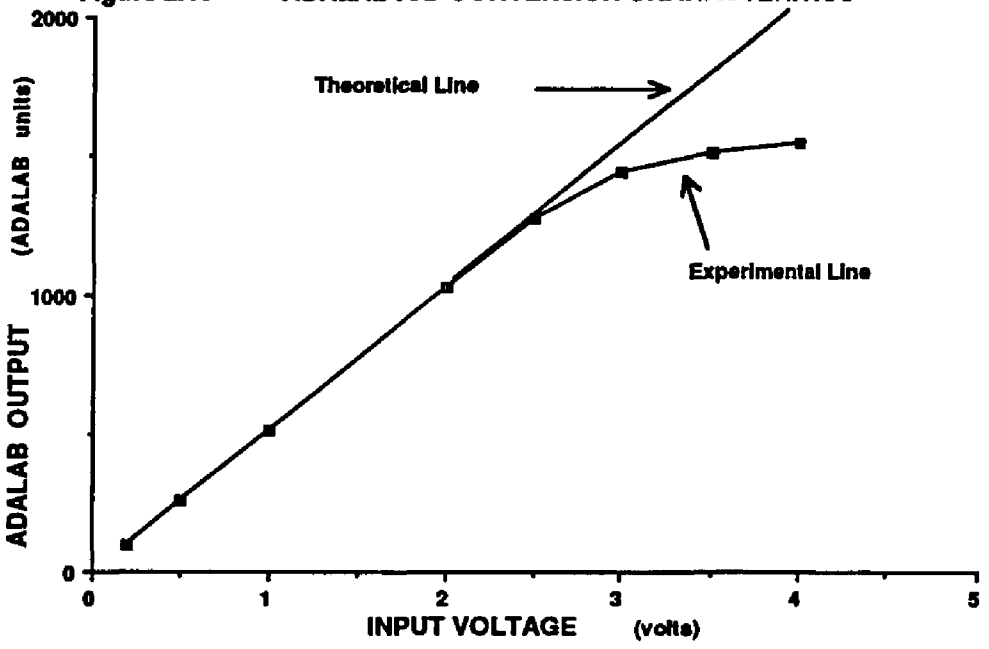

Precision of the A/D converter was experimentally found to be less than 0.1 percent. The A/D converter does not contribute significantly to the overall precision and accuracy of the measurements.

Data Acquisition With The Laser-Fiber Optic Instrument

Before the laser excited spectrometer can be utilized, protocols for data acquisition must be developed. In this section the components are evaluated on how they act in concert and a procedure is developed to correct for source drift.

Pulse-to-pulse variability and drift associated with the N_2/Dye laser, limit the accuracy and precision of data from a one channel measurement. Since fluorescence is proportional to source intensity, the fluorescence intensity must be referenced to the to the source intensity if the source is unstable. This requires a reference channel to monitor source intensity. To reference the source effectively, slope and y-intercept information must be generated for the range over which the source drifts. The slope and y-intercept data is then used in a source correction equation. Source corrections are efficiently performed with programmable calculators, Appendix 4, or directly by the computer. Once the correction parameters are established instrument calibration can be checked daily by generating 4 or 5 data points for different input signals and comparing them to the standard slope. Slope data were developed using both standard voltage sources and signals from the photomultiplier tubes.

A standard voltage source was split, with a three way BNC connector, and fed to the reference and sample integrator modules. Boxcar timing functions were held constant: ADR = 5 msec with a 10 % Delay, TC = 1 usec, and AD = 50 nsec, and the outputs of both channels were monitored on a two channel, 1 MHz, oscilloscope. Input voltages were varied from 0.10 mv to 100 mv and measured with a 1:10 signal reducing probe. Corresponding output signals were recorded, Table 2.12, and plotted, Figure 2.19. Because the 164 integrator units have 40x gain, a 100 mv input produces as output signal of 4.0 volts, which is the theoretical A/D conversion limit

Table 2.12: INTEGRATION OF A STANDARD INPUT VOLTAGES

INPUT (mv)	"Y" 164 (volts)*	"X" 164 (volts)
0	0	0
0.10	0	0
0.50	0.01	0.01
1.0	0.04	0.04
2.0	0.09	0.08
5.0	0.21	0.21
10.0	0.38	0.38
20.0	0.78	0.77
50.0	2.00	1.95
100	3.87	3.75

*Includes a 0.18 v correction

Figure 2.19: INTEGRATOR OUTPUT AS A FUNCTION OF VOLTAGE INPUT

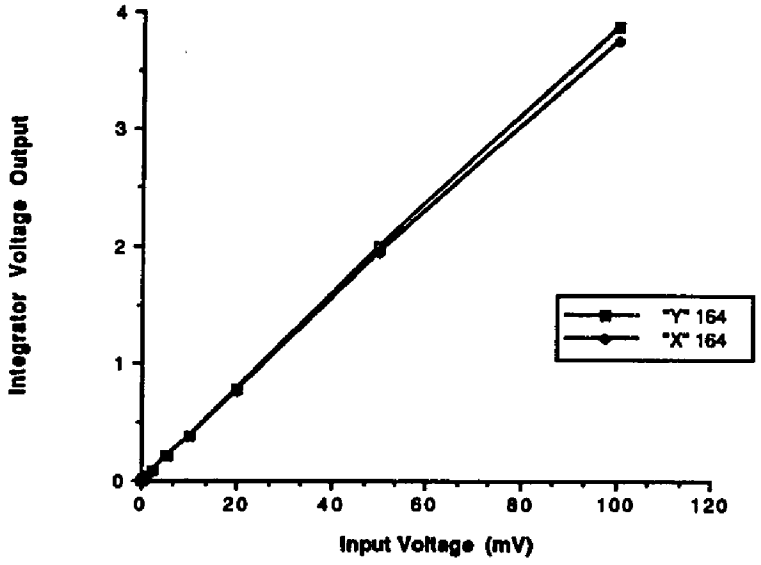

of the ADALAB interface card.

After correcting for the non equal initial levels, the correlation between the sample and reference channels was good, leading to a slope of 1.03 and a sample channel y-intercept of -0.004 volts, Figure 2.20. After determining that the boxcar response was essentially linear, the same experiment was performed using the computer as the readout device.

ADALAB corrections were performed by subtracting the reference and sample channel values, obtained with the PMT voltage off, from the ADALAB signal. Evaluation of the data shows that both channels responded similarly, indicating that the instrument should be amenable to source correction, Table 2.13 and Figure 2.20.

The inaccurate readings at high voltages have already been attributed to the ADALAB A/D conversion. At low voltages the 164 module, which had previously been sent out for repair, arbitrarily designated as "X", showed a better integration capacity than the "Y" 164. The "X" module was therefore used for the sample channel and the "Y" module for the less critical "reference" channel. The reference signal can be maintained at a high level where the integrator performs well, by adjusting the neutral density filter and/or the high voltage to the reference PMT.

To make sure that the difference in integration module performance was not due to mainframe difference, the units were switched. Module "X" still performed better with low input signals, Table 2.14. The slope and intercept, calculated from data derived from voltage inputs up to 50 mv, were 0.98 and 0.006 volts, respectively, Figure 2.21. These data compare well to the 1.03 slope and -0.004 volt y-intercept measured before switching the modules.

When the boxcar averager coupled to the ADALAB had been shown to yield reproducible slope and intercept values the same arrangement was utilized to measure reflected pulsed laser light. Before employing the computer as the signal

Figure 2.20: Slope of Boxcar Channels With A Steady State Source

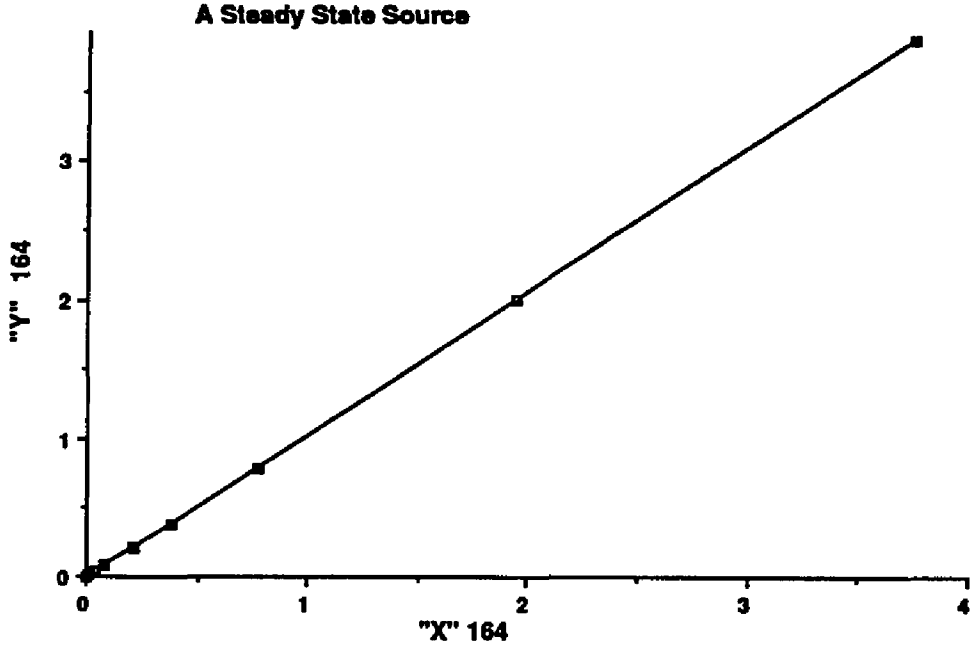

Table 2.13: INTEGRATION OF STANDARD VOLTAGES USING THE ADALAB/COMPUTER AS A READOUT DEVICE

	Corrected ADALAB DATA (ADALAB UNITS)		Corresponding Voltages (volts)	
Input (mv)	"Y" 164*	"X"164**	"Y" 164	"X" 164
0	0	0	0	0
0.1	0	2	0	.004
0.5	4	10	.008	.020
1.0	19	20	.037	.039
5.0	100	99	.20	.19
10.0	194	185	.38	.36
50.0	989	930	1.93	1.82
100.0	1697	1383	3.3	2.7

* correction value = +174 units
**correction value = -191 units

Table 2.14: INTEGRATION OF STANDARD VOLTAGES USING THE ADALAB/COMPUTER AS A READOUT DEVICE AFTER SWITCHING THE 164 MODULES

	Corrected ADALAB DATA (ADALAB UNITS)		Corresponding Voltages (volts)	
Input (mv)	"Y" 164*	"X"164**	"Y" 164	"X" 164
0	0	0	0	0
0.10	0.00	2	0	.004
0.50	5	9	.010	.018
1.0	15	18	.029	.035
5.0	94	94	.18	.18
10.0	185	184	.36	.36
50.0	940	931	1.8	1.8
100.0	1301	1746	2.5	3.4

* correction value = -286 units
**correction value = +237 units

Figure 2.21: Slope After 164 Units Switched

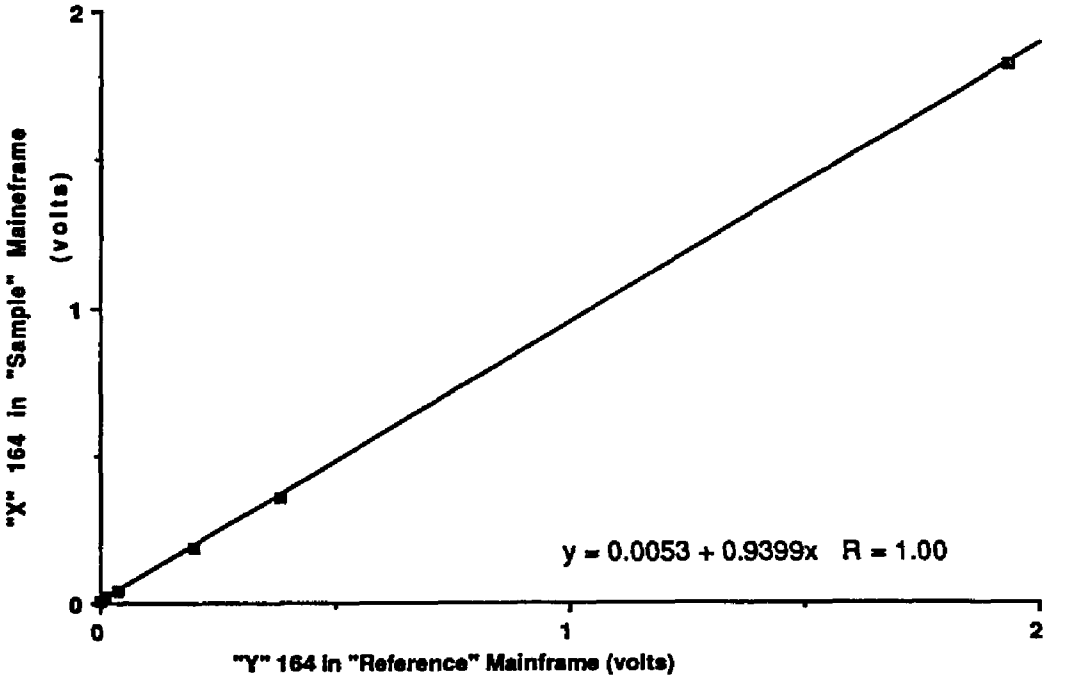

monitoring device, the oscilloscope was used to evaluate boxcar performance with the pulsed laser source.

Stray light reflected at a fiber/water interface was measured with a PMT coupled to a neutral density filter. Equal signals were directed to both the sample and reference boxcar channels by splitting one PMT output to the two 164 integrators. Boxcar triggering was provided by laser light collected by a PMT at output of the 4 Port ADC FOBS. A broad range of boxcar input voltages was obtained by varying the high voltage to the PMT. The instrument configuration for this series of tests is presented in Figure 2.22. The "zero" point was measured with no power supplied to the PMT.

The N_2 laser was computer fired at 1 pulse per second and replicate data points were collected for different PMT high voltage inputs from 500 to 900 volts, Table 2.15. A slope of 1.18 and a y-intercept of 56 ADALAB units (0.11 v) was calculated for the sample and reference channel data.

The fact that this slope derived from a pulsed source differs from the slope obtained with the steady state source indicates that the boxcars were not responding equally to a pulsed signal. However, repetitive testing showed that the slope and y-intercept values were reproducible. Therefore, the nonunity slope does not pose a problem because the computer can be programmed to account for it.

Including the ADALAB interface in the system simplifies data acquisition since the non zero starting points of the boxcars can be computer corrected. Therefore, an alternative procedure for obtaining the slope data was developed which improves on the above method in that instead of generating an average ground level reading, a separate correction is performed for each data point.

The improved procedure for acquiring slope data was as follows. Leads from two photomultiplier tubes were alternately connected to the two 164 integrators. One supplies the signal to be integrated, the other is from an unpowered PMT ac-

Figure 2.22: Block Diagram of Instrument

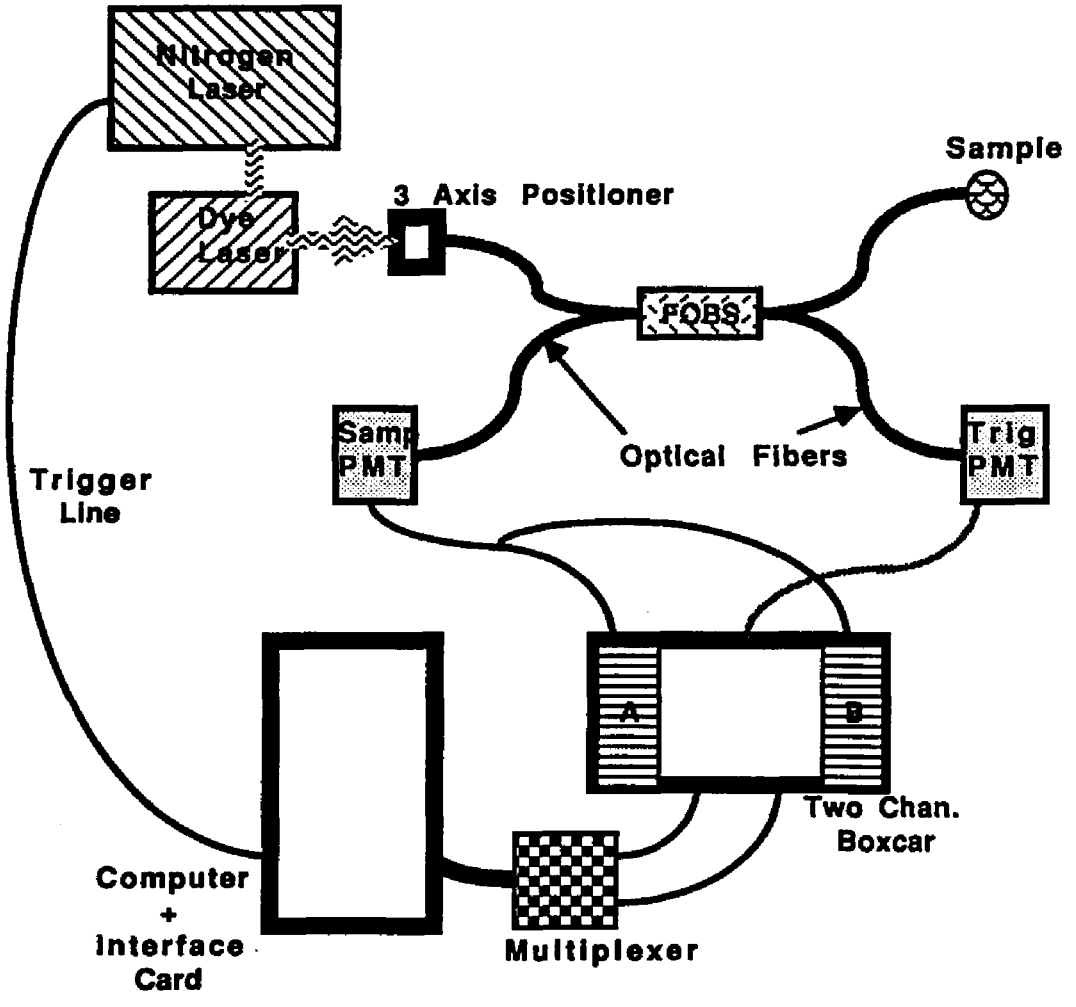

Table 2.15: BOXCAR OUTPUTS USING THE PHOTOMULTIPLIER TUBE AS A SIGNAL INPUT DEVICES

Voltage to PMT (volts)	Corrected Ave. Sample Sig. (volts)	Corrected Ave. Reference Sig. (volts)
500	0.18	0.15
600	0.58	0.50
700	2.0	1.6
800	5.0	3.8
900	10.0	8.5
corrected values with PMT power supplies off	-0.45	+1.05

ting as a zero point. After one point is determined by integrating 100 pulses, the leads are switched for a second 100 pulse integration. For each channel there are two sets of numbers, the integrated "raw" signal and the integrated ground point. Subtracting ground from the raw signal gives the actual signal strength. Sample data are displayed in Table 2.16.

The signal magnitudes are varied either by changing the high voltage to the PMT, or by adjusting the high voltage to the nitrogen pump laser. Holding the PMT power supply steady and varying intensity with the N_2 laser High Voltage control is the method of choice since it more closely mimics intensity fluctuations during experimentation.

Initial studies showed that a plot of corrected sample versus reference voltages is linear with an intercept slightly above zero. However, at higher ADALAB outputs the slope loses its linearity, Figure 2.23. While the curvature can be computer corrected, it is simpler to keep the signals within the linear range by adjusting the PMT high voltage input level. In repeated experiments the slope varied from 1.14 to a high of 1.50. Plotting the results of sixteen slope determinations, with a total of 142 data points, gave an overall slope of 1.18 with a 50 unit y-intercept, Figure 2.24. ADALAB units were converted to voltage by multiplying the ADALAB units by 4 volts, the ADALAB working range set by the jumper switch, and dividing by 2047, which corresponds to full scale A/D conversion. The results are similar to the 1.18 slope and 0.07 volt y-intercept observed when the oscilloscope was used to monitor boxcar output.

The slope of 1.18 and y-intercept of 50 ADALAB units, or 0.10 volts, was used to perform source corrections using signals from sample blanks and Rhodamine 6G standards.

Table 2.16: SAMPLE DATA FOR CALCULATING THE SLOPE AND INTERCEPT VALUES.

Ref PMT voltage = 600 v
Sample PMT = 550 v

ADR = 1 usec. w/ 10% Delay
TC = 1 usec. AD = 50 nsec.

	ADALAB Output	
	Corr. Samp. Sig	Corr. Ref. Sig.
Sig. to Ref. 164	-497	945
Sig. to Sample 164	-227	794
Difference	220	151
Sig. to Ref. 164	-495	920
Sig. to Sample 164	-305	790
Difference	190	130
Sig. to Ref. 164	-498	1018
Sig. to Sample 164	-170	796
Difference	328	222
Sig. to Ref. 164	-496	1014
Sig. to Sample 164	-194	796
Difference	302	218
Sig. to Ref. 164	-497	1045
Sig. to Sample 164	-168	795
Difference	329	250
Sig. to Ref. 164	-500	1252
Sig. to Sample 164	+ 85	786
Difference	585	466

SLOPE = 1.16
Y-INTERCEPT = 47 ADALAB units (0.09 volts)

Figure 2.23: PLOT OF REFERENCE AND SAMPLE ADALAB DATA

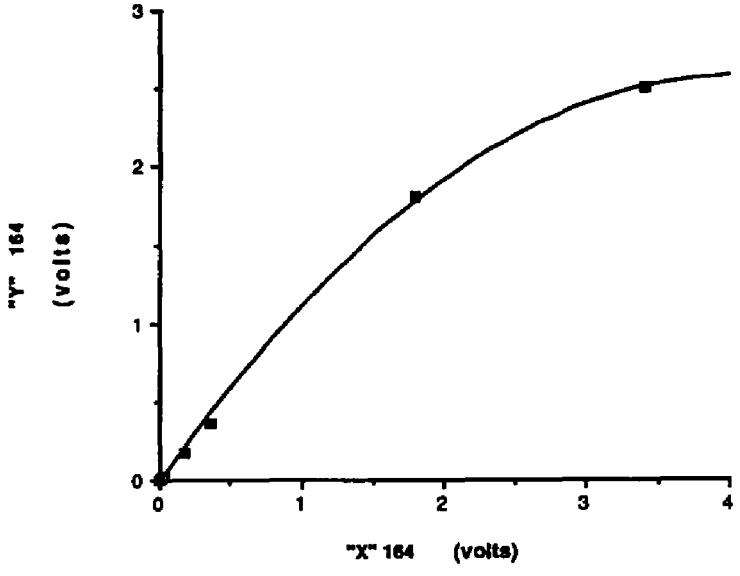

Figure 2.24: Slope Correction Curve

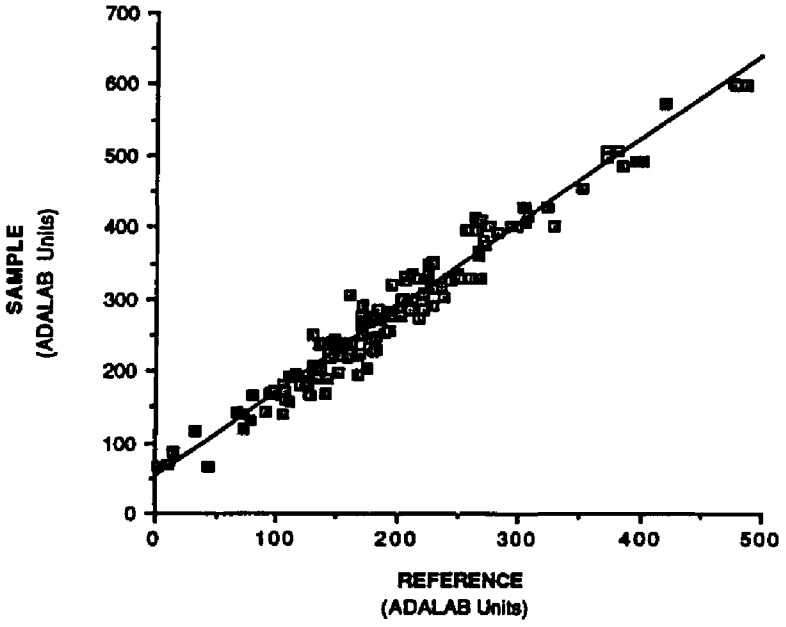

Response to Rhodamune Standards

The final task in evaluating the laser excited spectrometer was to generate and calculate working curves employing fluorescent standards. Rhodamine 6G was chosen since it is a benchmark fluorophor utilized in many fluorescence instrument characterizations. Rhodamine 6G (Rhodamine 590, Exciton Inc.), Figure 2.25, has a molar absorbtivity of 11×10^4 [85]. Excitation and emission wavelength maxima for the rhodamine, dissolved in pH 7.2 aqueous phosphate buffer, were 515 and 545 nm, respectively. Rhodamine standards were prepared by sequential dilution and were used to generate a Rh 6G working curve and to establish the instrument's detection limits.

Rhodamine 6G was excited by 510 nm radiation from a Coumarin 503 laser dye (6.0×10^{-3}M, in ethanol). Dye laser emission of 510 nm was achieved by tuning the micrometer slide to 1.490 units. Rhodamine emission was separated from the shorter wavelength stray light with interference filters. However, broad band fluorescence of the laser dye at the same wavelength as the sample emission can not be eliminated.

In the majority of the measurements the dye concentration was systematically increased. This minimized adsorption of the dye on the fiber end which would contaminate low concentration standards.

The instrument setup is displayed in Figure 2.26. The specific configurations for the Fiber Optic Beam Splitters, Figure 2.14-Configuration 3, and the boxcar integrators, Figure 2.17 have already been discussed. An extra length of fused silica fiber was connected to port 2 of the FOBS, making sure to include index of refraction matching gel in the SMA fiber connection. The extra fiber prevents the end of the FOBS from becoming contaminated and allows a fresh fiber surface to be used for every measurment. Boxcar timing functions are held constant with the Time

Figure 2.25: Structure of Rhodamine 6G

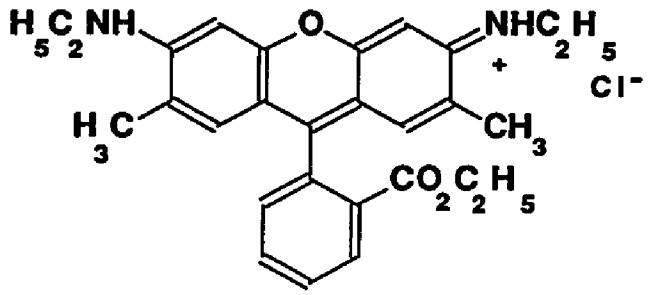

Figure 2.26: Instrumentation for Detection of Rhodamine 6G Emission

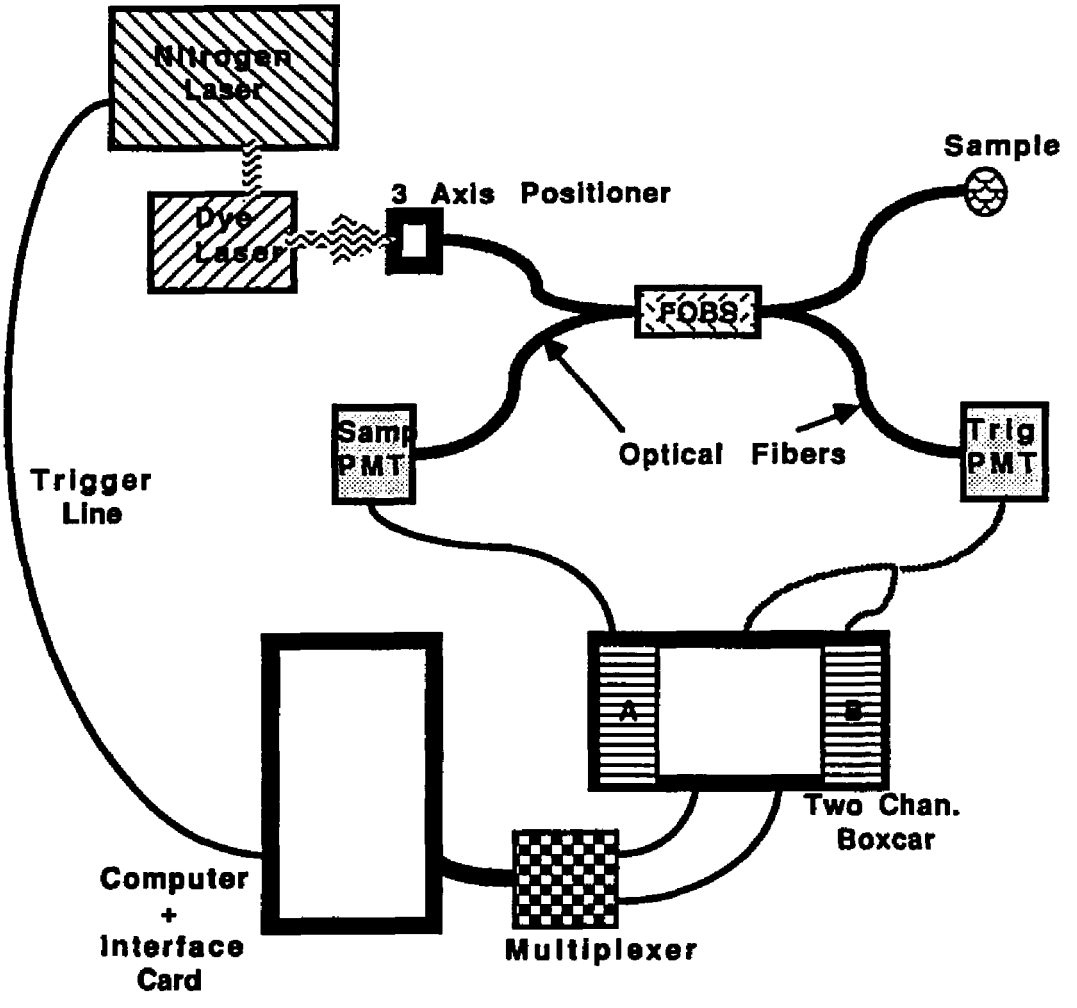

Constant and Aperture Delay Range set at 1 microsecond, a 10 % Delay, and a 50 nanosecond Aperture Duration. All electrical components are warmed up for one hour prior to use.

The high voltage to the Sample PMT was adjusted so that the highest concentration standard produced a signal corresponding to the maximum value of the ADALAB linear response range. Also, adjusting the Sample PMT voltage provides a simple way of varying the sensitivity of the instrument.

The reference signal is not as critical as the sample signal. Therefore, the reference PMT was powered so that the reference signal was roughly in the middle of the ADALAB range. Once set, the PMT voltages were held constant so that the slope correction values did not have to be reestablished.

It was determined that the source correction method used to establish the original slope and intercept values was too restrictive for practical experimentation. The 1.18 slope, with a 50 unit y-intercept, were only valid for measurements made with the same PMT voltages and boxcar settings thus removing a great deal of the inherent instrument versatility. In addition, that procedure was very laborious.

Individual sample and reference channel data were acquired in a multi step process. First, the integrator zero knob was used to adjust the trigger drift to less than 10 millivolts per 100 laser shots, monitored on the oscilloscope. Next, signal and baseline levels were measured for both the sample and reference channels. The baseline values were obtained with an unpowered PMT and are subtracted from the sample blank signal, collected with a powered PMT.

Next, the slope and y-intercept values are generated using the reference and raw sample data of the blank sample. Six to ten blank data points, of 100 pulses each, were integrated with the boxcar averagers, and the raw data was collected with the computer. A range of values is obtained by adjusting the nitrogen laser high voltage control. The slope and y-intercept values were calculated using the baseline

corrected raw sample and reference data. The source correction calculations for the blank raw sample data were then made using the slope and intercept values and the corresponding reference data. The same slope and y-intercept are also used to correct the sample data in the Rh 6G series.

Since leads do not have to be switched between the powered PMT and the unpowered PMT, the time to collect the necessary slope data is a fraction of the time required in the first method. In addition, the data generated to determine the slope value also produces the blank data for the working curve. Therefore, no time is lost and no information is wasted.

Besides significant time savings, the new slope generating procedure can be used with any PMT voltage, filter, or boxcar setting. Every change requires that a new slope be generated, but calculating the new slope takes no more time than it previously took to perform the daily instrument check. Considering that both the slope calculation and the source correction equation can be included in the computer program, the method is amenable to automation.

The slope data from this procedure were used to correct for source fluctuations in the Rh 6G working curve. Replicate measurements were made on a series of Rhodamine 6G standards and a blank solution. The source corrected data and standard deviations for a rhodamine series with a 550.6 nm interference filter (1 nm bandwidth at 1/2 height) is presented in Table 2.17 and produced a detection limit of about 1.0×10^{-9} M.

The importance of the slope correction method is reflected by the standard deviations of the corrected and uncorrected data. The standard deviations for the reference signal, raw sample signal, and the slope corrected data, are 13%, 8%, and 2%, respectively.

The same rhodamine working curve series was performed using a 560 nm filter with a 10 nm bandpass. The means and standard deviations are summarized in

Table 2.17: Rh 6G Working Curve Data Utilizing The New Slope and Intercept Values (I)

Rh Conc. (M)	Mean* and Stand. Dev. (ADALAB units)	% Deviation	Units Above Blank	Trials
Blank	100 +/- 2	2	-	9
1.0×10^{-10}	103 +/- 3	3	3	6
5.0×10^{-10}	104 +/- 3	3	4	5
1.0×10^{-9}	106 +/- 3	3	6	7
5.0×10^{-9}	109 +/- 3	3	9	6
1.0×10^{-8}	115 +/- 2	2	15	7
5.0×10^{-8}	147 +/- 4	3	47	6
1.0×10^{-7}	191 +/- 6	3	91	5

* Source Corrected: Slope = 0.31
y-intercept= 44 units

550.6 nm interference filter with 1 nm bandwidth.

Table 2.18. The average standard deviation is 1.7% which facilitates the resolution of low concentration standards which leads to better detection limits.

One trend noted in all the studies was that there is an unproportional correlation between concentration and fluorescence intensity. This non linear behavior is probably due to inner filter effects. Both the 1.0×10^{-7} and 5.0×10^{-8} M standards were visibly colored. This indicates that the inner filter effect sets the upper working range limit.

A similar fiber optic instrument, employing an Argon Ion Laser, using Rh 6G standards, had a detection limit of approximately 6×10^{-9} molar [73]. In addition, that design used separate excitation and emission fibers so backscatter was less of a problem.

Instrument Evaluation Summary

This instrument is unique because it is the first to use both Fiber Optic Beam Splitters and a nitrogen pumped dye laser. It is the combination of wavelength tunability, afforded by the dye laser, and the versatile optical design, allowed by the FOBS, which makes the instrument applicable to many different fiber optic chemical sensors.

Fiber Optic Beam Splitters simplify the optical design and alleviates alignment problems, making the instrument more rugged and potentially portable. Light throughput of the Aster beam splitter, fabricated from fused silica fiber, was an order of magnitude less than either of the ADC splitters and was thus not used. The two ADC splitters, with glass fibers, were configured so that the maximum information content could be extracted.

Another advantage of FOBS is that they allow single fiber measrements.

Table 2.18: Rhodamine 6G Working Curve Data Utilizing The New Slope and Intercept Values (II)

Rh Conc. (M)	Mean* +/- Stand. Dev. (ADALAB units)	Units above Blank	Trials
Blank	100 +/- 1	-	10
1.0×10^{-10}	99 +/- 1.5	N.S.	4
5.0×10^{-10}	102 +/- 0.8	2	5
1.0×10^{-9}	106 +/- 1	6	5
5.0×10^{-9}	119 +/- 2	19	5
1.0×10^{-8}	144 +/- 2	44	6
5.0×10^{-8}	212 +/- 4	112	5
1.0×10^{-7}	267 +/- 6	167	5

*Source Corrected: Slope = 1.00
y-intercept = 225 units

560 nm interference filter with 10 nm bandwidth.

Light collected efficiently when a single fiber is used to both excite the sample and collect the sample emission. Also, single fiber sensors are smaller than sensors with bifurcated fibers. The trade off is an increase in the amount of stray light. However, stray light can be reduced by an order of magnitude when index of refraction matching gel is used at all fiber interfaces and ends. In addition, gel inserted at the fiber interfaces increases light throughput by minimizing imperfections in fiber surfaces and retaining the higher order modes of light.

Since stray light results primarily from reflection of the laser light, the signal to background ratio can be further improved by the use of filters. Filters are placed in the photomultiplier tube housings to separate the longer wavelength sample light from the reflected laser light.

Wavelength versatility is a characteristic of the dye laser. Wavelength calibration relates directly to the alignment of the dye laser cavity, so that once set the alignment can not be altered.

Evaporation of the laser dye solvent, photobleaching of the laser dye, and even small changes in the position of the dye cell affect the intensity of emitted laser light. However, this long term source drift is of little consequence since it can be accounted for by utilizing a two channel measurement. The $\mp$ 10 percent pulse to pulse reproducibility of the nitrogen pump source is also corrected with the dual channel method. However, if the air and nitrogen pressure are not closely regulated the laser performance can decay to a point where data collection is not feasible.

Correcting for source fluctuations requires two integrators. The most successful boxcar configuration placed separate 164 module in individual 162 boxcar mainframes. This design eliminated the problem of mismatched timing functions and input load resistors. The non zero initial voltage integration points, of each 162 mainframe, were computer corrected. Performance of the boxcar integrators was marginal at times.

The primary problem associated with the boxcar averagers was trigger drift, which unlike source drift is not correctable. However, the boxcars are necessary since without them, the signals were indistinguishable from the background.

With careful zeroing of trigger drift the precision of the boxcars was approximately two percent with an accuracy of slightly better than one percent. The boxcars limited overall instrument precision. For Rh 6G working curves the relative standard deviation for source corrected data was about $\mp$ 2 percent.

The detection limit for rhodamine 6G was about 1.0×10^{-9} molar. The detection limit is set by broad band fluorescence of the dye laser. This improves on the detection limit reported for an argon laser, fiber optic fluorescence instrument.

CHAPTER III

INVESTIGATION OF DONOR-ACCEPTOR FLUORESCENT PAIRS FOR ENERGY TRANSFER

Introduction

The optical glucose sensor depends on both competitive binding and the transfer of fluorescence energy from a donor fluorophor to an acceptor fluorophor. To optimize sensor response it is necessary to find donor-acceptor pairs that undergo efficient energy transfer when donor (acceptor) labeled concanavalin A binds acceptor (donor) labeled dextran. This chapter describes the evaluation of donor-acceptor systems for the sensor.

Theory of Fluorescence Energy Transfer

Fluorescence energy can be transferred nonradiatively through space from an electronically excited donor to the excitation band of an acceptor inducing fluorescence from the acceptor dye. Closely aligned energy levels, between the donor emission and acceptor excitation bands allow energy transfer to take place with high efficiency.

Figure 3.1 represents an ideal donor-acceptor pair. There is excellent overlap between the donor emission and acceptor excitation bands, while both the two emission peaks and two excitation peaks are completely separated. Therefore, there is no direct electronic excitation of the fluorescence energy acceptor, and donor and acceptor fluorescence can be independently measured.

Förster developed the theoretical basis for long range fluorescence energy

Figure 3.1: Ideal Exitation and Emission Spectra for a Fluorescence Energy Transfer Pair

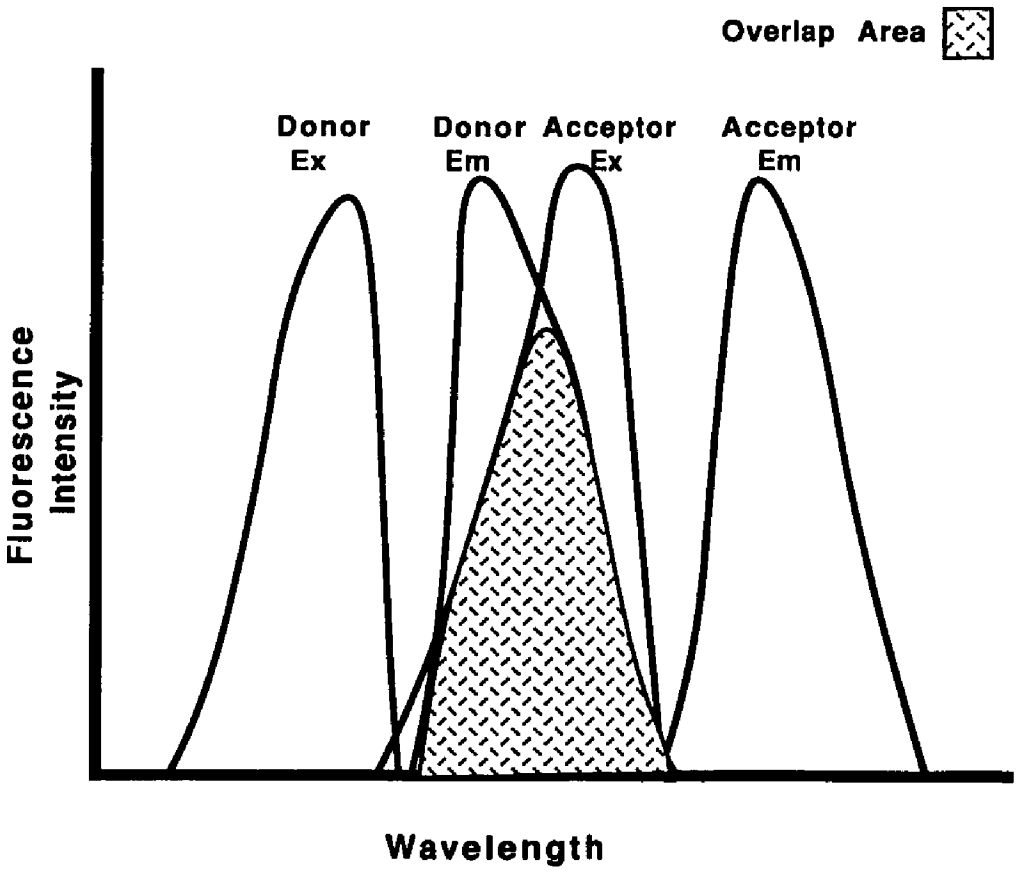

Ex = Excitation
Em = Emission

transfer in the mid 1950's [41]. For the system

$$D^* + A \leftrightarrow D + A^*$$

where D is the donor dye, A is the acceptor dye, and * denotes an electrically excited species, Förster calculated the rate of energy transfer as:

$$k_T = r^{-6}K^2Jn^{-4}k_F(8.71 \times 10)^{23}\ sec^{-1}$$

Where r is the distance between donor and acceptor dyes, and K is the orientation factor. K averages out to be 2/3 for fluorophors in solution. The degree of overlap between the fluorescence spectra of the donor and the excitation peak of the acceptor is described by J, the spectral overlap integral. Other spectroscopic variables include n, the refractive index of the solvent and k_F, the rate constant for fluorescence.

Stryer rearranged the Förster equation in terms of a critical radius, R_0.

$$R_0 = 9700\,\text{Å}\ (JK^2\phi_D n^{-4})^{1/6}$$

The critical radius is the distance at which there is a fifty percent probability that fluorescent energy will be transferred. R_0 depends on the spectral overlap, the orientation factor and the quantum efficiency of the donor, ϕ_D, in the absence of acceptor [86]. For small molecules in solution, the critical radius usually ranges from 15 - 50 Å. However, it has been demonstrated that, when the variables are favorable, R_0 can exceed 50 Å [41].

Selection of Energy Transfer Donor-Acceptor Pairs

When choosing donor-acceptor pairs for the sensor, the variables in the Förster equation must be considered. The donor emission peak must overlap the excitation band of the acceptor, and both the donor and the acceptor should have high quantum efficiencies.

There are several additional considerations. Not all dyes can be conjugated to dextran and concanavalin A. The number of dye molecules per substrate is also important because more dye increases the probability that donor and acceptor will be within the critical radius for energy transfer. In addition, because concanavalin A is sensitive to heat, pH and light a gentle labeling procedure and purification process is required. Finally, dextran binds to conA only between pH 5 and 8, eliminating fluorophors that do not emit strongly at these pH's [87].

Practical considerations also influence the choice of donor-acceptor fluorescent pairs. To eliminate the need for specialized and expensive optical components it is desirable to work in the visible region. Since a potential application of the optical glucose sensor is for in vivo blood sugar detection, the fluorophors need to function in water at physiological pH.

The following subchapters describe feasibility studies for a number of donor-acceptor systems. Successful pairs were evaluated for use in an optical glucose sensor. Energy transfer studies were initially carried out with conventional spectrofluorimeters. The most efficient fluorescent pairs were then tested with the laser, fiber optic spectrofluorimeter described in Chapter 2.

Experimental

Reagents - Energy transfer dyes are specified in the individual sections. Un-

less otherwise noted, all solutions were buffered to pH 7.2 with a 0.05 M phosphate buffer (monobasic sodium phosphate, Aldrich; dibasic sodium phosphate, Fisher). D(+)glucose (Aldrich) was used in all energy transfer reversal studies.

Cross linked dextrans, Sephadex (Sigma Chemical Co., ST Louis, MO), were used for affinity purification of the concanavalin A. Exhaustive dialysis was performed with different molecular weight cut off (MWCO) dialysis tubing (Spectrum Medical Industries, Los Angeles, CA).

Instrumentation - Initial energy transfer studies were performed on a Perkin Elmer model MPF44E fluorescence spectrophotometer (Norwalk, CT) but the bulk of the work was performed with a double monochromator SLM 8000/8000S spectrofluorometer (SLM-AMINCO Instruments Inc., Urbana, IL). A Perkin Elmer model 204 fluorescence instrument was utilized for the labeling efficiency studies.

Other instrumentation includes a Shimadzu Double Beam Spectronic UV-200S UV/VIS spectrophotometer and an Orion Ross combination pH electrode coupled to an Orion model 501 digital Ionalyzer.

Fluorescence Energy Transfer Studies

Dyes were immobilized on either concanavalin A or dextran. Energy transfer was studied by adding increasing amounts of the acceptor to solution with a constant concentration of the donor. Volume was maintained constant using buffers. Mixtures were allowed to equilibrate for 3 minutes before spectra were obtained. Spectra were recorded after setting the excitation monochromator to a wavelength at or near the maxima of the donor excitation peak and scanning across the emission band of both the donor and acceptor fluorophors. Spectra were recorded for the donor alone, a series of donor:acceptor ratios, and the acceptor in the absence of

the donor. When energy transfer occurs donor fluorescence is reduced upon addition of acceptor dye and acceptor, emission is enhanced by the presence of donor.

The reversal of energy transfer was tested by the addition of glucose to the dextran/conA solution. An excess of glucose was added to a dex/conA solution where energy transfer is taking place between the dye labels. As glucose displaces the dextran from the conA, the critical radius necessary for energy transfer is exceeded, leading to an intensity change. Reversal of energy transfer is indicated by an increase in donor intensity or a decrease in acceptor intensity.

Unless otherwise noted, this general procedure was followed in evaluating all dye pairs.

EVALUATION OF FLUORESCEIN ISOTHIOCYANATE AND TETRAMETHYLRHODAMINE ISOTHIOCYANATE AS FLUORESCENT LABELS FOR ENERGY TRANSFER

Introduction

The fluorescein and rhodamine pair is the most widely studied fluorescent energy transfer system. Ullman [42] used this pair in his pioneering work with energy transfer immunoassay. The system has since been utilized in numerous studies [88-94]. Most recently Schultz [95] investigated the FITC-Rhodamine system for use in his second glucose sensor. The attractiveness of this pair is due to their excellent spectral overlap, as well as the fact that both have very high quantum efficiencies.

Fluorescein, employed as the donor, has a broad excitation band in the visible region allowing direct excitation with a variety of sources [96]. This also facilitates the use of inexpensive glass optical fibers. Fluorescein-5-Isothiocyanate (FITC), Figure 3.2A, has excitation and emission wavelength maxima of 494 and 530 nm, respectively. FITC is used since it can be readily coupled to the dextran. FITC-labeled dextran with a variety of molecular weights are commercially available.

Several different rhodamines are available for energy transfer studies. Rhodamine can be purchased prelabeled to concanavalin A or can be conjugated in house to attain different labeling ratios.

Tetramethlyrhodamine-5-(and-6)-isothiocyanate (TRITC), Figure 3.2B, was chosen, as the fluorescence energy acceptor, for the initial investigation. The reported excitation, 541 nm, overlaps the FITC emission band, while the rhodamine emission peak, 572 nm, should be well resolved from the fluorescein emission. In addition TRITC has a slightly higher molar absorptivity than fluorescein, 8.2×10^4

Figure 3.2A: Structure of FITC

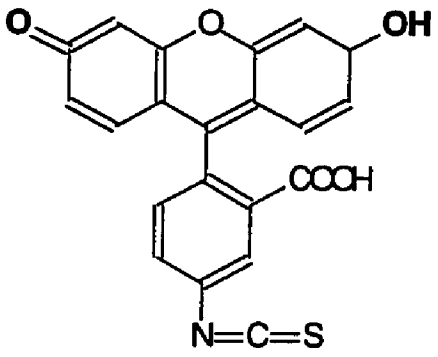

Figure 3.2B: Structure of TRITC

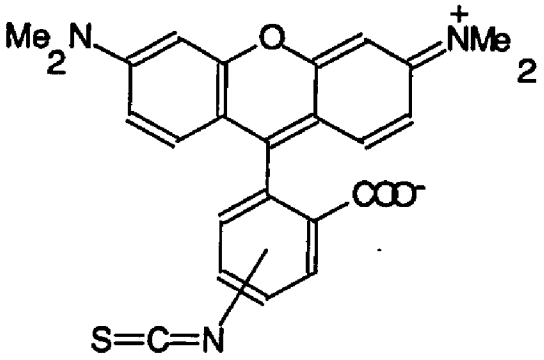

vs. 7.2×10^4, respectively [97].

Reagents - Stock solutions of dextran-FITC (Sigma, ST. Louis, MO) were prepared by dissolving a known mass of the solid in pH 7.2 phosphate buffer, 0.050M. A wide range of different molecular weight dextrans were used. A stock solution of conA-TRITC (Molecular Probes, Eugene, OR) was made by dissolving a known mass in the pH 7.2 buffer. According to manufacturer's literature, each conA tetramer reacts with just over two moles of TRITC [98].

Fluorescence Energy Transfer Studies - Excitation and emission spectra and the energy transfer studies were performed as described in the experimental section of this chapter. The excitation monochromator was set to 464 nm and emission was scanned from 480 to 630 nm.

RESULTS AND DISCUSSION

Figure 3.3 shows that there is excellent overlap between the FITC donor emission band and the TRITC excitation band with good resolution between the two emission peaks. In energy transfer studies the TRITC emission is usually less intense than the FITC emission, but was normalized for the figure.

Unfortunately there is some direct excitation of the TRITC at the FITC excitation wavelength maximum. This is reduced when the excitation is shifted to a shorter wavelength. To reduce direct excitation of the acceptor, while still maintaining good donor fluorescence efficiency, fluorescein was excited at 465 nm which corresponds to the small side peak on the FITC excitation band.

Figure 3.3 also shows a small TRITC peak at approximately 410 nm, which only materializes upon labeling to the concanavalin A. Fortunately it is far enough

Figure 3.3: Excitation and Emission Spectra of FITC and TRITC

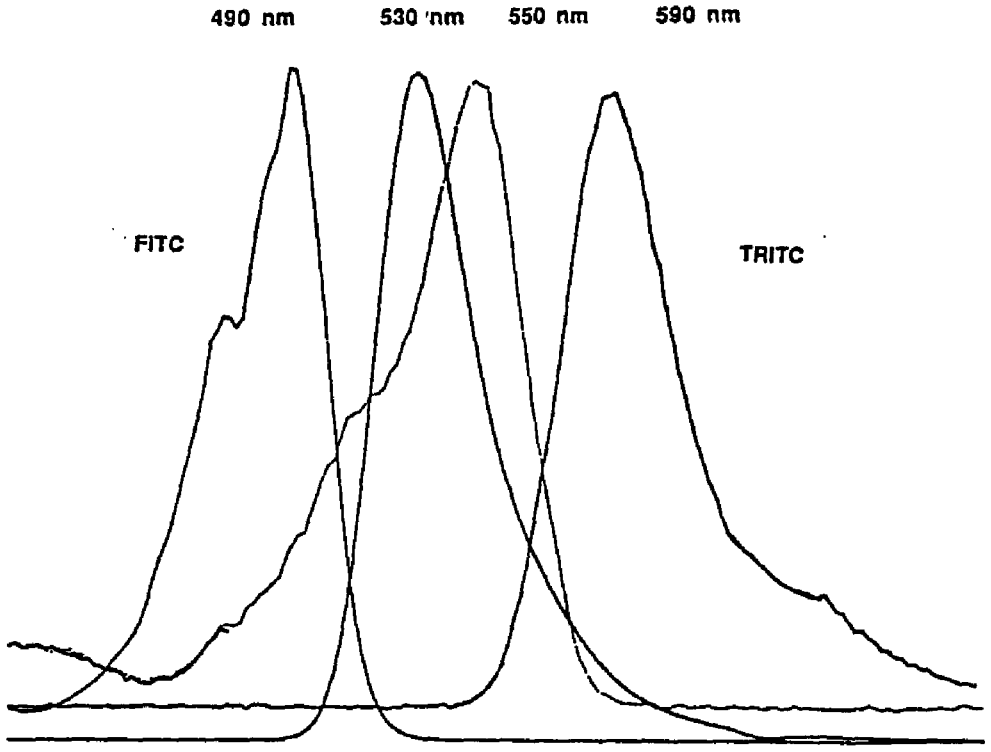

away so it does not overlap with the FITC excitation band.

Energy transfer was initially studied using conA-TRITC and 18,900 molecular weight dextran-FITC with 0.004 moles FITC per glucose unit (180 daltons) resulting in a dex-FITC ratio of about 2:1.

Data in Table 3.1, with corresponding spectra shown in Figure 3.4, show that energy is transferred from dex-FITC to conA-TRITC, causing a decrease in FITC intensity, at 530 nm, upon introduction to TRITC. TRITC quenching was reproducible and its impact on the relative FITC intensity is shown in Figure 3.5. Quenching ranged from 14 %, for the 3.4:1 conA-dex mixture to 23 % with an 11:1 conA excess.

Data in Table 3.2 and Figure 3.6 show that addition of glucose leads to an increase in FITC intensity. However, despite a large excess of glucose, FITC intensity does not return to its initial value in the absence of conA.

The probability of energy transfer increases as the average distance between the two fluorophors decreases. Shortening the distance between the FITC and TRITC is most easily accomplished by increasing the loading of the dyes on the two substrates. Since there is not much leeway with conA-TRITC, dextran-FITC concentrations were varied to increase the efficiency of energy transfer.

The wide selection of FITC-labeled molecular weight dextrans provides an opportunity to study the influence that dextran size and FITC concentration have on energy transfer. Each different molecular weight dextran has a unique FITC label concentration, Table 3.3. Different dextrans were compared while holding the other variables constant. Table 3.4 summarizes the experiment with the 4000 MW dextran. Energy transfer efficiency was determined by the relative decrease in FITC intensity at 530 nm, as conA-TRITC is added. Reversal of energy transfer is indicated by an increase of FITC intensity upon addition of glucose.

The spectra show that the greatest percentage FITC intensity changes occur

Table 3.1: Energy Tranfer Study From Dex-FITC (MW 18,900) To ConA-TRITC

	Volume Dex-FITC (3.5×10^{-4} M)	Volume ConA-TRITC (2.0×10^{-6} M)	Volume Buffer
1	5.0 uL	0	10.0 mL
2	5.0 uL	3.0 mL	7.0 mL
3	5.0 uL	5.0 mL	5.0 mL
4	5.0 uL	7.0 mL	3.0 mL
5	5.0 uL	10.0 mL	0
6	0	10.0 mL	0

Figure 3.4: Energy Transfer from Dex-FITC to ConA-TRITC

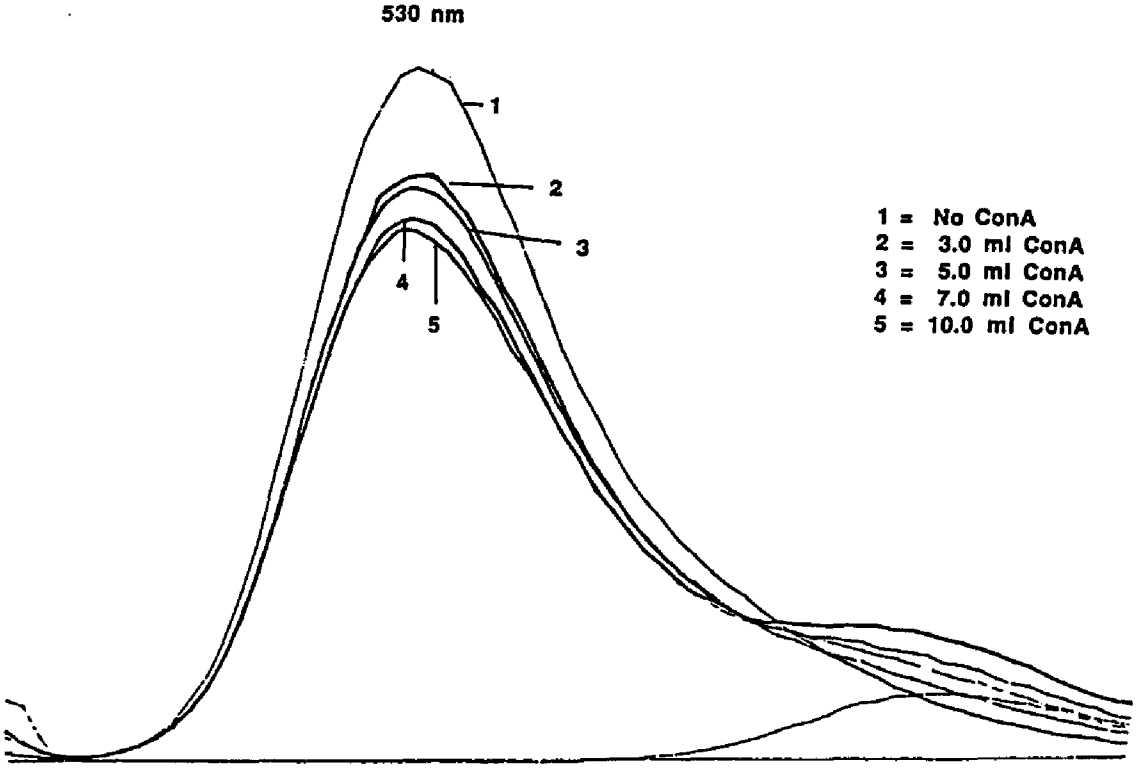

Figure 3.5: FITC Intensity Upon Addition of TRITC

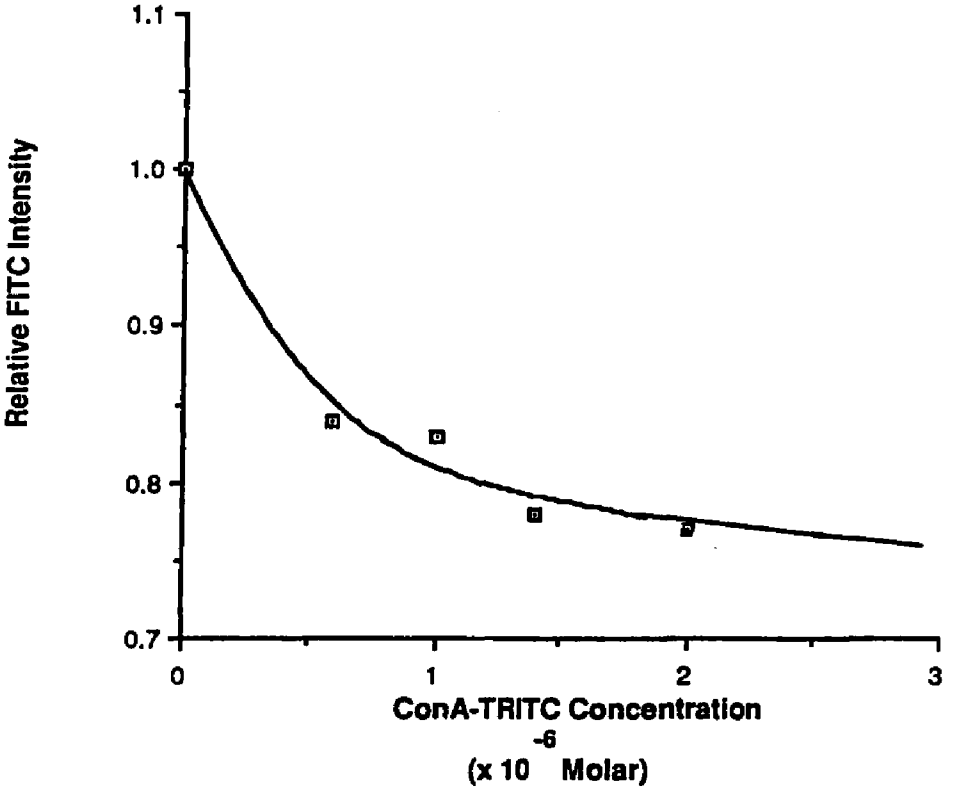

Table 3.2: Reversal Of Energy Transfer Upon Addition Of Glucose

	Volume Dex-FITC (3.5×10^{-4} M)	Volume ConA-TRITC (2.0×10^{-6} M)	Volume Buffer	Volume of 0.20 M Glucose
1	5.0 uL	0	4.0 mL	0
2	5.0 uL	3.0 mL	1.0 mL	0
3	5.0 uL	3.0 mL	0	1.0 mL

Figure 3.6: Glucose Reversal of Energy Transfer

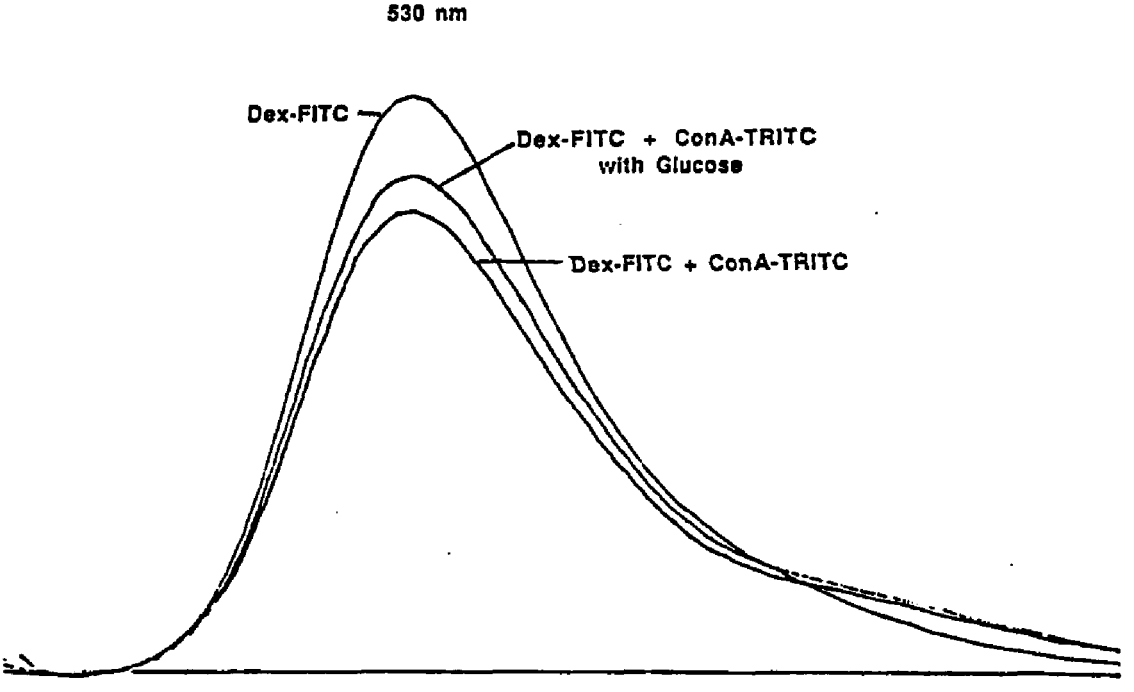

Table 3.3: FITC Labeling On Different Molecular Weight Dextrans

Dextran Molecular Weight	Moles FITC per Mole of Glucose	FITC:Dextran Mole Ratio
4057	0.004	1:10
9000	0.010	1:2
18900	0.004	1:2
40500	0.003	1:3
71600	0.004	1.6:1
148000	0.005	6:1

Table 3.4: Sample Experimental Set Up for Dextran Molecular Weight Series

	Vol. Dex-FITC (3.6×10^{-4} M)	Vol. ConA-TRITC (2.0×10^{-6} M)	Vol. Buffer	Vol. Glucose (0.10 M)
1	5.0 uL	0	5.0 mL	0
2	5.0 uL	2.0 mL	3.0 mL	0
3	5.0 uL	2.0 mL	2.0 mL	1.0 mL

Hold Dextran and ConA-TRITC concentrations constant

with the higher molecular weight dextrans. The 71,000 MW dextran produced a 12% decrease in FITC intensity upon addition of the acceptor while little or no energy transfer is observed with the low molecular weight species.

With small dextrans one would expect the fluorescent label to be closer to the conA binding site enhancing energy transfer. However, the smaller dextrans have fewer labels per dextran molecule (moles of FITC per mole of glucose), Table 3.3. Furthermore, fluorophors on the part of the dextran away from the conA binding site may actually interact more directly with fluorescent labels on the surface of the conA. And, since more than one conA can bind to the larger dextrans more efficient use is made of the donor fluorophor.

It was also discovered that a higher conA:dex ratio promotes better energy transfer. Figures 3.7A and 3.7B show the spectra for 10:1 and 100:1 conA:dex, using the 71,600 MW dextran. With the 10:1 ratio a 12 percent decrease in FITC intensity is observed upon addition of acceptor while a 100 fold excess of conA induces a 20% decrease. Addition of an excess of glucose to both solutions produced a 54 to 55 percent recovery of the FITC fluorescence. An additional advantage is that the TRITC emission peak has become clearly evident with the 100:1 molar ratio simplifying a dual wavelength measurement. These results are very similar to those of Schultz [95].

By greatly increasing the conA:dex ratio Schultz was able to produce a 40 % quenching of FITC intensity. It is surprising that such high conA:dex ratios could be attained considering the limited solubility of concanavalin A. The highest ratio in this work which still gave an acceptable FITC signal, was about 200:1.

SUMMARY

This dex-FITC/conA-TRITC system demonstrates that an optical glucose

Figure 3.7.A: Energy Transfer With a 10:1 ConA:Dex Ratio

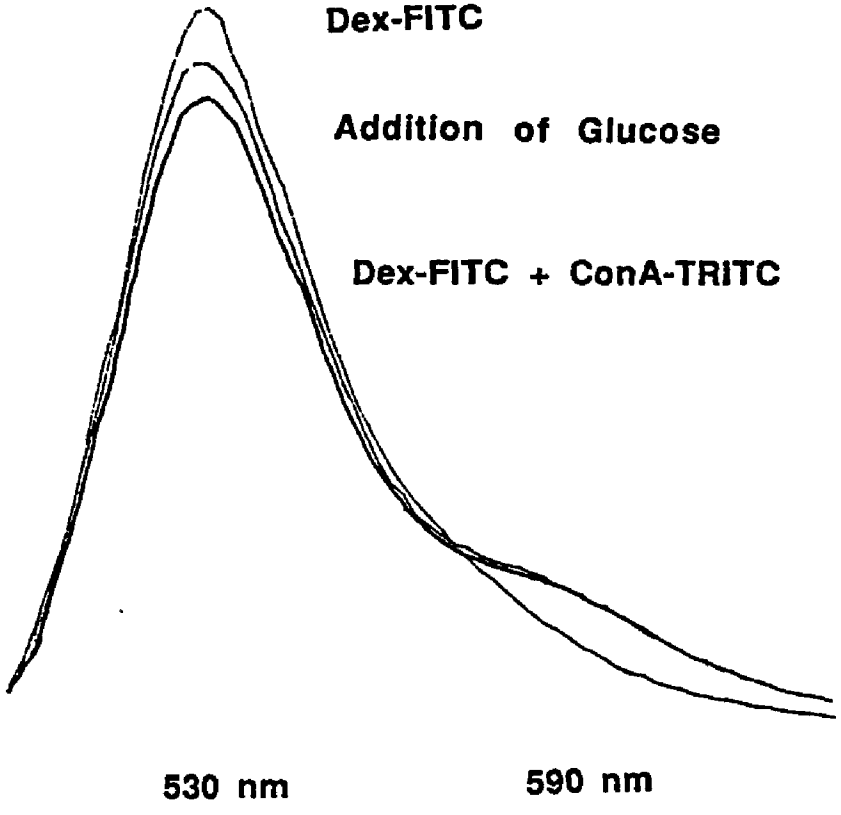

Figure 3.7.B: Energy Transfer With a 100:1 ConA:Dex Ratio

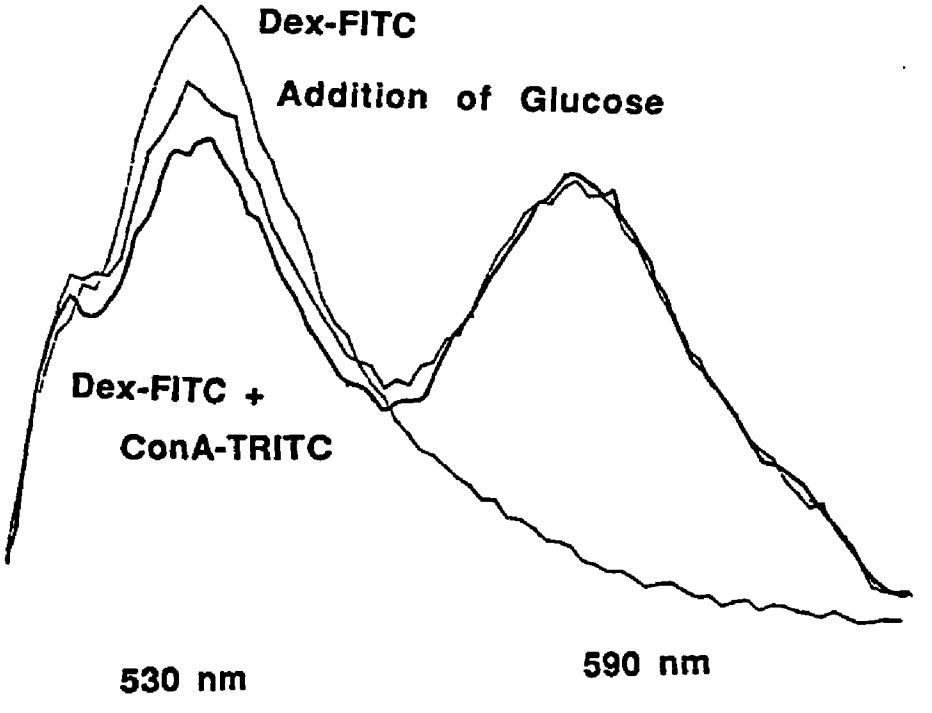

sensor based on competitive binding and energy transfer is feasible. Reproducible and reversible energy transfer was observed. Best results were achieved when more FITC labels are used and when the conA:dex ratio was maximized.

However, the system has a practical problem in that the TRITC emission is partially obscured by the FITC fluorescence tail, making a simultaneous dual wavelength measurement difficult. This problem is particularly acute at low conA-TRITC:dex-FITC ratios. To rectify the problem either the ratio of TRITC to FITC can be increased or a rhodamine derivative which emits at longer wavelengths can be employed.

To insure that dextran binds to conA the concentration of either one or both must exceed the binding constant which is approximately 1×10^{-4} at optimum conditions [44]. This corresponds to the maximum conA solubility in a pH 7.2 aqueous solution, thus eliminating the possibility of increasing the TRITC/FITC ratio by using a large excess of conA-TRITC.

A second option is to explore an alternative energy transfer dye pair with an acceptor that emits further from the FITC fluorescence peak. Two possible substitutes for TRITC are two other rhodamines, Texas Red and XRITC.

EVALUATION OF XRITC AND TEXAS RED DYES AS ENERGY TRANSFER ACCEPTORS FROM FITC

Introduction

The dextran-FITC to conA-TRITC system demonstrated the feasibility of utilizing energy transfer in an optical glucose sensor. Despite good resolution between FITC and TRITC emission peaks, even better resolution is attainable with alternative dyes. Increased spectral separation is afforded by both rhodamine X isothiocyanate (XRITC) and Texas Red, because ring substitution produces a bathochromic shift. XRITC and Texas Red have emission peaks at 604 and 615 nm, respectively [98]. Figure 3.8 shows emission spectra for Texas Red, TRITC and FITC, illustrating the improved separation with Texas Red.

In addition to the improved spectral resolution, both dyes are also highly fluorescent [98]. Texas Red has a molar absorbtivity of 8.5×10^4, which is slightly higher than the absorbtivity of XRITC and TRITC.

While the two are very similar, the isothiocyanato group of the XRITC, Figure 3.9A, makes it more hydrophobic than Texas Red, Figure 3.9B. Therefore, Texas Red, which is actually a mixture of two mono-sulfonylchloride substituted compounds, was initially preferred for this aqueous system. However, Texas Red is moisture sensitive [98], demanding a more refined labeling technique than XRITC.

The FITC and Texas Red energy transfer pair has been used in an ionic strength sensor [99] and to monitor the binding of the protein C5b to membranes [100]. Texas Red has also been employed as an energy transfer donor to B-Phycoerythrin [79].

Figure 3.8: Comparison of FITC, TRITC, and Texas Red Emission

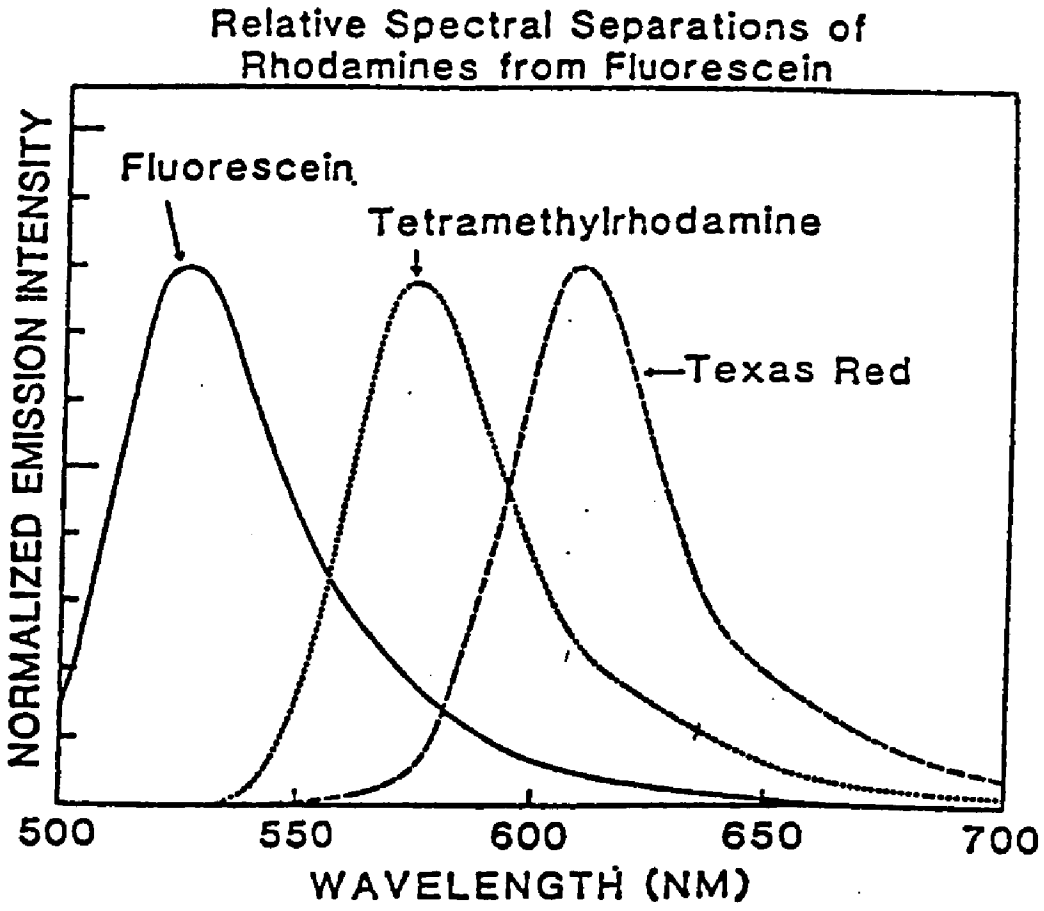

Handbook of Fluorescent Probes and Research Chemicals, by Richard Haugland, Molecular Probes Inc., P.O. Box 22010, 4849 Pitchford Ave., Eugene, OR January 1989, p. 37.

Figure 3.9A: XRITC Structure

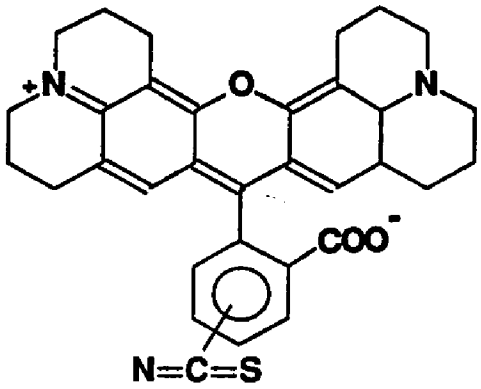

Figure 3.9B: Texas Red Structure

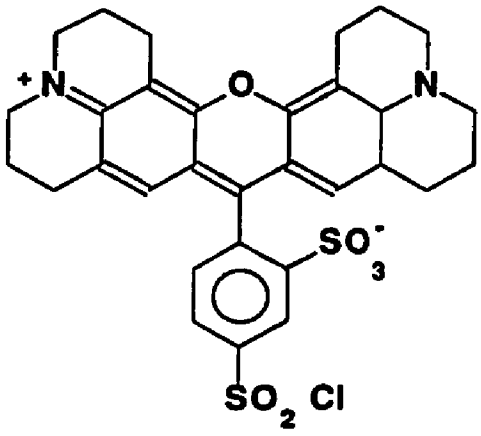

Experimental

Reagents - Prelabeled conA-XRITC is not available commercially so unlabled concanavalin A, 55000 MW (Sigma Chemical Co.) and the XRITC (Molecular Probes, Eugene, OR) dye were purchased separately. Concanavalin A is available prelabeled with Texas Red (conA-TR) (Molecular Probes) and a stock solution was made by dissolving a known mass in a pH 7.2 phosphate buffer. As in the TRITC work, stock solutions of different molecular weight dextran-FITCs (Sigma Chemicals) were prepared by dissolving known masses of the solid in pH 7.2 phosphate buffer. The purification process for the in house labeled conA-XRITC required 10,000 molecular weight cut off (MWCO) dialysis tubing and Sephadex beads, G 150-120, (Sigma Chemical Co.). Sephadex, a brand name for crossed linked dextrans, was used for affinity purification.

Labeling Procedure for conA-XRTIC (1:5 Ratio) - Using a vortex mixer, 190 ul of 9.2×10^{-3} M XRITC in dimethylformamide (DMF), was added to 100 ml of a 3.5×10^{-5} M aqueous conA solution, buffered at pH 9.2 (carbonate buffer, 0.05 M). The mixture was incubated for 2 hours at 0 to 5 °C, with stirring. The solution was then transferred to a 10,000 MWCO dialysis tube which was placed in a 2 L, pH 7.2, phosphate buffer bath for 12 to 18 hours at 0 to 5 °C, with stirring.

The conA-XRITC compound was purified using an affinity method [46]. A G 150-120 Sephadex column was prepared and equilibrated with 1.0 M NaCl. The conA-XRITC solution was poured through the column which passed the denatured conA and unbound XRITC. The undenatured conA was then eluted with a 0.1 M glucose/1.0 M NaCl wash solution and collected. Fractions were monitored at the 280 nm absorbance band of the protein using a Shimadzu Spectronic 200 UV/Vis spectrometer. Glucose removal from the purified conA-XRITC, required a 48 hour

dialysis process using 10,000 MWCO tubing in pH 7.2 buffer, at 0 to 5 °C, changing the bath every 12 hours.

Results and Discussion

The FITC to XRITC and Texas Red systems are grouped together because both acceptor dyes are derived from the sulforhodamine 101 precursor. Also neither system produced significant energy transfer.

The failure of the dex-FITC to conA-XRITC system is attributed to inefficient labeling, since conA-XRITC did not fluoresce after dialysis to remove excess fluorophor. The problem is at least partly due to XRITC insolubility in water since undissolved solid was observed when conA and XRITC were combined.

Examination of the excitation and emission spectra of dex-FITC and conA-TR shows that overlap between the FITC and Texas Red is limited, Figure 3.10. However, the benefits are that the FITC emission does not interfere with the Texas Red peak, 622 nm, and there is virtually no direct excitation of the Texas Red at the maximum FITC excitation wavelength.

Energy transfer between the two dyes proved to be negligible. The dex-FITC to conA-TR system showed only very slight decreases in FITC fluorescence intensity upon addition of the acceptor. Glucose reversal was therefore not attempted.

The minimal effect of the Texas Red on the donor dye is attributed to the poor overlap of the FITC emission peak and the Texas Red absorption band. The results are particularly disappointing since the FITC to Texas Red pair had been successfully utilized in an optical sensor for ionic strength based on competitive binding [99].

Figure 3.10: Excitation and Emission Spectra for FITC and Texas Red

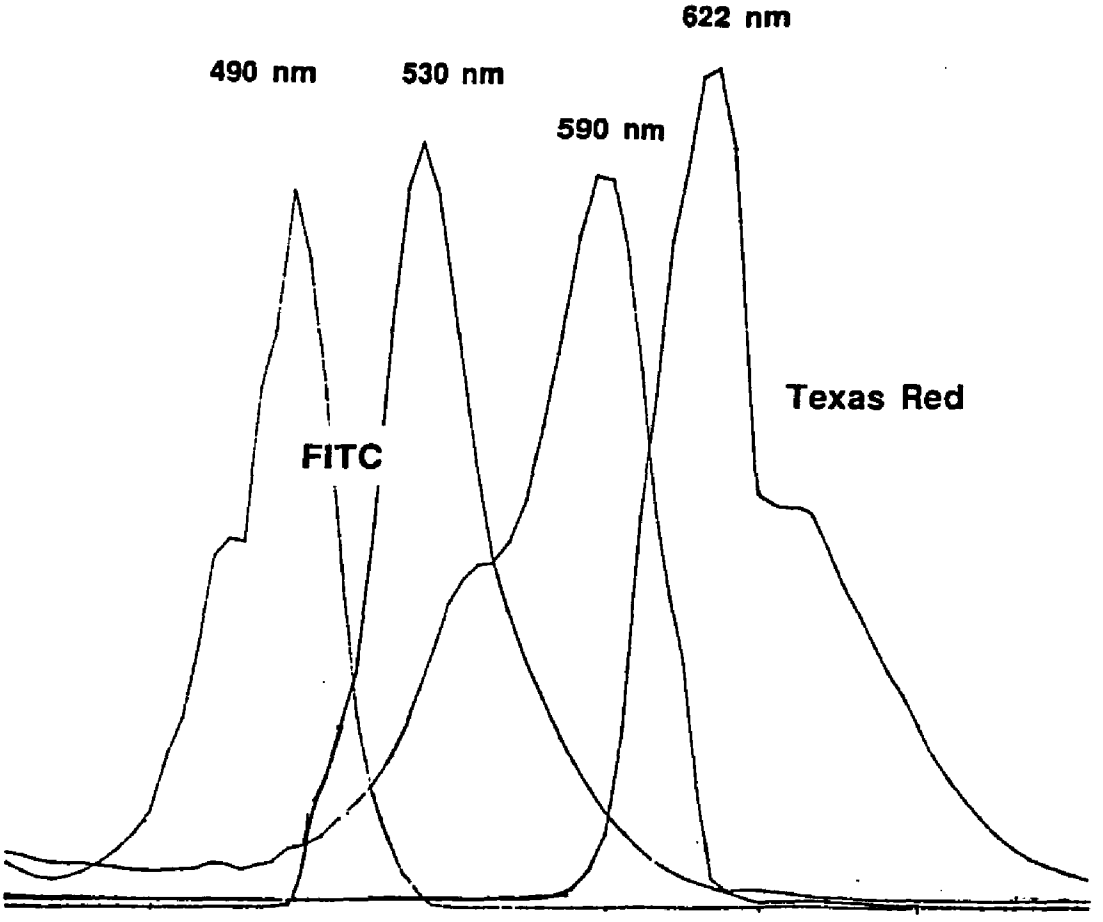

INVESTIGATION OF COUMARIN LABELED DEXTRANS AS AN ENERGY DONOR TO CONA-FITC

Introduction

This section describes systems in which dextran bound coumarins transfer energy to conA-FITC. Coumarin emission overlaps the FITC excitation band, while remaining separated from the fluorescein emission peak. However, many coumarins are excited in the ultraviolet region, which would require fused silica optical fibers in a sensor.

Since conA is available prelabeled with FITC the main problem was to label the dextrans. Because dextrans are not amenable to direct labeling with most coumarins, cyanuric chloride was employed as a linker.

Cyanuric chloride (cc) has previously been used to immobilize fluoresceinamine [14], and other reagents [101]. Cyanuric chloride, 2,4,6-trichloro-1,3,5-triazine, Figure 3.11, reacts with alcohols and amines. The reaction is temperature dependent. The first chloride reacts at 0 °C, the second above 30 °C, and the third above 90 °C [102]. Heating the compound above 150 °C destroys the ring. This temperature dependence provides the opportunity to sequentially attach the cyanuric chloride to the hydroxy groups on the dextran and the amino groups on the coumarin dyes.

A number of coumarin dyes were conjugated to dextran with cyanuric chloride. Coumarin dyes were selected based on their spectral characteristics and the presence of either a hydroxy group or a primary or secondary amino group. Out of the four dyes chosen, the first three all couple to the cyanuric chloride via amino groups. Structures are shown in Figure 3.12.

One of the attractions of this system is the wide variety of coumarin energy

Figure 3.11: Substitution Reactions of Amine and Hydroxyl Groups with Cyanuric Chloride

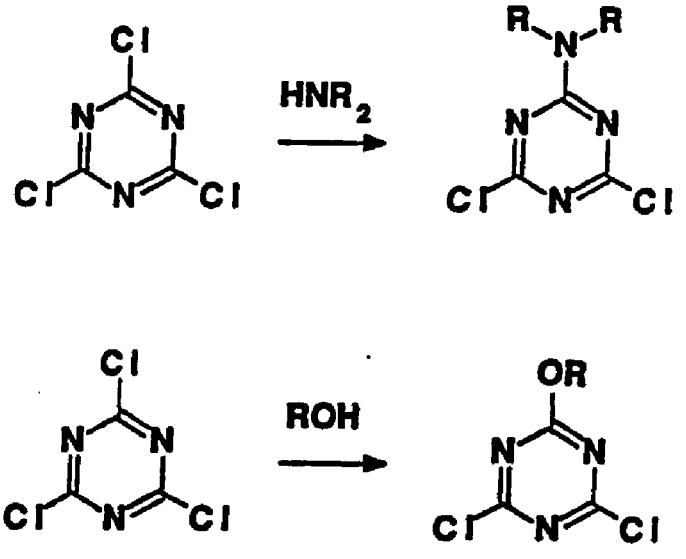

Figures 3.12A-D: Coumarin Structures

A:

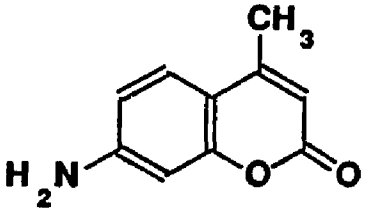

Ex 354 nm
Em 430 nm

Coumarin 120
(7-Amino-4-methylcoumarin)

B:

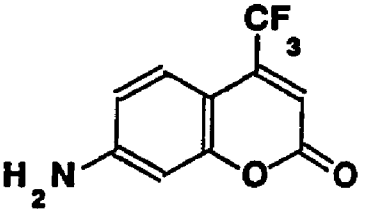

Ex 380 nm
Em 480 nm

Coumarin 151
(7-Amino-4-trifluoromethylcoumarin)

C:

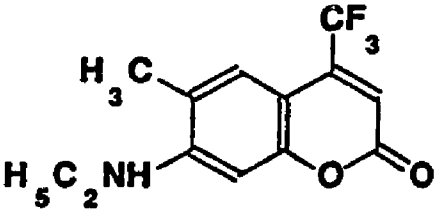

Ex 395 nm
Em 490 nm

Coumarin 307
(7-Ethylamino-6-methyl-4-trifluoromethylcoumarin)

D:

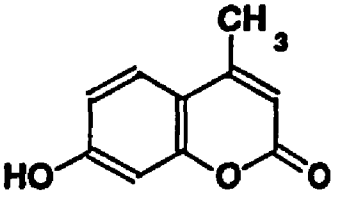

Ex 358 nm
Em 447 nm

HMC
(7-Hydroxy-4-methylcoumarin)

donors. Choosing from the above dyes, it should be possible to design an energy transfer pair which will have both excellent spectral overlap with good spectral separation.

Experimental

Reagents - Prelabeled conA-FITC (Sigma Chemical Co.) acts as the energy acceptor from the coumarin dyes. Coumarin 120, 151, and 307 (Eastman Kodak Co., Laboratory and Research Products, Rochester, NY) and 7-hydroxy-4-methylcoumarin (Aldrich Chemical Co., Milwaukee, WI) were coupled to different molecular weight dextrans (Sigma Chemical Co.) using cyanuric chloride (Aldrich).

Coumarin-Cyanuric Chloride-Dextran Labeling Procedure- The reaction of cyanuric chloride with the coumarin dyes and dextran follows a modified version of the de Belder method [103]. The basic procedure summarized here is typical.

Best results were obtained when the cyanuric chloride was coupled to the coumarin dyes before they were reacted with dextran. Different mole ratios of cyanuric chloride to coumarin dye were produced by dissolving the appropriate weights of both the compounds in an organic solvent (acetone, methanol, or absolute ethanol). While stirring, the mixture was heated to 30 to 35 °C for 20 minutes. The clear colorless solution was transferred to a round bottom flask and the solvent was removed with a rotary evaporator, until a pale yellow solid remained. This was assumed to be the coumarin-cyanuric chloride conjugate.

The coumarin-cyanuric chloride compound was dissolved in an appropriate amount of solvent (acetone, methanol, or absolute ethanol). Dextran was dissolved in water. The two solutions were combined and heated to 90 °C. While maintaining the high temperature the solvent was removed with a rotary evaporator. This

usually took about an hour. The remaining solution, approximately 50 ml, was cloudy with a white precipitate.

The solution was then filtered through Whatman #541 paper. A clear, colorless filtrate was collected and transferred to 10,000 MW (or pore size appropriate for MW dextran employed) dialysis tubing. The white precipitate was washed with copious amounts of solvent (methanol or acetone), tested for fluorescence, and was determined not to be the desired product. After saving a 10 ml aliquot of the solution as a reference, exhaustive dialysis was performed. The 0.025 M, pH 7.2, phosphate buffer bath was stirred at room temperature for up to 4 days, changing the bath a minimum of once a day. The liquid retained in the dialysis tubing was the coum-cc-dex solution.

Labeling efficiency was checked with a Perkin Elmer Model 204 fluorimeter. Fluorescence intensity for the coum-cc-dex solution was compared to the intensity for both the reference aliquot and the bath solution.

Variations on this procedure included: labeling the dextran with cyanuric chloride before reaction with the coumarin dye, varying the dextran to dye ratio, changing the solvents, using different molecular weight dextrans, altering reaction temperatures and times, and the coumarin dyes themselves.

Results and Discussion

The results for the dex-cc-coum to conA-FITC energy transfer pair were the most disappointing of all the pairs investigated. It proved extremely difficult to couple an appreciable amount of the coumarin dye to the dextran. During the dialysis step, most of the coumarin diffused into the bath, indicating that it had not reacted with the dextran or that the dextran had decomposed due to high labeling temperatures. The fluorescence of a 1:1 HMC:dextran (MW 40,000) solution

decreased to 22% of its initial value after an 18 hour dialysis. Higher percent losses were observed when the HMC:dex ratio was increased.

The amino-coumarins bonded somewhat more efficiently than the hydroxycoumarin. A 5:1 mole ratio of coumarin 120:dextran had a 10 % labeling efficiency compared to 3 % with the hydroxycoumarin. Percent efficiency is determined by measuring fluorescence intensity of the coumarin from the dialysis bag, subtracting the bath's fluorescence intensity, and comparing the difference with the reference aliquot.

Energy transfer studies were attempted with the coumarin 120-cc-dextran compound. Addition of conA-FITC caused neither a decrease in the coumarin emission peak height nor an increase in acceptor intensity, indicating a lack of energy transfer.

The above procedure was modified, without success, to try to improve the labelling efficiency. One of the principle problems was the solvent incompatibility between dextran and the cc-coum compound. The cc-coum is very soluble in acetone, slightly soluble in ethanol and methanol, and insoluble in water. Dextran is only soluble in water. This prompted the investigation of acetone, acetone/H_2O (20/50), ethanol, acetone/ethanol (30/70), methanol, acetone/methanol, and methanol/H_2O as possible labeling media. The methanol/water gave the best trade off between cc-coum solubility and minimum dextran precipitation. Reacting cyanuric chloride with dextran prior to coupling to coumarin also failed to improve labelling efficiency.

Experiments were also performed with coumarins purchased prelabeled with the cyanuric chloride linker. These also proved to be unsuccessful. Dextran labeled with 7-hydroxycoumarin produced energy transfer changes on the order of 5 percent. There was also a slight spectral shift of the emission band which can be noted upon reversal of energy transfer when glucose is added, Figure 3.13. The shift could

Figure 3.13: Energy Transfer from 7-Hydroxy-Coumarin to FITC

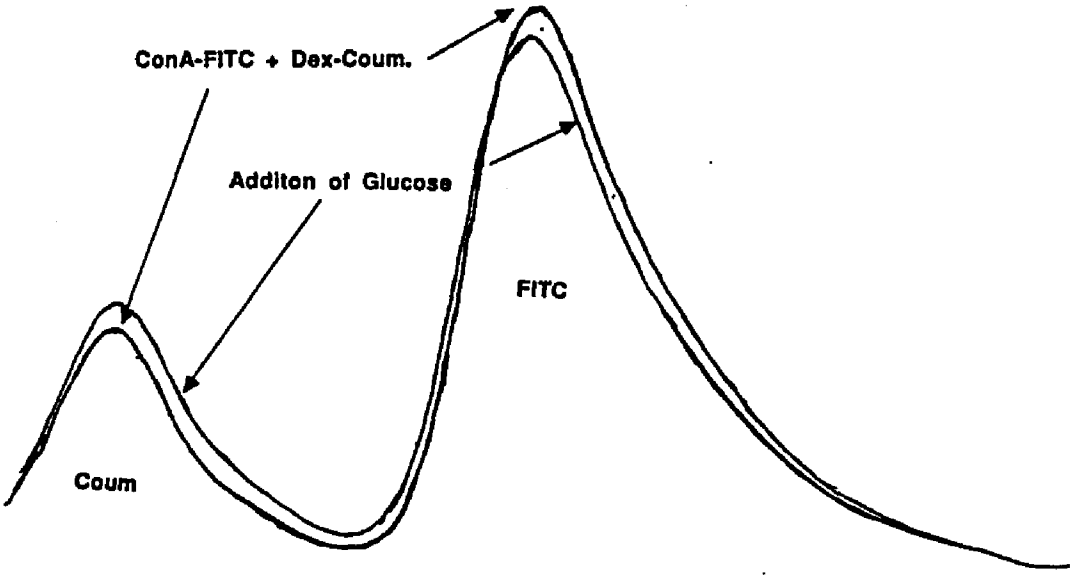

aid in monitoring energy transfer, but due to the small intensity changes the system was not further investigated.

Poor labeling may be due to weak aromatic and amine linkages at pH 7 and/or damage to the dextran molecule by the high labeling temperatures. In any case, this work emphasized the need to work with dyes which are compatible with the protein and dextran.

EVALUATION OF FLUORESCAMINE AND FLUORESCEIN ISOTHIOCYANATE AS FLUORESCENT LABELS FOR ENERGY TRANSFER

Introduction

The fluorescamine (FLNH) to fluorescein isothiocyanate (FITC) pair was evaluated because it has good spectral overlap and proven energy transfer ability. In addition, concanavalin A is readily labeled with FLNH dye. This system differs from previous systems in that the donor is coupled to concanavalin A rather than dextran.

Fluorescamine (4-phenylspiro[furan-2(3H), 1-phtalan]-3,3-dione), Figure 3.14-I, is ideally suited for labeling to primary amines [104,105] and proteins [106,107]. While non fluorescent at alkaline pH's and room temperatures, FLNH reacts almost instantaneously with primary amino groups to yield highly fluorescent pyrrolinones, Figure 3.14-II. Unreacted dye rapidly hydrolyzes to non fluorescent, water soluble furans, Figure 3.14-III [108]. This eliminates the need for dialysis to remove excess dye.

The FLNH to FITC system was successfully employed in an energy transfer immunoassay for study of the antidepressant drug, desmethylnortriptyline [92]. Excitation and emission maxima of the FLNH labeled drug are 390 and 490 nm, respectively, while the fluorescein-IgG conjugate maxima are at 490 and 530 nm.

The FLNH/FITC pair has many advantages. FLNH is exceedingly easy to use since it undergoes rapid, site specific labeling under mild conditions and does not require a lengthy purification process. FITC labeled dextran is readily available, with a wide range of molecular weights, and is soluble in aqueous solutions at the desired pH. In addition the pair has excellent spectral overlap and both are excited

Figure 3.14: Reactions of Fluorescamine with the Primary Amino Group on ConA (II) and Water (III)

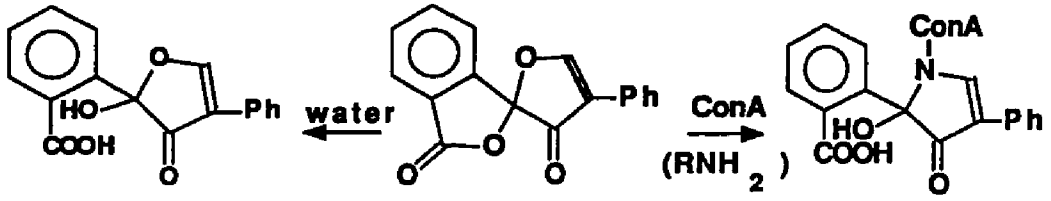

III
hydrolysate
(non fluorescent)

I
FLUORESCAMINE
(non Fluorescent)

II
conjugste
(fluorescent)

in the visible region, permitting the use of glass optical fibers.

Experimental

FLNH-conA conjugates were prepared using the procedure of Bhlem [106]. Concanavalin A (Sigma Chemical Co.) was dissolved in a pH 8.0 phosphate buffer (0.01 M) at room temperature to make a 5.0×10^{-6} M solution. Maximum labeling was achieved by running the reaction at high pH's [109]. A 2.5×10^{-2} M fluorescamine (Sigma Chemical Co.) stock solution was prepared by dissolving a known mass of the solid in 1,4-dioxane (Fisher). The FLNH/dioxane solution was added to 50 mL of the conA/buffer solution using a vortex mixer. Initial FLNH:conA ratios were varied from 2:1 to 50:1 by adding different volumes of the FLNH solution. The mixture was allowed to incubate at room temperature for 2 hours with gentle stirring. After incubation, the conA-FLNH solution was transfered to a 50,000 molecular weight cut off (MWCO) dialysis bag and placed in a 2.0 liter dialysis bath (pH 7.0, 0.25 M) for an additional 12 to 18 hours. Dialysis removes the unbound FLNH and lowers the working pH to a point where conA will bind dextran.

Results and Discussion

Because only fluorescamine which is conjugated to the protein fluoresces, it is not possible to measure labeling efficiency via fluorescence. FLNH binding to conA was estimated by comparing the fluorescence intensities for different initial FLNH:conA ratios. Maximum intensity was observed for 10:1 FLNH:conA, Figure 3.15. Above this ratio fluorescence efficiency fell off.

The fluorescamine and fluorescein energy transfer pair was initially investigated because it was thought that the spectral overlap between the FLNH emission

Figure 3.15 FLNH Intensity for Different FLNH:ConA Ratios

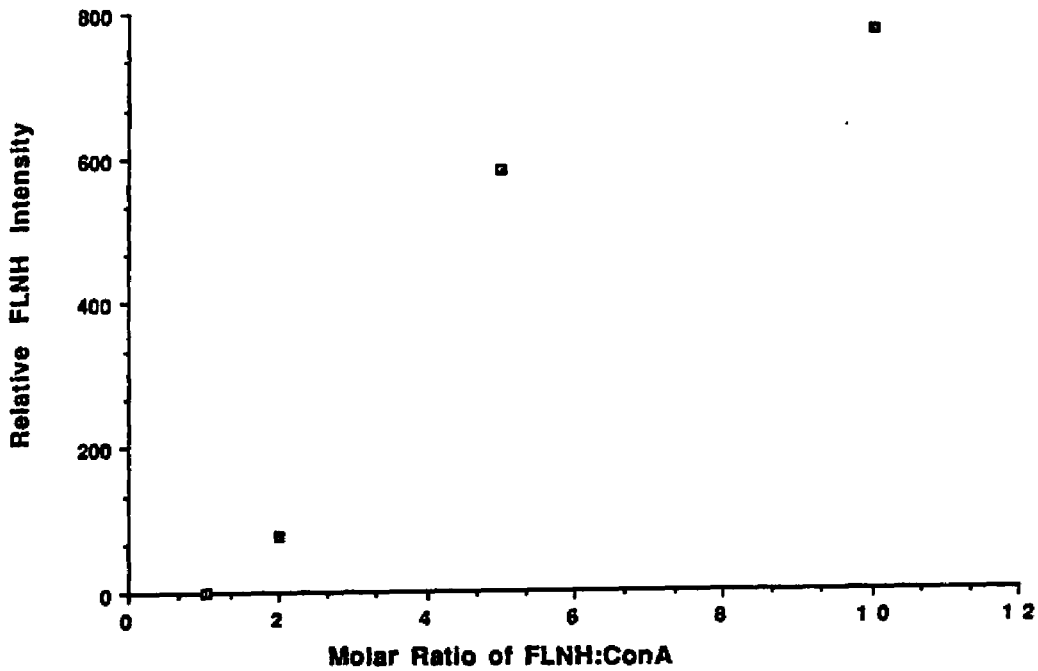

and FITC excitation peaks would lead to efficient energy transfer, Figure 3.16. As long as the critical radius is maintained, there exists a high probability that fluorescence energy will be transferred.

One weakness of this system is that the broad FLNH emission band also overlaps the FITC emission peak, Figure 3.16. A second problem is the small FITC excitation side peak at the same wavelength as the FLNH absorption maximum which results in direct FLNH excitation.

There is ample evidence that fluorescence energy is transferred from fluorescamine to fluorescein. One of the first experiments was to compare energy transfer for active concanavalin A to denatured conA. Protein was labeled with FLNH and half the sample was denatured by exposing it to high temperatures. Denatured protein retains its fluorescent label but does not bind dextran. Adding 1.0×10^{-6} M dex-FITC did not affect the FLNH intensity for the denatured protein. Yet, the same dex-FITC concentration induced a 24 percent decrease in donor intensity for the active conA-FLNH.

A series of energy transfer experiments were performed varying both the FLNH labeling on conA and the conA to dextran ratio. Results are summarized in Table 3.5. Analysis of the data indicates that both the amount of FLNH label on the protein and the conA:dex ratio influence the efficiency of energy transfer.

Increasing the labeling ratio from 5:1 to 10:1 produces a higher degree of energy transfer. This is expected since the larger FLNH concentration increases the probability that a fluorescent donor will be located near an acceptor. At 30:1, FLNH:conA the excess label inhibits protein activity as well as creating a larger background signal.

The probability that a fluorescent donor will be located within the critical radius of the acceptor is also increased when the protein to dextran ratio is raised. Increasing the conA:dex ratio from 6:1 to 9:1 causes a corresponding relative signal

Figure 3.16: Excitation and Emission Spectra for FLNH and FITC

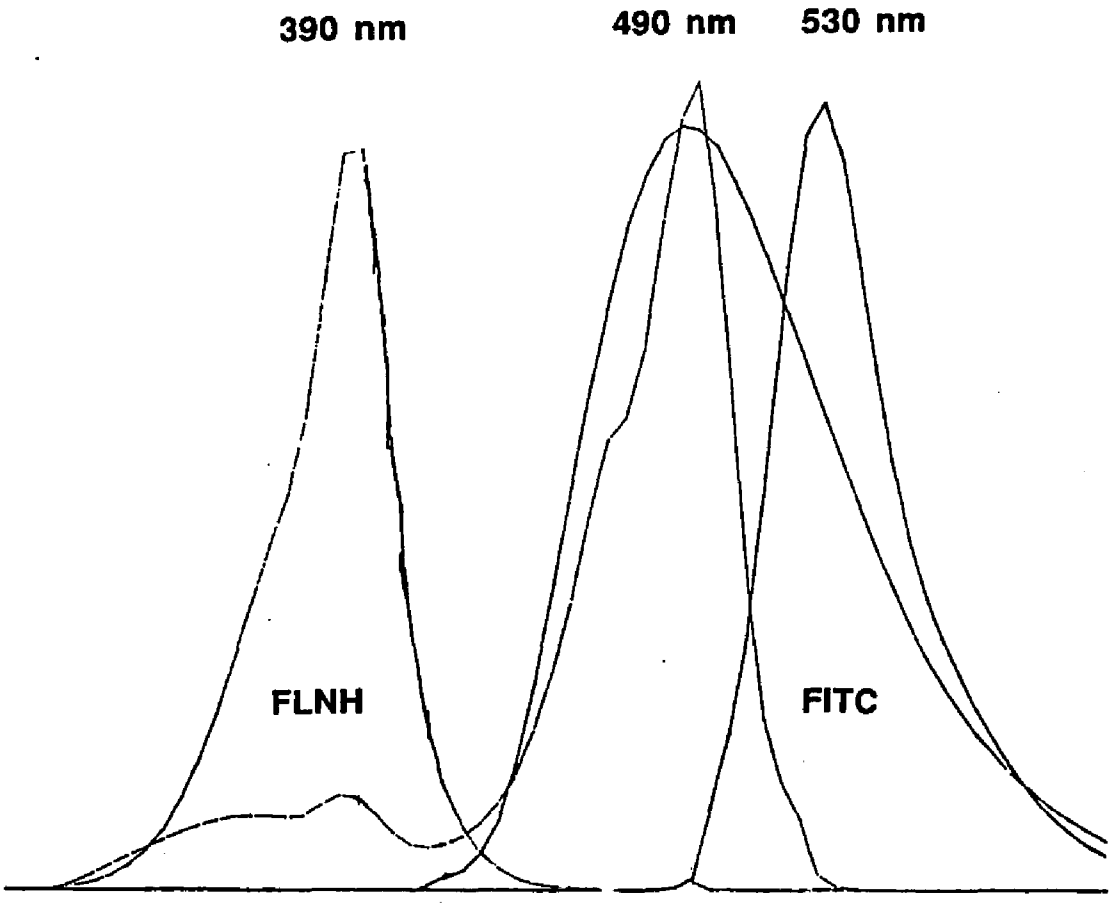

Table 3.5: Measure of Energy Transfer From ConA-FLNH to Dex-FITC

FLNH:ConA	ConA:Dex	% Decrease in FLNH Intensity
5:1	5:1	16 %
10:1	6:1	26 %
10:1	9:1	32 %
30:1	50:1	25 %

decrease of 26 to 32 percent. The higher efficiency may be partially due to the binding of multiple protein units to one dextran.

At very low dex-FITC concentrations the FLNH peak is easy to measure, but no FITC peak is present so a ratio measurement is not possible, Table 3.6, line 1. When both peaks are observed a ratio measurement is possible, lines 2-4, but due to the broad FLNH emission band which overlaps the FITC peak, the ratio is not proportional to added acceptor.

This lack of resolution precludes a routine simultaneous dual wavelength measurement. The resolution problem is exacerbated by a hump in the FITC excitation spectrum at the maximum wavelength of the FLNH excitation creating a large amount of directly excited FITC emission. Choosing an excitation wavelength off the peak maximum, 390 nm, reduces direct excitation of FITC but does not entirely eliminate the problem. Relative FITC emission, measured at 530 nm, varied with excitation wavelength with intensities of 50, 64, and 32 percent, of maximum FITC intensity, for excitation wavelengths of 380, 400, and 415 nm, respectively.

Table 3.6: Energy Transfer from FLNH to FITC

Vol. Dex-FITC (1.0×10^{-5} M)	FLNH Peak Height (cm)	FITC Peak Height (cm)	Ratio FITC/FLNH
0	8.6	-	
1 25 uL	7.2	n.p.	
2 50 uL	6.7	8.4	1.2
3 75 uL	7.4	11.1	1.5
4 100 uL	7.2	12.8	1.8

n.p. = no peak above FLNH base line.
ConA concentration = 1.8×10^{-6} M
ConA volume = 5.0 mL
n.p. = no peak

EVALUATION OF METHYLCOUMARIN AS AN ENERGY DONOR TO DEX-FITC

Introduction

This section describes the use of 7-diethylamino-3-(4'-isothiocyanatophenyl)-4-methylcoumarin (CPI), Figure 3.17, as an energy donor to fluorescein. The coumarin dye was conjugated to conA in house while prelabeled dex-FITC was employed as the acceptor. The coumarin/fluorescein pair has previously been utilized to demonstrate the energy transfer phenomenon [110] and to confirm Forster's Theory [111]. In addition, CPI has been studied as an energy donor to fluorescein for a laser dye application [100].

The advantage of utilizing coumarin as a donor is that the reported excitation and emission spectra are well suited for energy transfer to FITC [98]. Because coumarin's excitation band is at approximately 360 nm, far from the FITC excitation band at 490 nm, direct excitation of the acceptor dye should be minimal.

The reported CPI emission maximum is 460 nm in methanol, so there should be good spectral overlap with the FITC absorption band. In addition, these wavelengths could result in excellent spectral resolution between the donor and acceptor emission peaks. The only disadvantage is that coumarin is excited in the ultraviolet.

Experimental

Reagents - CPI was obtained from Molecular Probes Inc. and labeled to concanavalin A (Sigma Chemical Co.). Prelabeled dex-FITC (4000 MW dextran with 0.004 moles FITC/glucose, Sigma Chemical Co.) was employed as the energy accep-

Figure 3.17: Structure of CPI

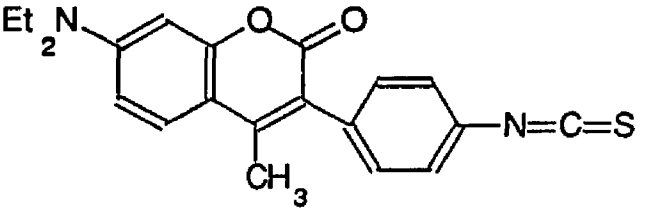

7-diethylamino-3-[4'-isothiocyanatophenyl]-
4-methylcoumarin (CPI)

tor.

Labeling Procedure - A known mass of 55,000 MW conA was dissolved in a pH 8.5 TRIS (Tris[hydroxy]aminomethane/HCl) buffer, 0.05 M. Addition of a known mass of coumarin, dissolved in dimethlyforamide (Aldrich), to the conA solution provided different dye:protein ratios. For a 1:1 CPI:conA label, 1.00 mL of 5.5 x 10^{-4} M CPI was added to 100.0 ml of 5.5 x 10^{-7} M conA (pH 8.5) using a vortex mixer. The solution was allowed to incubate for 2 to 4 hours at 0-5 °C.

An affinity separation was then performed using a cross linked dextran column (Sephadex G-70-50) equilibrated with 0.10 M NaCl. After adding the conA-coumarin mixture the column was washed with a pH 7.2 buffered 0.10 M NaCl solution to removed the denatured protein as well as any free coumarin. Active conA was eluted with a 0.10 M glucose/0.10 M NaCl solution buffered to pH 7.2. Fractions were monitored at 280 nm for the conA, and 390 nm for the coumarin with a Shimadzu Model 200UV Absorbance Spectrophotometer. Glucose was removed from the protein by exhaustive dialysis in a 0.05 M pH 7.2 bath, using 4000 molecular weight cut off dialysis tubing. The dialysis time was 3 to 4 days with 12 hour bath changes.

Results and Discussion

Despite the favorable spectral overlap of the donor emission and acceptor excitation bands and the good reported resolution, between coumarin and fluorescein emission, CPI does not serve as a practical energy donor to FITC.

Affinity purification studies showed that active conA was labeled with CPI. However, upon binding to the protein, the CPI emission peak shifted almost 60 nm from the literature value, placing it nearly on top of the FITC emission peak at 530 nm.

Figure 3.18 shows the excitation and emission spectrum for free CPI and dex-FITC. The overlap of CPI, and FITC, emission is already significant. Upon binding to the protein the CPI emission is shifted to about 515 nm. The shift confirms that labeling took place, but prevents a simple dual wavelength measurement.

In spite of the poor spectral resolution energy transfer studies were still performed, prompted mostly by the excellent overlap of the donor's emission with the excitation band of the acceptor.

The most successful system involved affinity purified conA with an initial 2:1 CPI:conA label. Addition of 1.0×10^{-4} M dex-FITC to 5.0 mL of conA-CPI produced a 19 % decrease in donor fluorescence, Table 3.7. However, if too high a ratio of dex-FITC:conA-CPI was used, energy transfer was not readily observed because the excess FITC signal masked the decrease in CPI intensity. Most of the CPI fluorescence intensity was restored when excess glucose was added to a conA-CPI/dex-FITC mixture, Table 3.8.

As with the fluorescamine to fluorescein pair, the problem with the CPI to FITC energy transfer pair is that the emission peaks of the donor and acceptor overlap, precluding a simple energy transfer measurement. Therefore, extensive studies to determine the final labeling ratio and conA concentration after purification were not deemed necessary.

Figure 3.18: Excitation and Emission Specta of CPI and FITC

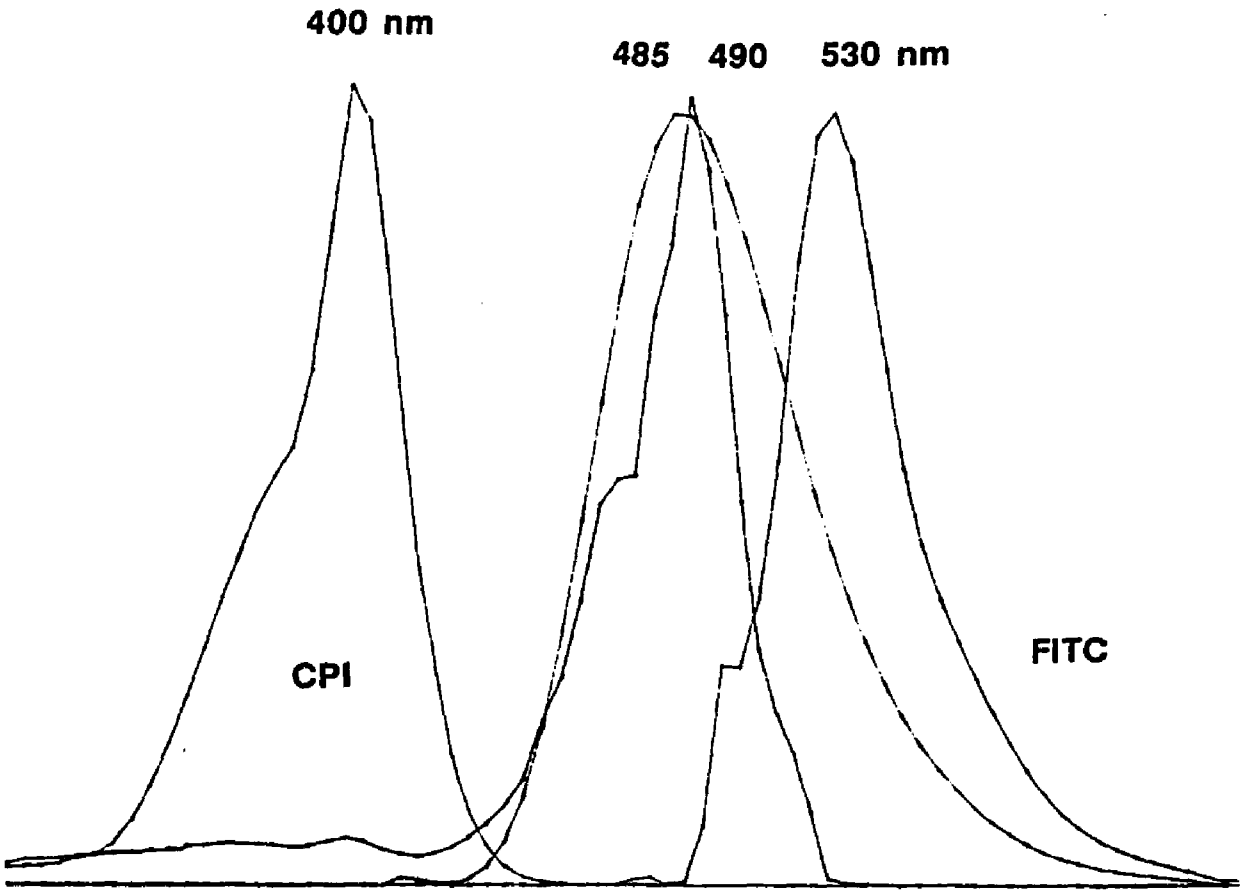

Table 3.7: Energy Transfer From CPI To FITC

Vol. Dex-FITC (1.0×10^{-6} M)	CPI Peak Height *	Percent Change
0	12.9 cm	-
10 uL	11.8 cm	14%
30 uL	10.4 cm	19%

* 5.0 mL of 4×10^{-6} M ConA

CPI Monitored at 485 nm

Table 3.8: Glucose Reversal of Energy Transfer

Vol. Dex-FITC (1.0×10^{-6} M)	CPI Peak Height	Percent Decrease	Percent Recovery
0	11.25 cm	-	-
10 uL	9.25 cm	18 %	-
10 uL + Glucose	10.70cm	-	72 %

CPI monitored at 485 nm

EVALUATION OF BOTH THE DONOR (COUMARIN) AND ACCEPTOR (FITC) DYES LABELED TO DEXTRAN

Introduction

Thus far all the energy transfer systems investigated involved separately labeled dextran and concanavalin A. Binding of dextran to conA brought the donor and acceptor dyes close enough for energy transfer to take place. A different approach is to conjugate both the donor and acceptor dyes to the dextran.

Dextran in solution is folded over on itself. Upon binding to the single site on each concanavalin A sub unit, the dextran stretches out. Partial uncoiling of the dextran is required for it to fit into the small binding pocket of conA [48].

It is proposed that when folded over on itself the donor and acceptor dyes, bound to the dextran, will maintain the critical radius necessary for energy transfer. Upon binding to conA, the dextran backbone is extended causing the critical radius to be exceeded and thus disrupting energy transfer. Addition of excess glucose displaces dextran from the binding site, allowing the dextran to once again fold over, reestablishing energy transfer, Figure 3.19.

The coumarin to FITC dye pair was chosen due to the good reported spectral resolution between the donor and acceptor fluorescence peaks, 430 and 530 nm, respectively.

Triazinyl coumarin (TPC), Figure 3.20, reacts directly with the hydroxy groups on the dextran [102].

Experimental

Reagents and Labeling Procedure - Dextran, MW 9000, was purchased

Figure 3.19: Idealized System With Both The Donor and Acceptor Dyes Labeled To Dextran

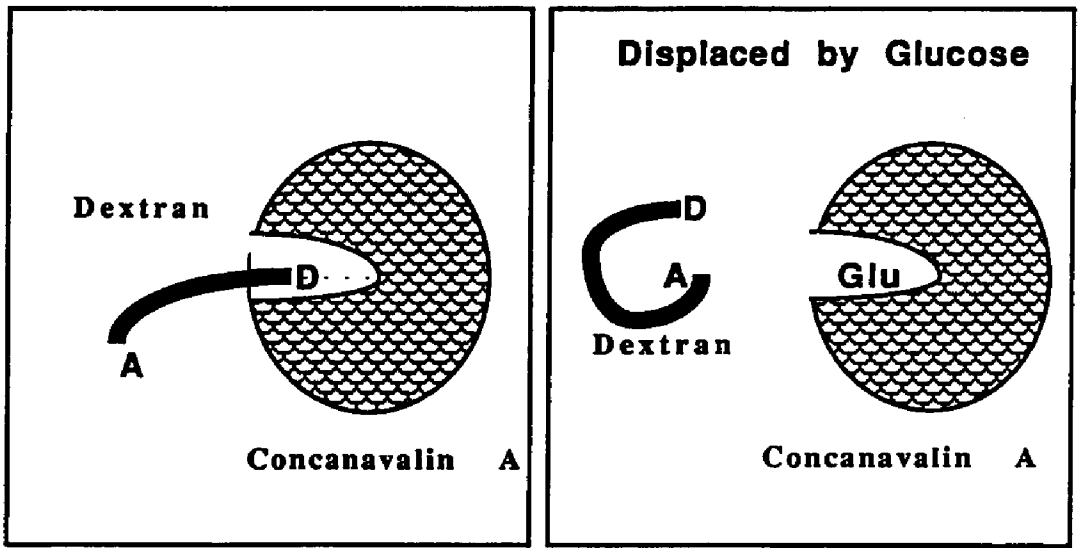

No Energy Transfer

Energy transfer

Figure 3.20: Structure of Triazinyl Coumarin (TPC)

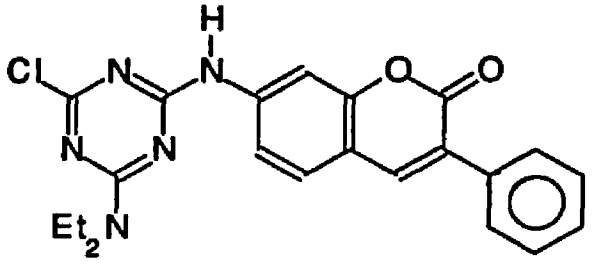

7-[[4-chloro-6-diethylamino]-s-triazin-2-yl]amino-3-phenylcoumarin

prelabeled with FITC, 0.010 moles FITC per mole of glucose (Sigma Chem. Co.) resulting in a dex:FITC ratio of 2:1. The dextran was then labeled with a 1:1 mole ratio of (7-(((4-chloro-6-diethylamino)-s-triazin-2-yl)amino)-3-phenylcoumarin), TPC (Molecular Probes).

To label the dextran, 0.0090 grams of TPC was dissolved in 10 mL of acetonitrile (Baker) and then added dropwise, with stirring, at room temperature, to 50.0 mL of a 1.0×10^{-5} M dex-FITC/phosphate buffer (pH 7.0) solution. A 1:2 conjugate of TPC:dex was also prepared. To deactivate the final chloride on the triazinyl ring, the solution was heated to 90 °C (∓5 °C) for 3 hours [102].

Results and Discussion

Unlike the previous energy transfer systems, a large excess of one dye over the other is not desirable. Therefore, donor:acceptor dye ratios of 1:1 and 2:1 were chosen for study. Also, a large molecular weight dextran is not beneficial. Since only the section of dextran in the binding site is disrupting energy transfer, the dextran extending out of the pocket will continue to be subject to transfer of energy. The larger the tail the greater the constant fluorescence background.

To minimize direct excitation of the FITC, while still maintaining high donor quantum yield, the excitation monochromator was set at 360 nm. Spectra were then recorded for TPC-dex-FITC with and without concanavalin A, and with excess glucose. The TPC peak intensities for the three spectra were measured and compared. Upon addition of conA the donor intensity increased and upon introduction of excess glucose a decrease in TPC intensity was observed. The trend was consistant for every experiment, but the actual changes were erratic, Table 3.9. Trials 1 and 2 are replicates as are trails 3 and 4. "Percent TPC Increase" is defined by the percent gain in TPC peak height, after addition of conA, over the TPC-dex-FITC

Table 3.9: Coumarin Intensity Changes Upon Exposure To ConA and Glucose

	TPC:FITC	% TPC Increase[1]	% TPC Decrease[2]
1	1:1	86 %	76 %
2	1:1	142 %	44 %
3	2:1	23 %	100 %
4	2:1	44 %	76 %

1. Mixture of 3.0 mL of 1.0 x 10^{-5} M TPC-Dex-FITC and 10.0 mL of 1.0 x 10^{-6} M ConA.

2. Mixture of 3.0 mL of 1.0 x 10^{-5} M TPC-Dex-FITC and 10.0 mL of 1.0 x 10^{-6} M ConA plus Glucose.

Reference Spectra is of 3.0 mL of 1.0 x 10^{-5} M TPC-Dex-FITC in 10.0 mL of Blank Solution.

without conA. "Percent TPC Decrease" is the intensity change of TPC-dex-FITC after addition of excess glucose.

Accuracy of the TPC peak height measurement was compromised by noise contributing to the reproducibility problem. The noise spikes are a result of the high gain necessary to amplify the TPC signal. Low TPC intensity is due both to its low molar absorptivity compared to FITC, 20000 versus 75000 [98], and poor labeling of the dye to the dextran. The labeling problems encountered in the dextran-cyanuric chloride section were not completely overcome with the triazine labeled coumarin.

The observed change is possibly due to energy transfer between TPC to FITC but is more probably a result of interaction between the conA and coumarin dye. If energy transfer were taking place the FITC emission would also change. However, this change is not observed, Figure 3.21.

Figures 3.21: Spectra of TPC and FITC Emission Upon Introduction of ConA and Glucose

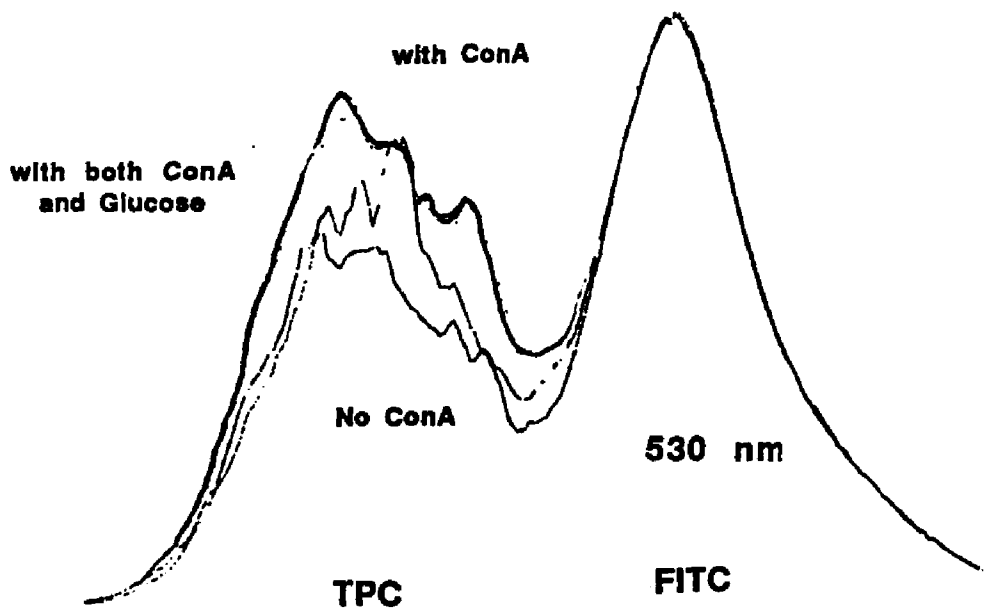

OTHER SYSTEMS

A number of energy transfer systems were investigated but not fully developed. Two of the more interesting ones include a non-energy transfer system using Dansyl Chloride, and a FITC to Procion Red energy transfer system.

Dansyl Chloride, which is an environment sensitive fluorophor, was labeled to dextran. Upon specific attraction of the dextran to the conA, the environment around the dansyl dye changes and its emission characteristics are altered. In practice the system did not show any change due to dextran-conA interaction.

However, the dansyl-dextran study did prompt work with procion red which in turn acted as the feasibility study for the coum-dex-FITC system. Procion Red does not fluoresce, but it can accept fluorescent energy from other dyes. The procion red was bonded to a dextran prelabeled with FITC. The energy transfer behavior is the same as with the TPC-dex-FITC. Fluorescence energy was transferred from the donor to the acceptor, in this case FITC and procion red, respectively. Exposure to conA causes the coiled dextran to extend in to the protein's binding site disrupting energy transfer. Glucose reestablished energy transfer when it displaced dextran.

Procion red accepted energy from the FITC and addition of conA produced a reproducible 4 to 6 % decrease in FITC intensity. An increase in FITC peak height was observed upon addition of glucose. Since procion red does not fluoresce it would not produce the desired dual wavelength measurement. While the changes were too small to warrant further study, the system did show that labeling both the donor and acceptor to dextran was feasible.

CHAPTER IV

THE FIBER OPTIC GLUCOSE SENSOR

Introduction

Results of the energy transfer studies were mixed. Some systems were successful, others were marginal or failed altogether. Systems that did not display promise were quickly discarded after a cursory investigation. It is possible that one or more of these systems could be significantly improved with further study.

The dextran-FITC to conA-TRITC system was most successful. Addition of conA-TRITC diminished the FITC donor intensity up to 20 percent, or more. Introduction of excess glucose enhanced the FITC intensity with up to a 55% peak recovery. The results compare favorably with Schultz's work, which produced a 20 percent decrease and a 60% recovery [95].

Energy transfer efficiency can be maximized by increasing the concentration of FITC. By increasing the donor concentration there is a greater chance that there will be an acceptor dye within the critical radius for energy transfer. Another favorable attribute of the FITC/TRITC pair is that both are excited in the visible region, allowing the use of inexpensive glass fibers in sensor work. More importantly, at certain FITC:TRITC dye ratios, there is sufficient resolution between the two emission peaks to allow a dual wavelength measurement. Therefore, the FITC to TRITC was chosen for use in the optical glucose sensor.

Although FITC-TRITC can be used for two wavelength intensity measurements, only the reduction of FITC emission intensity due to energy transfer was

monitored. The second detection channel was used to reference the source.

A working curve was generated with fluorescein standards to characterize the instrument's performance for use with the glucose sensor.

Response to Fluorescein

Isomer I of Fluorescein-5-isothiocyanate (FITC, Molecular Probes, Inc.), Figure 4.1, has a reported molar absorptivity of approximately 5 x 10^4, at λ_{max}(494 nm), in methanol, smaller than that of Rh 6G [95]. FITC excitation and emission wavelength maxima were determined with the SLM spectrofluorometer to be 490 and 520 nm, respectively, in pH 7.2 phosphate buffer. FITC standards were prepared by sequential dilution of a 1.0 x 10^{-5} molar solution.

Samples were excited with 480 nm light by setting the laser dye micrometer slide to 1.375 units. Three different interference filters were used in conjunction with the FITC standards. Two of the interference filters had a 10 nm bandwidth at 1/2 height, a 532 nm filter and a 550 nm filter. The third filter had a 1 nm bandwidth at 1/2 height with maximum transmittance at 550.6 nm.

When generating the FITC working curves all source corrected sample signals were calculated using the second slope method, where the slope and intercept are calculated from the reference and sample signal data of the sample "blank". (See Chapter 2.)

Tables 4.1 through 4.3 show the response to fluorescein standard solutions using the three different interference filters. The 532 nm filter was chosen since it is close to the emission maximum for FITC. In an attempt to reduce backscatter, two 550 nm interference filters were employed. Both of these filters provide improved spectral resolution from background due to laser dye fluorescence. A comparison of 10 nm and 1 nm bandwidth 550 nm filters are presented in Tables 4.2 and 4.3,

Figure 4.1: Structure of FITC

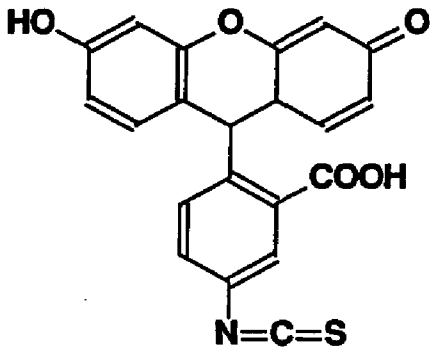

Table 4.1: FITC Working Curve Using 532 nm Interference Filter (10 nm bandwidth)

Sample	Corrected Signal	Rel. Std. Dev.	# of Data Points
Blank	1.00	0.01	12
1.0×10^{-9}	1.02	0.01	7
5.0×10^{-9}	1.03	0.01	7
1.0×10^{-8}	1.06	0.03	7
5.0×10^{-8}	1.13	0.01	4
1.0×10^{-7}	1.21	0.02	6
5.0×10^{-7}	1.69	0.03	4
1.0×10^{-6}	2.49	0.08	4

Slope = 0.81
y-intercept = 179 ADALAB Units

Table 4.2: FITC Working Curve Using 550 nm Interference Filter (10 nm bandwidth)

Sample	Corrected Signal	Rel. Std. Dev.	# of Data Points
Blank	0.99	0.02	8
1.0×10^{-9}	1.02	0.01	6
5.0×10^{-9}	1.01	0.02	9
1.0×10^{-8}	1.03	0.02	7
5.0×10^{-8}	1.30	0.01	6
1.0×10^{-7}	1.59	0.02	5

Slope = 0.52
y-intercept = 200 ADALAB Units

Table 4.3: FITC Working Curve Using 550 nm Interference Filter (1.0 nm bandwidth)

Sample	Corrected Signal	Rel. Std. Dev.	# of Data Points
Blank	0.99	0.04	13
1.0×10^{-9}	1.04	0.04	10
5.0×10^{-9}	1.10	0.04	10
1.0×10^{-8}	1.11	0.03	11
5.0×10^{-8}	1.32	0.06	9
1.0×10^{-7}	1.61	0.04	10

Slope = 0.76
y-intercept = 30 ADALAB Units

respectively.

In Table 4.1 the raw sample data was source corrected utilizing a slope of and y-intercept of 0.81 and 179 ADALAB units, respectively. These values reduced a 14 % raw sample signal variability to 1 %. The exceptional precision was partly due to the relative stability of the nitrogen laser pump source which had an average deviation of less than 4 percent for that particular experiment, well below the normal 10 % precision. A detection limit of about 5.0×10^{-9} M was obtained using FITC standards. Other FITC working curves were similar but with poorer precision.

The signal to background was improved with the use of 550 nm filters. Tables 4.2 and 4.3 show a greater increase in FITC intensity per standard, relative to background, than in Table 4.1. As with the 532 nm filter the detection limit is about 5.0×10^{-9} molar, Figure 4.2. Detection levels are not as low as those obtained with the Rhodamine 6G standards in Chapter 3.

Response to Glucose

The final experiment was to evaluate response to glucose using laser excitation through a single fiber. Intensities were measured with the 532 nm filter. Source fluctuations were corrected using the second slope correction method described in Chapter 2. Measurements were made by immersing the fiber end directly into the reagent solution and then adding the analyte, rather than containing the reagent in dialysis tubing. This allows for a more rapid and reproducible measurement.

Initially 25 ul of 1.0×10^{-6} M Dex-FITC was added to 4.0 mL of the blank solution, Figure 4.3-A. In place of the 18,900 and 71,600 molecular weight dextrans used in the FITC to TRITC energy transfer studies in Chapter 3, 148,000 MW dextran is utilized. Because this material is more heavily labelled, 0.005 moles FITC

Figure 4.2: FITC Working Curve with a 532 nm Interference Filter

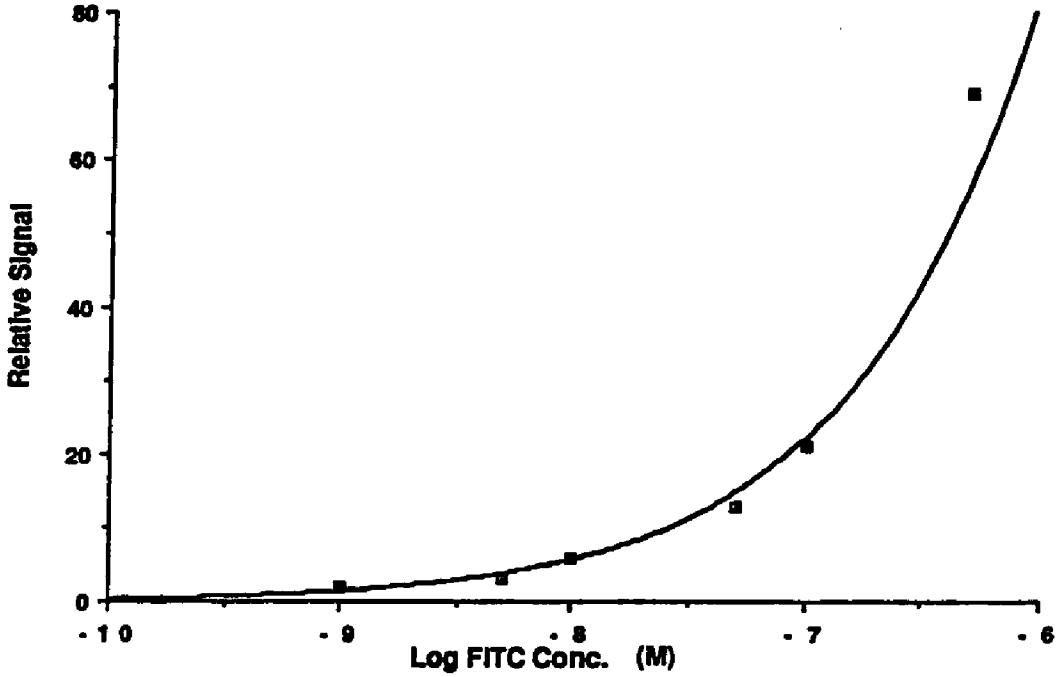

per mole of glucose, the probability of energy transfer is greater. After dilution, the concentration of dextran was 6.2×10^{-9} M and the corresponding FITC concentration was 2.5×10^{-8} M. The FITC signal intensity was measured several times, averaged, and the relative standard deviation was calculated.

The next procedure was to measure fluorescein intensity after adding 25 uL of the same Dex-FITC solution to 4.0 mL of 1.0×10^{-6} M ConA-TRITC, Figure 4.3-B. This mixture results in a conA:dex ratio of 170:1, which is higher than the ratios in Chapter 3 where it was shown that a higher ratio improves the probability of energy transfer.

Finally, energy transfer was reversed by adding 20 uL of 0.10 M D(+)Glucose to the Dex-FITC and ConA-TRITC solution, Figure 4.3-C. An increase in FITC intensity indicates that energy transfer is being reversed.

Raw data for the blank and three energy transfer solutions were corrected, using the procedure outlined in Appendix 4, for source fluctuations, averaged, and the relative standard deviations were calculated, Table 4.4. A summary of that data, Table 4.5, shows that after subtraction of the blank there was a decrease in FITC intensity when the ConA-TRITC solution was added. More importantly, FITC intensity was enhanced by adding glucose. The intensity of the 2.5×10^{-8} M FITC, in the absence of added ConA-TRITC, fell on the FITC calibration curve, Figure 4.2.

Although the data follow the expected trends and mimic the FITC-TRITC data from Chapter 3, the precision is too poor to draw any detailed conclusions. Examination of the data indicates that while the Dex-FITC/Blank solution, 9.6∓, is significantly different from both the Dex-FITC/ConA-TRITC solution, 8.0∓ 1.0 units, and the Glucose solution 8.5∓ 0.95 units, the Dex-FITC/ConA-TRITC is not significantly different from the glucose sample. The trend is there but the large deviation keeps the numbers from being significant. This was supported by other experiments which showed a similar trend but the associated error was even greater.

Figure 4.3: Energy Transfer Solutions

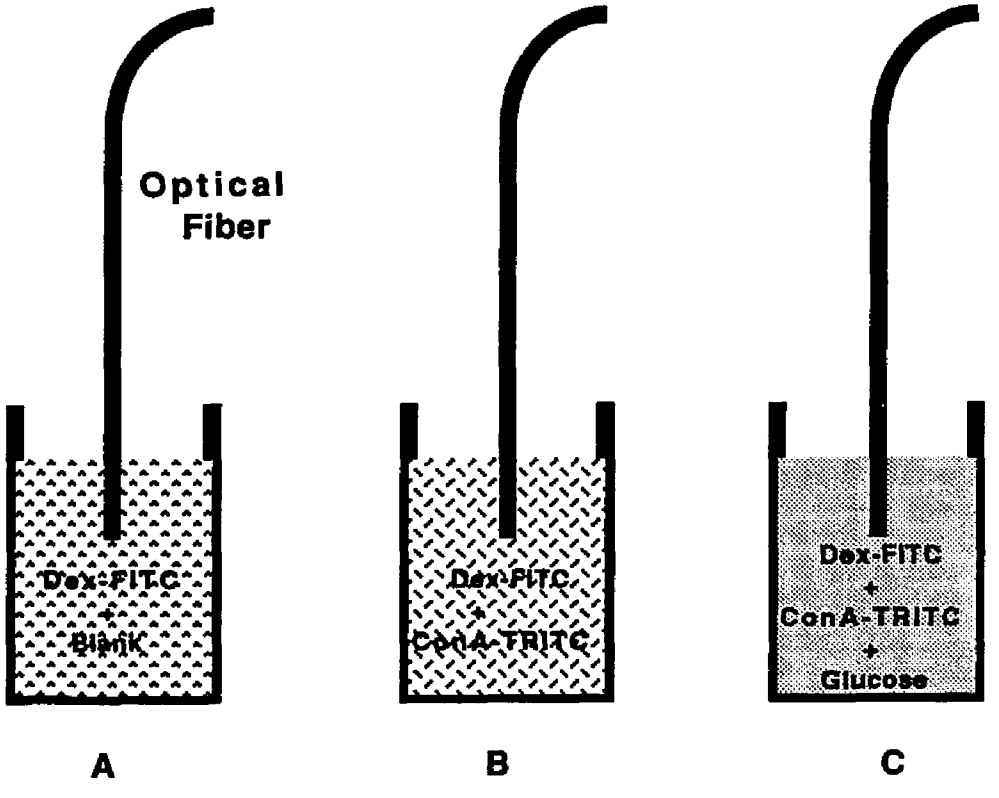

Table 4.4: Sample Data For Energy Transfer Study

	Raw Sample Signal	Corrected Sample	Reference Signal
Blank	693	0.99	658
	715	1.02	671
	684	1.01	609
	677	1.00	620
	653	0.97	602
	683	1.00	630
	690	0.98	678
	709	1.01	661
	658	0.97	623
	682	1.03	596
	683	1.00	630
	684+/-18	1.00+/-.020	635+/-29

Slope = 0.47, y-intercept = 388

Dex-FITC + Blank	763	1.092	662
	764	1.113	635
	763	1.101	650
	736	1.083	621
	741	1.098	612
	762	1.106	643
	738	1.079	631
	752+/-13	1.096+/-.011	636+/-17
Dex-FITC + ConA-TRITC	723	1.068	613
	766	1.097	659
	776	1.106	666
	722	1.071	609
	719	1.062	616
	739	1.080	630
	741+/-22	1.080+/-.016	633+/-22
Dex-FITC + ConA-TRITC + Glucose	750	1.088	642
	718	1.071	601
	778	1.104	674
	731	1.067	633
	738	1.086	620
	744	1.092	625
	743+/-19	1.085+/-.012	632+/-22

Table 4.5: Data Summary of FITC Intensity Changes Monitored With The Optical Glucose Sensor

	Averaged FITC Signal (ADALAB Units)
25 ul Dex-FITC + 4.0 ml of Blank Solution.	9.6 +/- 0.86
25 ul Dex-FITC + 4.0 ml of ConA-TRITC	8.0 +/- 1.0
25 ul Dex-FITC + 4.0 ml of ConA-TRITC + 20 ul of 0.10 M Glucose	8.5 +/- 0.95

Stock Solution Concentrations (M)	
Dextran	1.0×10^{-6}
FITC	4.0×10^{-6}
ConA	1.0×10^{-6}
TRITC	2.0×10^{-6}

Diluted FITC concentration is 2.5×10^{-8} M

For most applications the error problem could be minimized by increasing the reagent and ligand fluorophor concentrations so that the percent error is reduced. The error, ∓ 2% of a 1.00 unit corrected baseline, Table 4.4, is mostly dependent on the boxcar integrator and is thus fairly constant. However, when the percent error is calculated for the baseline corrected sample signal the actual percent error associated with the energy transfer data above is on the order of 15 percent. By increasing fluorophor concentration the sample signals increase while the absolute error remains almost constant.

Unfortunately the fluorophor concentrations in the glucose sensor are limited by a number of physical parameters. To assure that the ConA binds the dextran one or both concentrations have to exceed their binding constant, which requires a concentration of approximatly 1×10^{-5} M. Also, experimentation has shown that energy transfer is most efficient when the TRITC concentration exceeds the FITC concentration. This means that the TRITC labeled ConA concentration should be higher than the Dex-FITC concentration. However, the ConA solubility in the pH 7.2 phosphate buffer is about 1×10^{-5} M, which is the minimum concentration necessary for efficient binding of the ConA to the dextran. Therefore, only more efficient labeling can appreciably increase the concentrations of the TRITC and FITC. It may also be possible to manipulate the donor and acceptor dye concentrations by labeling the dextran with TRITC and the conA with FITC.

The glucose sensor proved feasible but impractical due to the large, constant error associated with the boxcar averagers. To improve sensor performance either the fluorescein concentration needs to be increased or the background needs to be reduced. A possible solution my be to label the conA with FITC and the dextran with TRITC.

CHAPTER V

CONCLUSION AND FUTURE WORK

An optical sensor based on competitive binding and energy transfer has several advantages over conventional solution fluorescence methods. Dual wavelength monitoring allows both the glucose concentration to be determined while compensating for source fluctuations. In addition, since all components are contained in a single homogeneous solution, the sensor would be easy to miniaturize. This is important to reduce response time which is primarily limited by mass transfer. Finally, the procedure is general and can be applied to a host of analytes including drugs and hormones using antibodies as reagents [79].

In practice the concentration range of the glucose sensor is limited by the insolubility and instability of the conA. To improve these characteristics it may be possible to chemically modify the protein.

To improve the sensor's sensitivity a higher degree of labeling is necessary. One possible system may be FLNH-conA/Rh-dextran. FLNH is easily labeled to conA and should overlap with the rhodamine excitation spectrum without interfering with emission.

In addition to improving the chemistry of the glucose sensor several instrument modifications would also enhance the performance of the sensor.

Using the ADALAB software the computer can be programmed to calculate the slope and intercept for each series of energy transfer experiments and then automatically correct each data point for more efficient source fluctuation corrections.

The computer program can be further refined and used in conjunction with an autoanalyzer and/or robotics for totally automated measurements.

The instrument used in this work utilized a single sample wavelength. The optical design can be configured so that there is a second sample PMT, with a suitable interference filter for a second fluorophor emission, as well as a source reference PMT, Figure 5.1. This arrangement provides an inexpensive dual wavelength instrument. One can also eliminate the use of the interference filter(s) by the use of a monochromator with a specially adapted output port, Figure 5.2. Wavelength selection is facilitated by inserting fiber bundles into different exit holes on the side of the monochromator. Monochromators are more costly but can produce higher stray light rejection.

A large portion of the stray light background is a result of the broad band fluorescence of the laser dye. For an increased cost the MICRO-DYE laser, using the Littman optical design, can be replaced with an Oscillator-Amplifier dye laser or a Ring Dye laser. Both optical designs should have increased rejection of the unwanted dye emission. An alternative would be to place a narrow bandwidth filter between the dye laser exit port and the optical fiber. The most logical choice would be to situate the filter just in front of the microscope objective which focuses the laser light into the fiber optic beam splitter.

Instrument flexibility and ease of adaptation make it applicable to a wide range of optical sensors. Slight modifications allow it to be used with sensors based on fluorescence intensity, absorbance, reflectance, and fluorescence and phosphorescence lifetimes. Instruments modeled after this prototype will find use in medicine, industrial and environmental applications.

Figure 5.1: Duel Wavelength Optical Arrangement

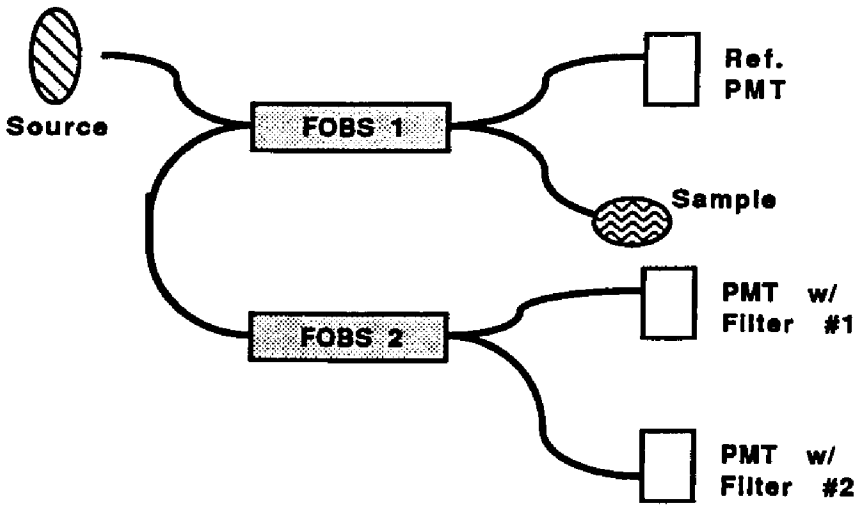

Figure 5.2: Block Diagram of Modified Monochromator for use with Laser/Fiber Optic Instrument

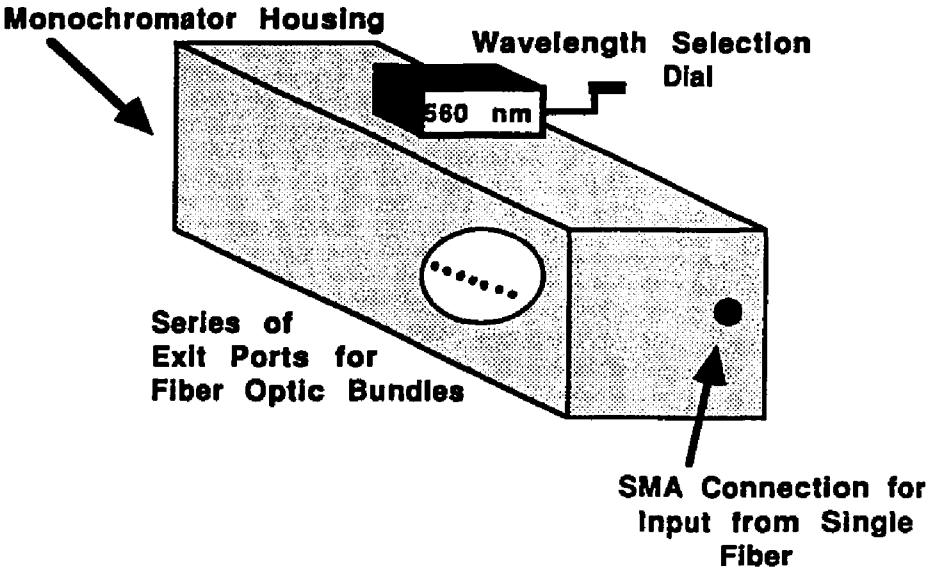

Appendix 1: BOXCAR TERMINOLOGY

EXPONENTIAL AVERAGING--Weighted averaging, output signal asymptotically approaches "G" time input level, where G is Gain. Time needed to reach final level is 5 times the observed time constant (OTC)
{A second option in Summation Averaging where all repetitions of signal are equal.}

APERTURE DURATION (AD)--Time when you are looking at the signal. Range is from 10 ns to 5 ms on the 162 and down to 2 ns on 166.
{AD Affects SNIR, analysis time and Resolution.}

APERTURE DELAY RANGE (ADR)--Interval over which the Aperture Duration is scanned.

% DELAY--Sets the leading edge of AD to any point in the ADR

TIME CONSTANT (TC)-- Time over which the capacitor is charged. Setting range from 1 usec to 10 msec. Time to perform experiment is directly proportional to TC.

OBSERVED TIME CONSTANT (OTC)--TC divided by aperture duty factor (ADF). ADF = AD/aperture period
Aperture Period = rep rate in Hz.

SIGNAL TO NOISE IMPROVEMENT RATIO (SNIR)--Improvement in SNIR varies with square root of TC. When exponential averaging is used
$SNIR = (2*TC/AD)^{1/2}$

TRIGGERING--Need up to a + or - 10 V input to initiate signal processing. Minimum trigger duration = 10 ns. {Trigger delay 30 ns from trigger to front of ADR and minimum time from ADR to leading edge of AD is 45 ns. Therefore first AD starts 75 ns after trigger.}

TRIGGER DRIFT-- Integration of trigger pulse which is measured, along with the signal, at the output jack. Theoretically this should remain constant and is eliminated with the ZERO CONTROL KNOB.

Miscellaneous Boxcar Controls and Functions

SCAN SELECT PUSH BUTTON--Use non-scan mode to fix AD in one position for every integration point.

INPUT VOLTAGE LIMITS-- + OR - 5 V

ZERO KNOB-- Used in an attempt to control trigger drift.

DROOP-- Some current is lost from capacitor in between samplings. Leakage depends on trigger period.

HOLD TIME-- lowest rep rate with out information loss.

MAXIMUM TRIGGER PERIOD (Pmax)-- Maximum sampling rate of boxcar. Depends on the TC, AD, and input capacitance. Consult Boxcar manual for maximum trigger periods.

INPUT CONTROLS:
INPUT IMPEDANCE--164: 1 MΩ or 50Ω
166: 10 kΩ or 50Ω
AC/DC-- Want DC for low frequency work and
AC when DC source drift is problem.

Additional Controls on 166 Module

SENSITIVITY-- Allows full scale sensitivities from 50 mV to 5 V. Determines Gain of 166 integrator. (Gain is fixed in 166 Module.)

APERTURE DURATION-- Additional AD's of 2,5,10, or 15 ns.

Appendix 2: SENSOR Program

```
1  HIMEM: 36095:D% = 0: DIM C%(5),Q%(5),D%(280): PRINT  CHR$ (4)"BRUNOUI
   CKI/O"
10  DIM A(280),B(280),R(280)
11  DIM AD(280),BD(280),SUM(280)
12  DIM C(280)
15  PRINT "INPUT CORRECTION FACTORS. INCLUDE '-' IF NUMBER IS TO BE SUBT
   RACTED"
16  PRINT
17  INPUT "SIG CORRECTION? ";SC
18  INPUT "REF CORRECTION? ";RC
19  PRINT
20  INPUT "INPUT NUMBER OF PULSES. MAX 280! TO EXIT PROGRAM INPUT 0 (ZER
   O).";NUM
21  IF NUM = 0 THEN  GOTO 500
22  PRINT
25  PRINT  TAB( 3);"SIG"; TAB( 10);"DIFF"; TAB( 17);"REF"; TAB( 23);"RDI
   FF"
26  FOR T = 1 TO 35
27  PRINT "-";
28  NEXT T
29  PRINT "-"
99  & DOO
100 B(COUNT) = D%
101  & A10: & A10.COUNT
120  FOR COUNT = 1 TO NUM
121  & DO1
124 DLAY = 400
126  FOR X = 1 TO DLAY: NEXT X
130  FOR CHANNEL = 0 TO 1
132 D% = (128 + CHANNEL): & POO:Q = Q
134  & A10: & A10.COUNT
135 DLAY = 25
136  FOR Z = 1 TO DLAY: NEXT Z
138  IF CHANNEL = 0 THEN A(COUNT) = D%: GOTO 144
139 B(COUNT) = D%
144  NEXT CHANNEL
148 DLAY = 100
150  FOR Y = 1 TO DLAY: NEXT Y
152  FOR H = 1 TO DLAY: NEXT H
153  IF COUNT < (NUM - 9) THEN  GOTO 160
155 REFSUM = C + A(COUNT):C = REFSUM
156 SIGSUM = S + B(COUNT):S = SIGSUM
160  NEXT COUNT
170 D% = 0
200  FOR COUNT = 1 TO NUM
202 AD(COUNT) = A(COUNT) - A(COUNT - 1)
204 BD(COUNT) = B(COUNT) - B(COUNT - 1)
219  PRINT COUNT; TAB( 5);
220  PRINT B(COUNT - 1); TAB( 10);
221  PRINT BD(COUNT - 1);
222  PRINT  TAB( 17);
```

```
223  PRINT A(COUNT): TAB( 23):AD(COUNT)
230  NEXT COUNT
250 REFAVE = REFSUM / 10 + RC
260 SIGAVE = SIGSUM / 10 + SC
275 R = SIGAVE / REFAVE
278  PRINT
280  PRINT "LAST 10 POINTS ARE AVERAGED AND THEN ADJUSTED WITH THE CORRE
    CTION FACTORS."
281  PRINT "SIG AVE = ";SIGAVE; TAB( 17);"REF AVE ";REFAVE
285  PRINT "SIG/REF RATIO = ";R
350 REFSUM = 0:SIGSUM = 0:REFC = 0:SIGC = 0:REFAVE = 0:SIGAVE = 0:R = 0
351 S = 0:C = 0
398  PRINT
399  PRINT
400  GOTO 20
500  END

]
```

Appendix 3: SENSOR2 Program

```
1  HIMEM: 36095:D% = 0: DIM C%(5),Q%(5),D%(280): PRINT  CHR$ (4)"BRUNQUI
   CKI/O"
10  DIM A(280),B(280),R(280)
11  DIM AD(280),BD(280),SUM(280)
12  DIM C(280)
15  PRINT "INPUT CORRECTION FACTORS. INCLUDE '-' IF NUMBER IS TO BE SUBT
   RACTED"
16  PRINT
17  INPUT "SIG CORRECTION? ";SC
18  INPUT "REF CORRECTION? ";RC
19  PRINT
20  INPUT "INPUT NUMBER OF PULSES. MAX 280! TO EXIT PROGRAM INPUT 0 (ZER
   O).";NUM
21  IF NUM = 0 THEN  GOTO 500
22  PRINT
25  PRINT  TAB( 3);"SIG"; TAB( 10);"DIFF"; TAB( 17);"REF"; TAB( 23);"RDI
   FF"
26  FOR T = 1 TO 35
27  PRINT "-";
28  NEXT T
29  PRINT "-"
99  & DOO
100 B(COUNT) = D%
101  & AIO: & AIO,COUNT
120  FOR COUNT = 1 TO NUM
121  & DO1
124 DLAY = 200
126  FOR X = 1 TO DLAY: NEXT X
130  FOR CHANNEL = 0 TO 1
132 D% = (128 + CHANNEL): & POO:Q = Q
134  & AIO: & AIO,COUNT
135 DLAY = 200
136  FOR Z = 1 TO DLAY: NEXT Z
138  IF CHANNEL = 0 THEN A(COUNT) = D%: GOTO 144
139 B(COUNT) = D%
144  NEXT CHANNEL
148 DLAY = 25
150  FOR Y = 1 TO DLAY: NEXT Y
152  FOR H = 1 TO DLAY: NEXT H
153  IF COUNT < (NUM - 9) THEN  GOTO 160
155 REFSUM = C + A(COUNT):C = REFSUM
156 SIGSUM = S + B(COUNT):S = SIGSUM
160  NEXT COUNT
170 D% = 0
200  FOR COUNT = 1 TO NUM
202 AD(COUNT) = A(COUNT) - A(COUNT - 1)
204 BD(COUNT) = B(COUNT) - B(COUNT - 1)
219  PRINT COUNT; TAB( 5);
220  PRINT B(COUNT - 1); TAB( 10);
```

```
221  PRINT BD(COUNT - 1);
222  PRINT  TAB( 17);
223  PRINT A(COUNT); TAB( 23);AD(COUNT)
230  NEXT COUNT
250 REFAVE = REFSUM / 10 + RC
260 SIGAVE = SIGSUM / 10 + SC
275 R = SIGAVE / REFAVE
278  PRINT
280  PRINT "LAST 10 POINTS ARE AVERAGED AND THEN ADJUSTED WITH THE CORRE
    CTION FACTORS."
281  PRINT "SIG AVE = ";SIGAVE; TAB( 17);"REF AVE ";REFAVE
285  PRINT "SIG/REF RATIO = ";R
350 REFSUM = 0:SIGSUM = 0:REFC = 0:SIGC = 0:REFAVE = 0:SIGAVE = 0:R = 0
351 S = 0:C = 0
398  PRINT
399  PRINT
400  GOTO 20
500  END
```

]

Appendix 4: Slope Correction Program on Texas Instrument TI55-III Calculator.

Slope Correction $y = mx + b$

y = Sample Signal
x = Reference Signal
m = slope
b = y-intercept

Source Corrected Sample Signal $= \frac{\text{Raw Sample Sig.}}{mx + b}$

Program on TI55-III Calculator:

Enter each calculator key in the order shown. The only variables are "Slope and "y-Inter.":

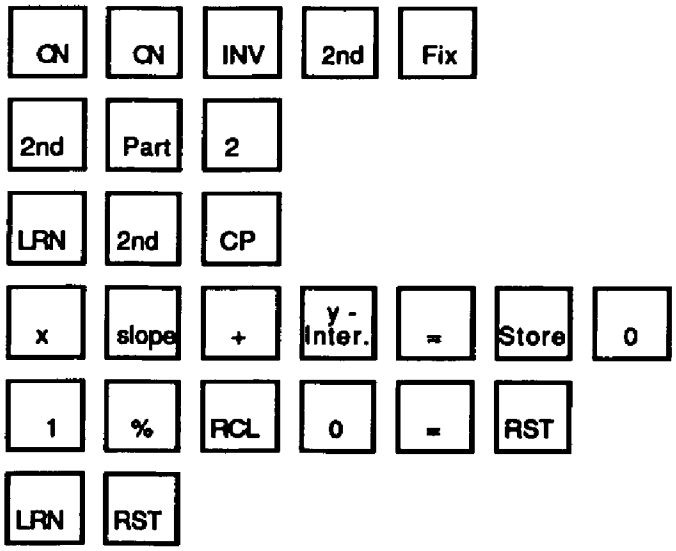

Source correction is accomplished by entering the Reference signal, hitting the R/S key, to start the program, and multiplying the output by the Raw Sample siganl.

REFERENCES

1. Seitz, W. R. **Anal. Chem.** 56, 16A, 1984.

2. Seitz, W. R. **CRC Crit. Rev. in Anal. Chem.** 19, 135, 1988.

3. Peterson, J. I.; Vurek, G. G. **Science** 224, 123, 1984.

4. Wolfbeis, O. S. **Trends Anal. Chem.** 4, 184, 1985.

5. Wolfbeis, O. S. **Fresenius Z. Anal. Chem.** 325, 387, 1986.

6. Angel, S. M. **Spectroscopy** 2, 38, 1987.

7. Raju, T. N. K.; Vidyasager, D. **Med. Instrum.** 16, 154, 1982.

8. Gerdt, D. W.; Gilligan, L.H., Manufacturers Literature, Sperry Marine Inc., Charlottesville, VA 22906.

9. Hardy, E. E.; David, D. J.; Kapany, N. S.; Unterleitner, F. C. **Nature** 257, 666, 1975.

10. Luebbers, D. W.; Opitz, N.; Speiser, P. P.; Bisson, H. J. **Z. Naturforsh** 32C, 133, 1977.

11. Freeman, T. M.; Seitz, W. R. **Anal. Chem.** 50, 1242, 1978.

12. Peterson, J. I.; Goldstein, S. R.; Fitzgerald, R. V.; Buckhold, D. K. **Anal. Chem.** 52, 864, 1980.

13. Gehrich, J. L.; et. al. **IEEE Trans. Biomed. Eng.** BME-33, 117, 1986.

14. Saari, L. A.; Seitz, W. R. **Anal. Chem.** 54, 821, 1982.

15. Zhujun, Z.; Seitz, W. R. **Anal. Chim. Acta.** 160, 47, 1984.

16. Wolfbeis, O. S.; Furlinger, E.; Kroneis, H.; Marsoner, H. **Fresenius Z. Anal. Chem.** 314, 119, 1983.

17. Kautsky, H. **Trans. Faraday Soc.** 35, 216, 1939.

18. Bergman, I. **Nature** 218, 396, 1969.

19. Wolfbeis, O. S.; Offenbacher, H.; Kroneis, H.; Marsoner, H. **Mikrochemica Acta.** 1, 153, 1984.

20. Peterson, J. I.; Fitzgerald, R. V.; Buckhold, D. K. **Anal. Chem.** 56, 62, 1984.

21. Zhujun, Z.; Seitz, W. R. **Anal. Chem.** 58, 220, 1986.

22. Vurek, G. G.; Feustel, P. J.; Severinghaus, J. W. **Annals Biomed. Eng.** 11, 499, 1983.

23. Zhujun, Z.; Seitz, W. R. **Anal. Chim. Acta** 160, 305, 1984.

24. Wolfbeis, O. S.; Weis, L. J.; Leiner, M.; Zeigler, W. **Anal. Chem.** 60, 2028, 1988.

25. Kawahara, F. K.; et. al. **Anal. Chim. Acta** 151, 315, 1983.

26. Chudyk, W. A.; Carrabba, M. M.; Kenny, J. E. **Anal. Chem.** 57, 1237, 1985.

27. Milanovich, F. P. **Environ. Sci. Technol.** 20, 441, 1986.

28. Giuliani, J. F.; Wohltjen, H.; Jarvis, N. L. **Optics Letters** 8, 54, 1983.

29. Arnold, M. A.; Ostler, T. F. **Anal. Chem.** 58, 1137, 1986.

30. Saari, L. A.; Seitz, W. R. **Analyst** 109, 655, 1984.

31. Urbano, E.; Offenbacher, H.; Wolfbeis, O. S. **Anal. Chem.** 56, 427, 1984.

32. Zhujun, Z.; Seitz, W. R. **Anal. Chim. Acta** 171, 251, 1985.

33. Bright, F. V.; Poirier, G. E.; Hieftje, G. M. **Talanta** 35, 113, 1988.

34. Schultz, J. S.; Sims, G. **Biotech. Bioeng. Symp.** 9, 65, 1979.

35. Schultz, J. S.; Mansoure, S.; Goldstein, I. J. **Diabetes Care** 5, 245, 1982.

36. Schultz, J. S. United States Patent # 4,344,438, Aug. 17, 1982.

37. Tromberg, B. J.; et. al. **Anal. Chem.** 60, 1901, 1988.

38. Tromberg, B. J.; Sepaniak, M. J.; Vo-Dihn, T.; Griffin, G. D. **Anal. Chem.** 59, 1226, 1987.

39. Petrea, R. D.; Sepaniak, M. J.; Vo-Dihn, T. **Talanta** 35, 139, 1988.

40. Sutherland, R.; Dahne, C.; Place, J.; Ringrose, A. S. **Clin. Chem.** 30, 1533, 1984.

41. Förster, J. **Discussions Faraday Soc.** 27, 7, 1959.

42. Ullman, E. F.; Schwarzberg, M.; Rubenstein, K. E. **J. Biological Chem.** 251, 4172, 1976.

43. Jordan, D. M.; Walt, D. R.; Milanovich, F. P. **Anal. Chem.** 59, 437, 1987.

44. Sharon, N.; Lis, H. **Science** 177, 954, 1972.

45. Summer, J. B.; Howell, S. F. **J. Bacteriol.** 32, 227, 1936.

46. Agrawal, B. B. L.; Goldstein, I. J. **Biochim. Biophys. Acta** 147, 262, 1967.

47. Olson, M.; Liener, I. E. **Biochemistry** 6, 105, 1967.

48. Edelman. G. M.; et. al. **Proc. Nat. Acad. Sci. USA** 69, 2580, 1972.

49. Goldstein, I. J.; Hollerman, C. E.: Smith, E. E. **Biochemistry** 4, 876, 1965.

50. Hardman, K. D.; et. al. **Proc. Nat. Acad. Sci. USA** 68, 1393, 1971.

51. Quiocho, F. A.; et. al. **Proc. Nat. Acad. Sci. USA** 68, 1853, 1971.

52. McKenzie, G. H.; Sawyer, W. H.; Nichole, L. W. **Biochim. Biophys. Acta** 263, 283, 1972.

53. Yariv, J.; Kalb, A. J.; Levitzki, A. **Biochim. Biophys Acta** 165, 303, 1968.

54. Hassing, G. S.; Goldstein, I. J.; Marini, M. **Biochim. Biophys. Acta** 243, 90, 1971.

55. Agrawal, B. B.; Goldstein, I. J.; Hassing, G. L.; So, L. L. **Biochemistry** 7, 4211, 1968.

56. Poretz, R. D.; Goldstein, I. J. **Biochemistry** 9, 2890, 1970.

57. Vurek, G. G.; Bowman, R. L. **Anal. Chem.** 29, 238, 1969.

58. Hirschfeld, T.; et.al. **J. Lightwave Tech.** 5, 1027, 1987.

59. Wyatt, W. A.; Poirer, G. E.; Bright, F. V.; Hieftje, G. M. **Anal. Chem.** 59, 572, 1987.

60. Fuh, M. S.; Burgess, L. W.; Christian, G. D. **Anal. Chem.** 60, 433, 1988.

61. Munkholm, C; Walt, D. R.; Milanovich, F. P. **Talanta** 35, 109, 1988.

62. Bright, F. V. **Applied Spec.** 42, 1531, 1988.

63. Carroll, M. K.; Bright, F. V.; Hieftje, G. M. **Applied Spec.** 43, 176, 1989.

64. Luo, S; Walt, D. R. **Anal. Chem.** 61, 174, 1989.

65. Hirschfeld, T; Deaton, T; Milanovich, F; Klainer, S. **Optical Engineering** 22, 527, 1983.

66. Exciton Laser Dye Catalog, Exciton Chemical Co., Overlook Station, Dayton, OH, 1986.

67. Sarri, L. A.; Seitz, R. W. **Anal. Chem.** 54, 821, 1982.

68. Sarri, L. A.; Seitz, R. W. **Anal. Chem.** 56, 810, 1984.

69. Wolfbeis, O. S.; Posch, H. E.; Kroneis, H. W. **Anal. Chem.** 57, 2556, 1985.

70. Vo-Dihn, T; Griffin, G. D.; Ambrose, K. R. **Applied Spec.** 40, 696, 1986.

71. Peterson, J. I.; Goldstein, S. R.; Fitzgerald, R. V.; Buckhold, D. K. **Anal. Chem.** 52, 864, 1980.

72. Suzuki, K.; et.al. **Anal. Chem.** 61, 382, 1989.

73. Reichert, W. M.; Ives, J. T.; Suci, P. A. **Applied Spec.** 41, 1347, 1987.

74. Keiser, Gerd "Optical Fiber Communications" McGraw-Hill Book Co., New York, NY, 1983.

75. Fuh, M. S.; et.al. **Analyst** 112, 1159, 1987.

76. Hill, K. O.; Johnson, D. C.; Lamont, R. G. **SPIE** Vol. 574 Fiber Optic Couplers, Connectors, and Splice Technology, 1985.

77. Gerdt, D. W.; Gilligan, L. H. "Variable Coupler Fiber Optic Sensor" personnel correspondence, Sperry Marine Inc., Charlottesville, VA.

78. Gerdt, D. W.; Gilligan, L. H. United States Patent #4,634,858, Jan. 6, 1987.

79. Anderson, F. P.; Miller, W. G. **Clin. Chem.** 34, 1417, 1988.

80. Liu, K; Littman, M. G. **Optics Letters** 6, 117, 1981.

81. Hecht, J. **Lasers and Applications** 3, 53, 1984.

82. Operating and Service Manual, Model 162 Boxcar Averager Including Model 164 Gated Integrator. Publication MDL 162, EG&G Princeton Applied Research P.O. Box 2565, Princeton, NJ 08540.

83. Model 162 Boxcar Averager Product Literature, Publication T-399, EG&G Princeton Applied Reseach, P.O. Box 2565, Princeton, NJ 08540.

84. Laser Dye Catalog, 1986, Exciton Chemical Co., P.O. Box 31226, Overlook Station, Dayton, OH 45431.

85. Kodak Laser Dyes, Publication JJ-169, Laboratory and Research Products Division, Eastman Kodak Co., Rochester, NY 14650.

86. Streyer, L. **Ann. Rev. Biochem.** 47, 819, 1978.

87. So, L.L.; Goldstein, I.S. **Biochim. Biophys. Acta** 165, 398, 1965.

88. Khanna, P.L.; Ullman, E.F. **Anal. Biochem.** 108, 156, 1980.

89. Boguslaski, R.C.; Li, T.M. **Applied Biochem. and Biotech.** 7, 401, 1982.

90. Eimstad, W.M.; et.al. **Clin. Chem.** 24, 1015, 1978.

91. Miller, J.N.; Lim, C.S.; Bridges, J.W. **Analyst** 105, 91, 1980.

92. Lim, C.S.; Miller, J.N.; Bridges, J.W. **Anal. Biochem.** 108, 176, 1980.

93. Becker, J.S.; Oliver, J.M.; Berlin, R.D. **Nature** 254, 152, 1975.

94. Rodgers, R.; et. al. **Clin. Chem.** 24, 1033, 1978.

95. Meadows, D.; Schultz, J.S. **Talanta** 35, 145, 1988.

96. Smith, D.S.; Nargess, R.D.; Hassen, H. in "Modern Fluorescence Spectroscopy", Vol 3, Wehry, E.L., Ed., Plenum Press, New York, 1981, p. 143.

97. Molecular Probes: Handbook of Fluorescent Probes and Research Chemicals, Richard Haugland P.O. Box 22010, 4849 Pitchford Ave., Eugene, OR 1989 edition.

98. Molecular Probes: Handbook of Fluorescent Probes and Research Chemicals, Richard Haugland P.O. Box 22010, 4849 Pitchford Ave., Eugene, OR 1985 edition.

99. Christian, L.M. "The Characterization of an Ionic Strength Sensor Based on Competitive Binding and Fluorescence Energy Transfer", UNH Thesis, 1986.

100. Chen, K.; Wiedmer, T.; Sims, P.J. **J. of Immunology** 135, 459, 1985.

101. Ditzler, M.A. personel correspondince to W. R. Seitz.

102. Smolin, E.M.: Rapoport, L. in "The Chemistry of Heterocyclic Compounds, S-Triazines and Derivatives" Arnold Weissberger, Ed., Interscience Publishers, Inc., New York, 1959, p. 55.

103. DeBelder, A.N.; Granath, K. **Carboydrate Research** 30, 375, 1973.

104. Undenfriend, S.; et. al. **Science** 178, 871, 1978.

105. Weigele, M.; et. al. **JACS** 94, 5927, 1972.

106. Bhlem, P.; et. al. **Arch. Biochem. Biophys.** 155, 213, 1973.

107. Weigele, M.; DeBernardo, S; Liemgruber, W.; Cleeland, R.; Grumburg, E. **Biochem. Biophys. Res. Comm.** 54, 899, 1973.

108. Handschin, U.E.; Ritschard, W.J. **Anal. Biochem.** 71, 143, 1976.

109. Titus, J.A.; Haugland, R.; Sharrow, S.; Segal, D.M **J. Immunogical Methods** 50, 193, 1982.

110. Godvindanunny, T; Sivaram, B.M. **J. of Luminescence** 21, 397, 1980.

111. Goodall, D.M.; Roberts, D.R. **J. Chem. Ed.** 62, 711, 1985.